CHAPTER 2

THE LIGHT-GAS-GUN MODEL LAUNCHER

by

Robert E. Berggren and Robert M. Reynolds

NASA-Ames Research Center

THE LIGHT-GAS-GUN MODEL LAUNCHER

Robert E. Berggren and Robert M. Reynolds

2.1 INTRODUCTION

The conventional powder gun – the forerunner of the present day ballistic-range model launcher – has been the object of theoretical and experimental research for two centuries. The foundations for formal systematic research on guns were laid by Robins[2.1] and Lagrange[2.2], who formulated the basic problems of classical internal ballistics. Many other notable names form the roster of those early workers who made significant contributions to the fascinating study of ballistics: Poisson[2.2], Résal[2.3], Hélie[2.4], Sarrau[2.5], Moisson[2.6], Hugoniot[2.7], Gossot and Liouville[2.8], Charbonnier[2.9], Röggla[2.10], Love and Pidduck[2.11], Cranz[2.12], and many others. Historical reviews of the earlier development of ballistics are given by Cranz[2.12], Corner[2.13], Thornhill[2.14], Hunt[2.15], and Nelson[2.16].

With the introduction of the free-flight ballistic range the gun became a laboratory tool which provided a convenient means for generating high speeds for the study of the physics of flight. Early ranges were used by Charbonnier[2.9], Cranz[2.12], and Fowler et al.[2.17], to investigate the aerodynamics of spinning shells. Since that period, a large number of modern ballistic ranges have evolved to study many aspects of flight at high speeds, not necessarily related to the weapons of ordnance. As the flight speeds of interest increased, new classes of projectile launchers were required, but the conventional powder gun has remained an important test device for research at speeds below approximately 3 km/s.

The powder gun is limited to such speeds because of the high molecular weight of powder gas. In accelerating a projectile by the expansion of a heavy gas, a large share of the total available energy of the gas is expended in accelerating the gas itself and thus the energy available for accelerating the projectile is relatively small; even with a very light projectile the maximum velocities attainable are relatively low. A much more favorable distribution of energy between the gas and the projectile, giving higher projectile velocities, is obtained with the use of a light gas such as hydrogen or helium.

The first gun utilizing a light propellant gas (helium) was developed by Crozier and Hume[2.18], in 1946 at the New Mexico School of Mines. Since that time, a large variety of "light-gas" guns have evolved, differing mainly in the manner in which the propellant gas is compressed to the high pressures and temperatures required to produce high speeds. Early further development of the type of gun introduced by the New Mexico group was made by Charters, et al.[2.19], at Ames Research Center (1955). Development of a second type of light-gas gun was carried out at the same time at the US Naval Ordnance Laboratory under the direction of Z. I. Slawsky[2.20, 2.21]. Further improvements in the technology of light-gas guns have since been made by many ballistic laboratories in the United States, Canada, and England, with the result that this type of model launcher has become an invaluable tool to generate flight speeds up to 11 km/s. The development of the high-speed computer and new instrumentation techniques have aided greatly in obtaining a better understanding of the complex internal ballistic processes, as evidenced by the large gains in velocity that have been achieved in the last decade, but much remains to be learned.

A number of other methods for accelerating projectiles or discrete particles have been explored and are well documented in the literature. Scully, et al.[2.22] report the attainment of velocities up to 20 km/s with small silicate spheres (10^{-8} to 10^{-6}gm) with an electrothermal gun. The spheroids are accelerated by aerodynamic drag in a stream of dense lithium plasma which is energized by an electric arc discharge. Small charged particles (0.1 to 10 microns diameter) have been accelerated electrostatically to velocities as high as 28 km/s, as reported by Friichtenicht et al. in Reference 2.23. Kronman and Kineke[2.24] report that discrete particles of larger mass (0.01 to 1.0 gm) have been accelerated with explosive shaped-charge techniques to approximately 21 km/s. Electromagnetic accelerators of a variety of types have been tested but have not produced results to date that would make this launcher competitive with the light-gas gun. A novel innovation to the two-stage light-gas gun has been developed by Howell and Orr[2.25], whereby spherical projectiles are given an additional increment in velocity as they are impulsively accelerated through a convergent section attached to the muzzle of the gun. Velocities in excess of 11 km/s have been obtained by this technique. A new development by Godfrey and Moore (reported in Reference 2.26), utilizing a light-gas gun in which the propellant gas is compressed in a controlled manner by an explosive lens, has produced velocities up to 12.2 km/s and shows promise of achieving substantially higher velocities. A brief description of this gun is contained in Section 2.7.

The light-gas gun has proven to be a particularly versatile device in comparison with other launchers because it has the capability of launching models of complex shape having a wide range of weights, sizes, and materials. It has the advantage that high velocities may be achieved under conditions which subject the model to relatively low accelerations and stresses. Although this gun has not produced velocities as high as desired, its present capabilities encompass a flight regime of interest for much present day research. Photographs of two representative light-gas guns may be seen in Figures 2.1 and 2.2.

This chapter will be confined to a discussion of the light-gas gun with major emphasis on the two-stage gun now in wide use as a laboratory model launcher.

2.2 SYMBOLS

a	speed of sound
A	cross-sectional area
b	co-volume term
c	modified speed of sound (see Equation (2.114))
d	diameter of projectile
D	diameter of gun components
f	factor in real-gas equation of state
F	factor in real-gas relations (see Equation (2.114))
G	mass of gas
h	enthalpy
k	factor in real-gas equation of state
l	length of projectile
L	length of gun components
m	mass
M	molecular weight
N	number of moles
p	pressure
$\mathcal{R}$	universal gas constant
R	gas constant for a mole of gas $= \mathcal{R}/M$
s	specific entropy
S	entropy
t	time
T	temperature
u	velocity
U	projectile velocity at muzzle of launch tube
v	specific volume
V	volume
w	cylinder wall ratio $= \dfrac{\text{outer diameter of cylinder}}{\text{inner diameter of cylinder}}$
x	distance
α	acceleration
β	factor in real-gas equation of state
γ	ratio of specific heats
ρ	density

σ	Riemann function
σ_y	yield stress
$\bar{a}, \bar{u}, \bar{t}$, etc.	nondimensional quantities defined in text
$\tilde{p}$	average pressure

Subscripts

a	ambient conditions
b	conditions at base of pump piston
c	conditions at entrance of transition section, or conditions in powder chamber
e	conditions at entrance to launch tube
f	final conditions at point specified which affect motion of the model in barrel (see Equation (2.134))
g	gas conditions
p	relating to piston or pump tube
r	reservoir conditions
R	conditions at release of model (diaphragm rupture)
s	relating to projectile, conditions at base of projectile, or launch tube
v	conditions at vertex of parabolic characteristic lines of similarity solution
o	initial loading or starting conditions
1	length or time corresponding to condition when first rare faction wave returns from reservoir and reaches projectile base
*	sonic conditions

2.3 SIMPLE LIGHT-GAS GUN

In the following paragraphs the fundamental problem of the expansion of an ideal propellant gas in a simple gun, consisting only of a reservoir and gun barrel, will be examined. The relationships which govern the expansion process will be developed and the factors that predominate in the determination of the projectile motion, the selection of the propellant gas, and the geometrical configuration of the gun will be considered.

2.3.1 Basic Parameters Influencing Projectile Velocity

The basic factors which determine the motion of a projectile or "shot" as it is accelerated in the bore of a gun under ideal conditions are related by Newton's equation of motion, as follows, with the notation shown in Figure 2.3:

$$a = \frac{du_s}{dt} = \frac{p_s A_s}{m_s}, \tag{2.1}$$

or, in terms of the distance traveled,

$$a = u_s \frac{du_s}{dx_s} = \frac{p_s A_s}{m_s}. \tag{2.2}$$

Not considered at this point are the retarding forces due to friction between the model and bore, and the pressures developed on the front face of the model by residual gases in the bore.

In virtually all guns, the pressure, p_s, acting on the base of the model during launch is not constant but varies over a wide range, and is some function of x or t. The launch velocity or muzzle velocity, U, achieved by accelerating the model through the entire barrel length, L_s, is obtained by integrating Equation (2.2):

$$U = \left[\frac{2A_s}{m_s}\int_0^{L_s} p_s dx_s\right]^{1/2} \tag{2.3}$$

For purposes of simplification, consider an ideal case in which the model is accelerated by a base pressure, $\tilde{p}_s$, which is constant during the entire launch. (For the real case, $\tilde{p}_s$ represents the average pressure for the full launch distance). Equation (2.3) then becomes:

$$U = \left[\frac{2A_s}{m_s}\tilde{p}_s L_s\right]^{1/2} . \tag{2.4}$$

In terms of a nondimensionalized barrel length and model length this becomes, for a cylindrical projectile,

$$U = \left[\frac{2\tilde{p}_s}{\rho_s}\frac{L_s/D_s}{l_s/D_s}\right]^{1/2} . \tag{2.5}$$

Projectile velocities can be maximized, then, by maximizing $\tilde{p}_s$ and L_s/D_s and minimizing ρ_s and l_s/D_s. With a gun of specified bore diameter, the velocity is seen to increase with an increase in barrel length. However, increasing gun size by scaling up all dimensions proportionately will not result in increased performance, at least for the ideal conditions considered here, since the values of l_s/D_s and L_s/D_s remain unchanged.

It is informative to compute the launch velocities that might be attained under conditions of pressure, barrel length, model length, and density in Equation (2.5) that appear to be reasonable or realistic. Velocities calculated for several representative model weights and base pressures are plotted as a function of launch-tube length in Figure 2.4. Model density for all cases is 1 gm/cm^3, a value about equal to that of the plastics frequently used. Several typical model lengths were chosen ranging from ½ to 4 barrel diameter (calibers) long. The launch tube was limited to lengths no greater than 400 calibers, although construction of barrels appreciably longer than this is quite feasible. If one chooses an average base pressure of 10 kilobars, a value well within the strength capabilities of certain plastic models, a one-caliber-long model is accelerated to almost 30 km/s in the 400 caliber distance. This velocity is approximately three times greater than that actually achieved for this type of model. The primary reason is that the gun configurations in use at this time have not produced constant base pressures for lengths as long as 400 calibers, or an average pressure for this length where the peak pressures are low enough to be withstood by the model or the gun itself. An average base pressure of 1.5 kilobars, more representative of that attainable presently, is used for a second case. Actually it is difficult to maintain even this lower value of pressure for launch distances greater than 200 to 300 calibers (as will be shown in a later section) without producing peak pressures which are very much greater than the average value. The problem of achieving high launch velocities, then, is, in part, one of developing methods whereby acceptable pressures can be applied to the model for extended distances. One factor of primary importance in achieving this is the proper selection of propellant gas, and the effect of gas properties as well as other considerations will be examined in the following sections.

2.3.2 Expansion of Gas in Constant-Diameter Tube - Gas Properties

With the thought in mind that maintaining a high base pressure during the entire launching process is an important factor in obtaining high velocities, it is appropriate to examine briefly the behavior of a gas during the process of expansion to determine which parameters most strongly influence the relationship between the pressure and velocity.

Consider the case of the simple launcher shown in Figure 2.5, consisting of a reservoir and launch tube (or barrel) of the same bore diameter. The reservoir contains a perfect gas at initial conditions p_r, ρ_r, and T_r, separated from the projectile by a diaphragm. The launch-tube bore is evacuated to eliminate the retarding effects of any gas ahead of the projectile. When the diaphragm is ruptured in some manner, the subsequent expansion of the gas will accelerate the model, and part of the potential energy of the gas will be converted to kinetic energy in both the gas and projectile. If this expansion process is continued for a sufficiently long time, the limiting conditions will be reached where (neglecting friction and other losses) all potential energy will be converted to kinetic energy and the pressure will have decreased to zero. The limiting speed is termed the escape speed of the gas. The expansion process is nonsteady and one-dimensional, and the assumptions are made that the changes in the flow are continuous and that the process is isentropic. The fundamental relations which apply are:

Conservation of mass,

$$\frac{\partial\rho}{\partial t} + \rho\frac{\partial u}{\partial x} + u\frac{\partial\rho}{\partial x} = 0 . \tag{2.6}$$

Conservation of momentum,

$$\frac{\partial u}{\partial t} + u\frac{\partial u}{\partial x} + \frac{1}{\rho}\frac{\partial p}{\partial x} = 0 . \tag{2.7}$$

Constancy of particle entropy,

$$\frac{\partial S}{\partial t} + u\frac{\partial S}{\partial x} = 0 . \tag{2.8}$$

Isentropic process,

$$p = f(\rho) . \tag{2.9}$$

A solution to the nonlinear partial differential equations is possible using the "method of characteristics" given in Reference 2.27.

Introducing the speed of sound relationship,

$$a^2 = \left(\frac{\partial p}{\partial \rho}\right)_s ,$$

into the conservation of momentum equation, (2.7), gives

$$\frac{\partial u}{\partial t} + u \frac{\partial u}{\partial x} + \frac{a^2}{\rho} \frac{d\rho}{dx} = 0 . \tag{2.10}$$

Multiplying the continuity equation, (2.6), by a/ρ and combining with Equation (2.10) leads to two equations which, when rearranged, become:

$$\frac{\partial(u + \sigma)}{\partial t} + (u + a) \frac{\partial(u + \sigma)}{\partial x} = 0 , \tag{2.11}$$

$$\frac{\partial(u - \sigma)}{\partial t} + (u - a) \frac{\partial(u - \sigma)}{\partial x} = 0 , \tag{2.12}$$

where, σ , the Riemann function, is defined as

$$\sigma = \int_0^\rho \frac{a}{\rho} d\rho , \tag{2.13}$$

and $\sigma = 0$ when $\rho = 0$.

Equations (2.11) and (2.12) are known as characteristic equations in which the fluid properties are defined in the $x-t$ plane along lines having slopes $dx/dt = (u \pm a)$. Along the $dx/dt = (u + a)$ curves the flow properties are related by

$$d\rho = -\frac{\rho}{a} du \tag{2.14}$$

or, in terms of pressure,

$$dp = -\rho a \, du . \tag{2.15}$$

For the $dx/dt = (u - a)$ characteristic lines,

$$d\rho = \frac{\rho}{a} du \tag{2.16}$$

or

$$dp = \rho a \, du . \tag{2.17}$$

The directions or velocities represented by $dx/dt = u \pm a$ are the paths in the x-t plane of disturbances or acoustic waves which propagate upstream at the speed of sound, a, relative to the particle speed, u .

When a projectile is accelerated by an expanding gas, an infinite number of acoustic waves originate continuously in the gas at the base of the projectile and propagate upstream at velocity $(u - a)$ causing a continuous drop in pressure. In a sense, increasing projectile and fluid velocity is gained at the expense of a diminished pressure. It can be seen from Equations (2.15) and (2.17) that *the rate of change of pressure with velocity is dependent upon* ρa *, termed the acoustic impedance.* To obtain a high increment in velocity for a given incremental pressure drop requires that the acoustic impedance be low. This is a fundamental relationship, then, that governs the selection of the propellant gas to be used in a high-speed gun.

An expression for the acoustic impedance in terms of the reservoir conditions can be obtained from the following equation of state, sound speed equation, and isentropic relations:

$$p = \rho \frac{\mathcal{R}}{M} T \tag{2.18}$$

$$a^2 = \gamma RT \tag{2.19}$$

$$\frac{a}{a_r} = \left(\frac{\rho}{\rho_r}\right)^{(\gamma-1)/2} = \left(\frac{p}{p_r}\right)^{(\gamma-1)/2\gamma} \tag{2.20}$$

$$\frac{du}{dp} = \pm \frac{1}{\rho a} = \pm \frac{a_r}{\gamma p_r}\left(\frac{p_r}{p}\right)^{(\gamma+1)/2\gamma} \tag{2.21}$$

or

$$\frac{du}{dp} = \pm \left(\frac{RT_r}{\gamma M p_r^2}\right)^{1/2}\left(\frac{p_r}{p}\right)^{(\gamma+1)/2\gamma} . \tag{2.22}$$

It can be seen that, for a fixed value of reservoir pressure, p_r and pressure ratio, p_r/p, a reduction in γ and an increase in reservoir sound speed will increase the velocity gained with a given pressure loss. The sound speed is the more important factor since it can be varied over a wide range while the variation in γ for suitable propellant gases is quite limited. A reduction in acoustic impedance is also obtained by reducing the molecular weight of the gas. The requirement of a low molecular weight gas to obtain high projectile velocities can be readily appreciated when one considers that in the process of accelerating a projectile a substantial portion of the total available potential energy of the gas is expended in accelerating the gas itself. A gas must thus be chosen which requires the least energy to achieve a given gas velocity and this then dictates a gas of low molecular weight. Equation (2.22) shows also that increasing reservoir temperature will serve to reduce the acoustic impedance. Note that an increase in reservoir pressure, p_r, adversely affects the acoustic impedance by increasing the density, ρ_r.

To gain further insight into the manner in which pressure is diminished in exchange for increasing velocity in an expansion, let us examine again the characteristic Equations (2.11) and (2.12). Integration of the expression for the Riemann function, σ, for a perfect polytropic gas gives the simple relation:

$$\sigma = \frac{2a}{\gamma - 1} . \tag{2.23}$$

The quantities $(u + \sigma)$ and $(u - \sigma)$, referred to as Riemann invariants, are thermodynamic functions which remain constant along the characteristic lines of slope $(u + a)$ and $(u - a)$. Thus:

$$u + \sigma = u + \frac{2a}{\gamma - 1} = \text{constant} , \tag{2.24}$$

along downstream characteristics having slope $dx/dt = (u + a)$, and

$$u - \sigma = u - \frac{2a}{\gamma - 1} = \text{constant} , \tag{2.25}$$

along upstream characteristics having slope $dx/dt = (u - a)$.

These disturbance paths are illustrated in the $x-t$ diagram of Figure 2.6, for a simple launcher having an infinitely long reservoir of the same diameter as the barrel.

The conditions in the barrel can be related to the conditions in the undisturbed region in the reservoir where the flow velocity is zero, along downstream characteristics by:

$$u + \frac{2a}{\gamma - 1} = \frac{2a_r}{\gamma - 1} . \tag{2.26}$$

Combining this equation with the isentropic relation

$$\frac{p}{p_r} = \left(\frac{a}{a_r}\right)^{2\gamma/(\gamma-1)} ,$$

gives the relationship between pressure and flow velocity for the expansion of a perfect gas:

$$\frac{p}{p_r} = \left[1 - \left(\frac{\gamma - 1}{2}\right)\frac{u}{a_r}\right]^{2\gamma/(\gamma-1)} , \tag{2.27}$$

or

$$\frac{u}{a_r} = \frac{2}{\gamma - 1}\left[1 - \left(\frac{p}{p_r}\right)^{(\gamma-1)/2\gamma}\right]. \tag{2.28}$$

In the limit $\gamma \to 1$ these equations reduce to

$$-\log_e \frac{p}{p_r} = \frac{u}{a_r}, \tag{2.29}$$

as noted in Reference 2.28. Curves of Equation (2.27), presented in Figure 2.7 for several values of γ, show that the pressure ratio is highly sensitive to changes in the velocity ratio. If the flow velocity is very much less than the sound speed, there is only a small reduction in pressure below the initial reservoir pressure, but as flow velocity is increased to values greater than the reservoir sound speed, the pressure reduction becomes exceedingly great. Thus, in a realistic gun in which the maximum reservoir pressure, p_r, is limited by the strength of the reservoir, the propelling pressures can be maximized during expansion only by choosing a propellant gas having a high sound speed. It can also be seen again that the "best" propellant should have a low ratio of specific heats, γ.

The limiting velocity of an expanding gas is reached if the gas is expanded completely to zero pressure. This "escape velocity" can be seen from Equation (2.28) to be:

$$u_{esc} = \left(\frac{2}{\gamma - 1}\right) a_r . \tag{2.30}$$

This represents a theoretical maximum to which a projectile could be accelerated in a constant-bore gun under ideal conditions, without losses, if the launch tube were infinitely long to allow complete expansion of the gas to zero pressure.

Table 2.1 gives the physical properties of several gases that have been used as propellants. Hydrogen and helium are clearly superior to powder gas in fulfilling the requirements of a low acoustic impedance, ρa, and a high sound speed, a. At the high pressure, more representative of gun conditions, the two light gases are closely competitive in these properties. However, in regard to low molecular weight and a low ratio of specific heats, γ, hydrogen is substantially superior. Thus, in a given gun, hydrogen will achieve the highest ultimate performance, or, when used under comparable conditions to produce the same performance, will have the advantage of operating at considerably lower temperatures than those required for helium. As a consequence, at high-performance levels the erosion of the launch tube surfaces with hydrogen can be very much less – as much as an order of magnitude less – than for helium. This can be the difference between a tolerable rate of deterioration of the launch tube and an unacceptable rate requiring frequent replacement of eroded components. Erosion should be minimized for the added reason that the metallic vapor is a contaminant which can degrade performance by increasing the molecular weight of the propellant gas. Helium, while second best to hydrogen, is still an important propellant, since considerations of safety, in certain situations, outweigh the advantages gained with hydrogen.

2.3.3 Gas Dynamics Related to Model Motion

2.3.3.1 Infinite-Length Reservoir – Constant-Diameter Tube

The motion of the projectile, as given by Newton's law (Equation (2.2), Section 2.3.1), can be combined with the unsteady isentropic expansion relation, Equation (2.27), to obtain:

$$\frac{du_s}{dt} = u_s \frac{du_s}{dx} = \frac{p_s A_s}{m_s} = \frac{p_r A_s}{m_s}\left[1 - \left(\frac{\gamma - 1}{2}\right)\frac{u_s}{a_r}\right]^{2\gamma/(\gamma-1)}. \tag{2.31}$$

The expression for distance becomes:

$$x_s \frac{p_r A_s}{m_s} = \int_0^{u_s} u_s \left[1 - \left(\frac{\gamma - 1}{2}\right)\frac{u_s}{a_r}\right]^{-2\gamma/(\gamma-1)} du_s . \tag{2.32}$$

Changing x_s and u_s to a dimensionless form $\bar{x}_s$ and $\bar{u}_s$:

$$\bar{x}_s = \frac{p_r A_s x_s}{m_s a_r^2} \tag{2.33}$$

$$\bar{u}_s = \frac{u_s}{a_r} \tag{2.34}$$

and, completing the integration, one obtains the following expression for distance (see References 2.19, 2.29, and 2.30):

$$\bar{x}_s = \frac{2}{\gamma - 1}\left\{\frac{\frac{2}{\gamma+1} - \left[1 - \left(\frac{\gamma-1}{2}\right)\bar{u}_s\right]}{\left[1 - \left(\frac{\gamma-1}{2}\right)\bar{u}_s\right]^{(\gamma+1)/(\gamma-1)}} + \frac{\gamma-1}{\gamma+1}\right\}. \tag{2.35}$$

For time, where

$$\bar{t} = \frac{p_r A_s t}{m_s a_r}, \tag{2.36}$$

one obtains:

$$\bar{t} = \frac{2}{\gamma+1}\left\{\left[1 - \left(\frac{\gamma-1}{2}\right)\bar{u}_s\right]^{-(\gamma+1)/(\gamma-1)} - 1\right\} \tag{2.37}$$

and by combining Equations (2.35) and (2.37):

$$\bar{x}_s = \frac{2}{\gamma-1}\left\{1 + \bar{t} - \left[1 + \left(\frac{\gamma+1}{2}\right)\bar{t}\right]^{2/(\gamma+1)}\right\}. \tag{2.38}$$

These are the basic relationships for projectile velocity, as a function of distance and time, for unsteady isentropic flow of an ideal gas in a gun with an infinitely long reservoir, of the same diameter as the launch tube. Equation (2.35) is plotted in Figure 2.8, for various values of γ.

2.3.3.2 Finite-Length Reservoir - Constant-Diameter Tube

Consider now, the acceleration of a projectile by the expansion of gas from a reservoir of finite length. As in the previous section, let the reservoir diameter be the same as the barrel diameter.

At $t = 0$, representing the start of projectile acceleration, an expansion wave travels rearward at the speed of sound of the reservoir gas, a_r, setting the gas in motion, which in turn causes a decrease in pressure. Upon reflection from the rear wall of the reservoir, this acoustic wave will return in a downstream direction at a velocity $(u + a)$, acting to retard the motion of the reservoir gas and further reduce the reservoir pressure. If the launcher barrel is sufficiently long, the "reflected" rarefaction will, on arriving at the base of the projectile, lower the base pressure and projectile acceleration to values below those which would have occurred had the rarefaction not caught up with the projectile. The characteristic lines for this case are shown in Figure 2.9. The reservoir length, L_{r_1}, which will cause the first reflected rarefaction to catch the projectile just as the projectile leaves the muzzle of the launcher depends on projectile mass, launch-tube length, and the gas conditions. Any reservoir of length L_{r_1} or greater can be considered as "effectively" infinite because the projectile will have left the barrel before receiving communication from the gas signaling the existence of a reservoir wall. Heybey[2.30] developed an analytical relationship for the point at which the first reflected wave reaches the projectile base, as a function of the reservoir length L_{r_1}. This is given (in a different form) as a function of projectile velocity in Equation (2.39) below, for the expansion of an ideal gas in a constant diameter tube.

$$\bar{L}_{r_1} = \frac{p_r A_s L_{r_1}}{m_s a_r^2} = \frac{2}{\gamma+1}\left\{\left[1 - \left(\frac{\gamma-1}{2}\right)\frac{u_{s_1}}{a_r}\right]^{-\frac{1}{2}(\gamma+1)/(\gamma-1)} - 1\right\}. \tag{2.39}$$

In the limit $\gamma \to 1$ Equation (2.39) becomes

$$\bar{L}_{r_1} = e^{\bar{u}_s/2} - 1. \tag{2.40}$$

It may be noted that this relationship is part of a general analytical solution to the longstanding Lagrange Ballistic Problem solved by Heybey by tracing the flow properties with a network of characteristic lines. Previous to this, Love and Pidduck[2.11] and Kent[2.31] had derived restricted "special" solutions to the Lagrange problem. A relationship for the distance traveled by the projectile at the time the first reflected wave reaches the projectile base can be obtained as a function of the reservoir length $\bar{L}_{r_1}$ by combining Equations (2.39) and (2.35) to give:

$$\bar{x}_s = \frac{4}{\gamma^2-1}\left[\left(\frac{\gamma+1}{2}\right)\bar{L}_{r_1} + 1\right]^2 - \left(\frac{2}{\gamma-1}\right)\left[\left(\frac{\gamma+1}{2}\right)\bar{L}_{r_1} + 1\right]^{4/(\gamma+1)} + \frac{2}{\gamma+1}. \tag{2.41}$$

A plot of the barrel length, where $\bar{x}_s = \bar{L}_s$, is presented in Figure 2.10 as a function of the effectively infinite chamber length, for several values of γ (as given in Reference 2.28). Here, it is seen that for this criterion the chamber length is a nearly linear function of barrel length.

2.3.3.3 The Effects of Chambrage

When a gun has a reservoir diameter that is larger than the barrel or launch-tube diameter, as sketched in Figure 2.11, it is said to have "chambrage" or chamberage. In the expansion process in a chambered gun, rarefaction waves originating at the projectile base and moving toward the reservoir are partially reflected at the transition section, proceeding as compression waves directed back toward the projectile. The portion of the rarefaction not reflected is transmitted through the transition section to the reservoir, reflecting from the breech wall and lowering the reservoir pressure. The proportion of the rarefaction wave that is reflected at the transition section, towards the projectile, as a compression wave increases as the ratio D_r/D_s increases, approaching complete reflection as $D_r/D_s \to \infty$. This is in contrast to the situation in the constant-diameter gun (no chamberage) with an infinitely long reservoir, in which neither rarefactions or compressions can be reflected to the projectile. Hence, with other factors being equal the performance of a highly chambered gun would be expected to exceed that of a gun with smaller or no chamberage.

One other significant difference between the gas dynamics of the chambered gun and one with no chamberage is due to the quasi-steady flow in the transition section of the chambered gun, which is described by the following equation:

$$u\,du = -\frac{dp}{\rho} . \tag{2.42}$$

It is readily seen that for the chambered gun it is a low "ρ" as a function of pressure which is required to minimize the loss in pressure exchanged for an increase in velocity, rather than the low "ρa" requirement for the constant-diameter gun.

The most extensive treatment of the chamberage problem has been given by Seigel in References 2.28 and 2.32 to 2.34. Stephenson[2.35] presents some particular solutions, using Seigel's approach, for guns having helium as the propellant gas, and Vasiliu[2.36] and Zondek[2.37] have obtained solutions for the chambered gun using the method of characteristics in a digital computer program. The detailed analysis of the chamberage problem will not be considered here. We will be content, instead, to briefly outline the problem and summarize some of the conclusions regarding chamberage, leaving it to the interested reader to delve further into the references.

While the flow processes in the reservoir and launch tube may be readily treated by the one-dimensional characteristics equations previously outlined, the flow in the transition section joining the two bores is two-dimensional as well as unsteady. Seigel simplifies the problem by assuming that the flow at the entrance and exit planes of the transition section is one-dimensional, and that the time rates of change of mass and energy of the gas in the transition section are negligible. Hence, at any instant of time, the quasi-steady continuity and energy equations may be used to relate the conditions at the entrance to those at the exit of the transition section:

$$\rho_c A_r u_c = \rho_e A_s u_e , \tag{2.43}$$

and

$$h_c + \frac{u_c^2}{2} = h_e + \frac{u_e^2}{2} . \tag{2.44}$$

For an ideal gas, in a gun having an infinitely long reservoir $(L_r = \infty)$ with chamberage, the following equations are applied:

$$a = \left(\frac{\gamma - 1}{2}\right)\sigma , \qquad \frac{p}{p_{r_o}} = \left(\frac{\sigma}{\sigma_o}\right)^{2\gamma/(\gamma-1)} ,$$

$$h = \left(\frac{\gamma - 1}{4}\right)\sigma^2 , \qquad \frac{\rho}{\rho_{r_o}} = \left(\frac{\sigma}{\sigma_o}\right)^{2/(\gamma-1)} , \tag{2.45}$$

$$u_c + \sigma_c = \sigma_o , \tag{2.46}$$

and

$$u_r + \sigma_r = \sigma_o . \tag{2.47}$$

(Equations (2.45) and (2.46) relate the conditions of the gas at the entrance of the transition section and at any point in the reservoir, respectively, to those of the gas in the undisturbed region of the reservoir where u_{r_o} is considered to be 0).

(Continuity)

$$\frac{A_r u_c}{A_s u_e} = \frac{\rho_e}{\rho_c} = \left(\frac{\sigma_e}{\sigma_c}\right)^{2/(\gamma-1)} . \tag{2.48}$$

(Momentum)

$$\frac{u_c^2}{2} + \frac{\gamma - 1}{4}\sigma_c^2 = \frac{u_e^2}{2} + \frac{\gamma - 1}{4}\sigma_e^2 . \tag{2.49}$$

(In the barrel)

$$\frac{\partial}{\partial t}(u \pm \sigma) + (u \pm a)\frac{\partial}{\partial x}(u \pm \sigma) = 0 . \tag{2.50}$$

(Equation of motion)

$$\frac{m_s du_s}{dt} = p_{r_o} A_s \left(\frac{\sigma_s}{\sigma_o}\right)^{2\gamma/(\gamma-1)} . \tag{2.51}$$

For the limiting case of infinite chamberage ($D_r/D_s = \infty$) and infinite reservoir length ($L_r = \infty$), application of the preceding equations by the method of characteristics leads to the results shown in Figure 2.12. It is readily seen that for infinite reservoir length, according to this simplified analysis, the effect of chamberage increases with projectile velocity. However, increasing chamberage from unity to infinity (case shown) gives, as a maximum, an increase in velocity of $a_r/2$ over that of the gun with no chamberage.

For the more general case of finite chamberage and reservoir lengths, Seigel presents, in Reference 2.28, results calculated using both the method of characteristics, outlined herein, and the method of von Neumann and Richtmyer[2.38]. The variation of $\bar{u}_s$ as a function of $\bar{x}_s$ was calculated for all combinations of chamberage equal to 1, 2, 5, and ∞, with various reservoir lengths, expressed as $G/m_s = 0.25$, 0.5, 1, 2, 5, and ∞, and for $\gamma = 1.1$, 1.4, and 1.67. The parameter G/m_s is the ratio of the mass of gas initially loaded in the reservoir to the projectile mass, and is related to the nondimensional reservoir length, as follows:

$$\frac{G}{m_s} = \frac{\rho_r A_r L_r}{m_s} = \gamma \frac{A_r}{A_s}\bar{L}_r . \tag{2.52}$$

A typical plot of Seigel's results, for $\gamma = 1.4$ and $G/m_s = 5$, is shown in Figure 2.13. When compared at equal values of G/m_s, the calculations indicate the following:

(1) During the early stages of motion of the projectile, $\bar{x}_s$ small, while only a few reflections of the acoustic waves have occurred between the reservoir and projectile, increased projectile velocities result from increased chamberage. The largest gains in velocity occur with the initial increases in chamberage; that is, beyond a value of chamberage of 4 ($A_r/A_s = 16$) only negligibly small additional increases in velocity may be obtained.

(2) As the expansion is allowed to proceed to larger values of $\bar{x}_s$, the effect of chamberage gradually diminishes, resulting ultimately in the same projectile velocity for all values of chamberage.

2.4 TWO-STAGE PISTON-COMPRESSION GUN

The simple single-stage gun described in Section 2.3, consisting of a reservoir of gas of constant volume, is not capable of providing the highest model velocities frequently required. Even with an infinite size reservoir the projectile base pressure drops rapidly from its initial peak, as the model accelerates (as seen in Figure 2.7), so that the average base pressure is, for many cases, too low to yield the desired velocity. Further, the models to be launched are often of complex shapes or are composites of several materials, encased for support in in a multiple piece carrier (sabot), and hence are relatively fragile (see Chapter 3). Thus the allowable peak base pressure (equal to reservoir pressure, p_r, in this case) is often limited by model strength and may be very much lower than the strength capability of the reservoir. The decrease in base pressure caused by the expansion of the propellant gas can, in principle, be counteracted by the addition of energy to the gas after start of model motion. The reservoir pressure, if initially limited by the strength of the model, may then be increased progressively until the reservoir strength is reached, in a manner to give a more uniform pressure history at the base of the projectile. In a single-stage gun, the energy can be augmented by electrical means, using an arc discharge (Refs. 2.39 to 2.42), or by chemical means, using combustible gases or explosives (Refs. 2.43 to 2.46).

The addition of energy to the propellant gas during the time that the model is being launched can be effectively accomplished with a two-stage light-gas gun, as sketched in Figure 2.14. The two-stage gun has two gas

chambers: energized gas in the first stage compresses the light propellant in the second stage, which in turn accelerates the projectile. In some cases the two gas regions are separated only by a diaphragm, and the second-stage propellant gas is compressed and heated, as in a shock tube, by shock waves generated as the first-stage gas expands into the second stage. However, for the conditions required in a high-performance launcher, a more effective transfer of energy is made between the first and second stages by means of a free piston. Compressed helium (see Reference 2.47) or combustible mixtures of hydrogen and oxygen with helium (see References 2.21 and 2.48) have been used as first-stage driver gases, but more generally the first-stage propellant is a gun powder gas. The operation of a typical two-stage gun, then, starts with the ignition and burning of a solid gunpowder propellant. The gas generated from this combustion drives the piston, which, in turn, compresses hydrogen or helium in the second stage to high pressures and temperatures. A diaphragm which serves to isolate the model from the light gas ruptures at some specified pressure and the model accelerates through the barrel or launch tube. The significant factor to be noted concerning the operation of the two-stage gun is that the compression or pumping process continues during a substantial part of the time that the model is being launched, adding energy to sustain the base pressure.

Two-stage piston-compression guns can be grouped into two general classes according to the manner in which the propellant gas is compressed and heated. In one type, the piston speed is low, and compression occurs nearly isentropically; in the other, the piston speed is high, and compression is accomplished by the strong shock waves which precede the piston. There are considerable differences in the pressure and temperature histories that occur with each type, as well as differences in gun geometry. A discussion of the relative merits of each type is presented in the following sections.

2.4.1 Isentropic-Compression Guns

When the second-stage propellant gas is compressed nearly isentropically (not considering viscous effects or heat transfer to the walls), the pressure in the reservoir rises smoothly and continuously, as shown in Figure 2.15. This is accomplished by driving the piston at a slow speed in relation to the gas sound speed so that strong shock waves are not formed, (see fluid-dynamics text, e.g., References 2.27 or 2.49). A reasonably smooth pressure rise during compression becomes important in launching models to high velocity when the pressure applied to the base of the model approaches the limit of the model's strength. In this case, large pressure jumps associated with strong shock waves can result in model failure.

The energy necessary to compress the propellant gas is provided by the kinetic energy of the "free" piston. With a low piston speed, a high piston mass is needed to provide the energy, so guns employing isentropic compression are sometimes referred to as "heavy-piston" guns.

The gas properties during compression are related to the initial properties by the following isentropic expressions:

$$\left(\frac{p}{p_o}\right) = \left(\frac{V_o}{V}\right)^{\gamma} = (\text{Comp. Ratio})^{\gamma} = \left(\frac{\rho}{\rho_o}\right)^{\gamma} = \left(\frac{T}{T_o}\right)^{\gamma/(\gamma-1)} = \left(\frac{a}{a_o}\right)^{2\gamma/(\gamma-1)} . \tag{2.53}$$

These relations are plotted in Figure 2.16. The high sound speeds required for high performance can be achieved with a large volume (high compression ratio) pump tube. Sound speeds and temperatures developed by compressing isentropically to an arbitrary pressure of 10 kilobars from a range of initial gas-loading pressures (representative of a large number of guns in current operation) are given in Figure 2.17.

2.4.2 Shock-Compression Guns

The method of heating a gas by shock compression has been used sucessfully in the operation of a number of two-stage guns. Typically, a light piston is accelerated by the first-stage driver gas to relatively high speeds, 1500 to 3000 m/s, to produce the desired strong shock waves in the second-stage propellant gas. The effect of piston speed on the pressure, density, and temperature ratios may be seen by examining the approximate relationships for a strong normal shock (i.e., $p_2/p_1 \gg 1$):

$$\frac{p_2}{p_1} \simeq \frac{\gamma(\gamma+1)}{2}\left(\frac{u_2}{a_1}\right)^2 , \tag{2.54}$$

$$\frac{\rho_2}{\rho_1} \simeq \frac{\gamma+1}{\gamma-1} , \tag{2.55}$$

$$\frac{T_2}{T_1} \simeq \left(\frac{\gamma-1}{\gamma+1}\right)\frac{p_2}{p_1} , \tag{2.56}$$

$$U_{shock} \simeq \left(\frac{\gamma+1}{2}\right)u_2 , \tag{2.57}$$

where U_{shock} denotes the shock speed, and subscripts 1 and 2 refer to the conditions ahead of and behind the shock, respectively. (For exact shock relations, see, for example, References 2.49 to 2.51.)

During operation of such a gun, the shock traveling at a speed up to approximately $(\gamma+1)/2$ times the piston speed, moves through the length of the pump tube, is reflected from the end of the pump, and travels rearward to be reflected by the piston. The shock may make several oscillations between piston and end of reservoir, further compressing and heating the gas. (Pressure, temperature, and density relations for multiple shock transits and reflections are given in Reference 2.52). Model motion begins upon rupture of a diaphragm separating the propellant gas from the model. Diaphragm rupture is generally designed to occur at the first or second shock reflection. During the time that the model is accelerated, the back and forth motion of the shock continues and may reflect from the base of the model several times, producing large and rapid pressure increases at the model base. A time-distance plot describing the motion of the piston, shock, and model is given in Figure 2.18. A plot of model base pressure during launch (Fig. 2.19) serves to show that the relatively violent shocking process exposes the model to large and rapid pressure fluctuations. Model damage may occur not only from the high peak pressures but also from the rapid rate of change in pressure which generates compressive and tensile stress waves within the model (see Reference 2.53).

Nonisentropic heating of the propellant gas yields higher temperatures than obtained by isentropic compression for the same increase in pressure. Baker[2.54] has shown that as an upper limit under ideal conditions a 30% increase in temperature is calculated for a piston velocity of 1800 m/s over that attained by isentropic compression to the same pressure. Real-gas effects, however, may reduce this gain. Stollery and Maull[2.55] show that for shock compression of air, real-gas effects will lower temperatures and increase the pressures so that if a comparison is made at equal final pressures, the temperature gained with a real gas will be significantly less than the ideal case.

The shock-compression gun has been widely used by a number of laboratories. A two-stage shock-compression gun described in Reference 2.56 uses a powder charge in a helium chamber for a first stage, with a light piston separating the first- and second-stage gases to transfer energy between the two stages. An example of such a gun used at Ames Research Center is shown in Figure 2.20.

In the combustion-driven shock-compressed light-gas gun, developed at the Naval Ordnance Laboratory (Ref. 2.21), the first-stage driver gas (helium) is energized by the combustion of a H_2–O_2 mixture. Expansion of the heated gas mixture upon rupture of a diaphragm separating the first and second stages, serves to shock compress and heat the second-stage propellant gas. (Other guns of this type are described in References 2.57 and 2.58.)

Further description of the design and performance of shock-heated light-gas guns, including analytical methods for computing velocity may be obtained from References 2.35, 2.41, and 2.58 to 2.63.

2.4.3 Comparison of Shock- and Isentropic-Compression Guns

The higher temperatures generated by shock-heating allow one to use a smaller-volume pump tube having a lower compression ratio than the isentropic gun. Further, the light piston used with the shock-heated gun provides some advantage in that the forces imposed on the high pressure end of the second stage, when the piston decelerates to rest, are generally less than the pressures resulting from deceleration of the heavy piston of the isentropic gun, making possible a somewhat simpler construction. The shock-compression gun, thus, may require less laboratory space and be more economical to construct and operate, but the difference need not be great.

On the other hand, it has been demonstrated through actual experience with both types and by analytical comparisons (see Lemcke, Reference 2.64) that the slow-piston isentropic gun has the capability of achieving higher model velocities. Temperatures as high as those achieved by shock heating can be attained isentropically, simply by increasing the size of the compressor to obtain a high compression ratio. The important advantage to be gained by isentropic compression is the more favorable pressure history at the base of the moving model, resulting generally in lower peak pressures (and more slowly varying pressures) imposed on the model to obtain comparable average base pressures. Thus, the model is subjected to lower stresses to obtain the same velocity. This means that fragile saboted models as well as rugged simple models can be launched to substantially higher velocities by a gun which has a more nearly isentropic mode of compression. Guns in present use are in many cases a compromise between the two types.

2.4.4 Two-Stage Isentropic-Compression Gun

From considerations given previously it was seen that it is desirable that the propellant gas be compressed isentropically. In the following section (2.4.5) it will also be seen that, ideally, the gas should be compressed in a manner which will result in a constant driving pressure at the base of the model throughout its full length of travel in the barrel. Although these requirements, strictly speaking, cannot be readily achieved, this has, however, become a widely accepted goal in the design and operation of laboratory model launchers. (In practice, a departure from constant base pressure operation is intentionally made to obtain higher velocities: the launch tube length is extended beyond that distance over which base pressures can be held relatively constant, to obtain an additional increment in velocity from further expansion of the gas to some low pressure at which the model acceleration becomes insignificant). The class of light-gas gun, in use currently, in which the compression process can be made to most closely approach the ideal conditions is the two-stage isentropic-compression gun, two types of which are described in the following discussion.

The first type of two-stage isentropic-compression gun is shown in Figure 2.21. (See, e.g., References 2.19, 2.39, and 2.62). The basic operation is that described in Section 2.4. A gunpowder propellant provides the energy to accelerate a relatively heavy piston to the required velocity to compress the light gas (in most cases, hydrogen). The piston generally reaches its maximum velocity at a time, or position in the pump tube, when the

second-stage pressure is still only a small fraction of the final value (at this time the expanding powder gas has dropped in pressure to about this same low value). Further compression of the hydrogen results from the kinetic energy of the piston, and thus the piston mass and velocity must be sufficient at this point to provide the energy required for compression. This gun has a square-ended or a relatively abrupt transition from the end of the pump to the breech of the launch tube. To prevent damage to this end a sufficient quantity of hydrogen must be loaded initially so that the piston will decelerate almost to rest when it reaches this point. To provide a buffer which will insure some margin of safety, a quantity of gas substantially larger than that necessary to launch the projectile must be used. This has the effect of lowering the compression ratio of the pump with the result that peak temperatures are reduced. This buffer may be eliminated by using an expandable transition section (see Reference 2.39), so that only the quantity of gas dictated by the launching requirements is needed. The expandable end section acts to stop the piston and is replaced after each firing.

Another type of two-stage isentropic gun presently in wide use is shown in Figure 2.22. The geometry of this gun, developed by Curtis[2.65], is similar to that of the gun previously discussed except for two important features: (1) the transition between pump tube and launch tube is made with a slender taper section (total included angle of taper generally between 6 and 16 degrees), and (2) the heavy piston is made of a deformable but relatively incompressible plastic such as polyethylene. During the compression cycle the piston enters the taper and starts to deform. The retarding forces imposed by the tapered wall as well as the rising gas pressure act to decelerate the piston to rest. These forces are frequently of approximately equal values. The piston comes to rest typically as its front face reaches the breech of the launch tube, although in some cases, with a relatively small mass of gas and high piston velocities, a portion of the piston may be driven into or even through the launch tube. If the transition section is sufficiently strong and massive there is relatively little damage incurred during each shot. A gradual deterioration occurs but usually many rounds may be fired before replacement is necessary. The taper, then, provides the means for stopping the piston without the need for any additional gas buffer, and only that quantity of gas required to launch the model is necessary. Thus, for a pump tube of given size, the tapered transition section enables one to maximize compression ratio in a manner that is not destructive to the gun. The slender taper also provides a gradual transition to give smoother flow. However, shock waves traveling through the pump tube are strengthened in the convergent taper (References 2.66 and 2.67). Additional shock waves may also be generated when the piston enters the taper. The front face of the piston must increase in velocity as it intrudes into the taper (the increase in velocity being inversely proportional to the change in area for an incompressible piston) and if the acceleration is great enough the compression waves generated will quickly coalesce into shock waves. These shock waves may serve to increase the model velocity but also produce the undesirable abrupt increases in base pressure.

Curtis suggests an additional factor that might result in increased model performance with the use of a slender taper. This is related to the fact that the front face of the piston increases in velocity as it traverses the taper, reaching much greater velocities than that portion of the piston in the constant diameter section of the pump. It is suggested the gas particles will be accelerated to sufficiently high velocities that the additional kinetic energy thus gained will add substantially to the total available energy, serving to lessen the ultimate pressure drop occurring between the reservoir and model. This effect will, of course, be greater with guns having relatively high piston speeds but may not be significant for guns having large values of chambrage that operate with very slow pistons.

The effects of gun geometry and variations in operating conditions on model performance with the deformable-piston isentropic-compression gun will be discussed in Section 2.5.

2.4.5 Ideal Isentropic Compression - Constant Base Pressure

In concept, or ideally, the maximum velocity that can be imparted to a particular model in a gun of fixed length results when the highest propellant pressure consistent with the steady-load strength characteristics of the model is maintained at the base of the model during the full launching time. In the sense of producing the highest possible performance, then, the application of a constant base pressure, resulting in uniform acceleration of the model for the full launch time, is regarded to be an ideal cycle for gun operation, and was first considered for use in a two-stage gun by Curtis[2.65], Charters[2.68], Wilenius[2.69], and Smith[2.70]. Subsequent extensions of these solutions and/or other considerations relating to the constant base-pressure cycle have been published in References 2.28, and 2.71 to 2.79. At this point we will not be concerned with the practical difficulties or limitations arising from application of this concept, such as the adverse dynamic effects (destructive shock waves in the model) which may occur with the sudden application of pressure to the base of the model at the start of the launching cycle. We wish to examine here the requirements for producing flow in a gun barrel that will maintain a constant pressure at the projectile base.

2.4.5.1 Gas Conditions for Uniform Acceleration in Unchambered Gun

To meet the requirements for constant pressure at the projectile base, the basic one-dimensional equations for unsteady flow (given in Section 2.3.2) must be satisfied:

Continuity Equation

$$\frac{\partial \rho}{\partial t} + \rho \frac{\partial u}{\partial x} + u \frac{\partial \rho}{\partial x} = 0 . \qquad (2.6)$$

Momentum Equation

$$\frac{\partial u}{\partial t} + u\frac{\partial u}{\partial x} + \frac{1}{\rho}\frac{\partial p}{\partial x} = 0 . \tag{2.7}$$

Stanyukovich[2.80] was the first to show that the assumption $u = u(t)$, that is, gas velocity is a function of time only rather than time and distance, leads to

$$u = \alpha t , \tag{2.58}$$

as an exact solution of Equations (2.6) and (2.7), which satisfies the imposed requirement that the pressure be constant on the surface of the projected body (for elaboration on this point and demonstration that the same conclusion is reached by other lines of reasoning, see References 2.28, 2.69, 2.70, and 2.74).

To visualize the physical consequences of Equation (2.58) in the operation of a gun consider a column of gas and projectile being uniformly accelerated in a barrel by a piston, as sketched in Figure 2.23. The pressure in the first layer of gas at the base of the projectile, p_s, is constant, and dependent only on the acceleration, α, and the projectile mass, m_s, since $p_s A_s = m_s \alpha$. Similarly, at any other layer in the gas the pressure is also constant (a different constant), since that layer must accelerate the mass of gas and projectile ahead of it. Hence, along any given particle path the pressure will be constant. There will be no relative motion of the gas particles in one part of the flow with respect to any other part, so no expansion or compression waves will be generated. In the Lagrangian coordinate system, then, the flow is steady and there is no change in velocity with respect to distance. Velocity is a function of time only.

For an Eulerian coordinate system with its origin $x = 0$ fixed at the barrel entrance, and with $t = 0$ when $x = 0$, the projectile motion in the gun barrel is simply defined by

$$u_s = \alpha t = \frac{p_s A_s}{m_s} t , \tag{2.59}$$

and

$$x_s = \frac{\alpha t^2}{2} = \frac{p_s A_s t^2}{2 m_s} = \frac{u_s^2}{2\alpha} . \tag{2.60}$$

The variation of enthalpy required for the constant base pressure solution is obtained by combining Equations (2.7) and (2.58) with the isentropic relation $dh = dp/\rho$, giving

$$h - h_s = \frac{\alpha^2 t^2}{2} - \alpha x , \tag{2.61}$$

where h_s is the initial enthalpy when $x = t = 0$, which is the enthalpy of the gas at the base of the projectile.

For an ideal gas subject to an isentropic process ($a^2 = \gamma p/\rho$ and $p\rho^{-\gamma} = \text{constant}$) Equation (2.61) becomes:

$$a^2 = a_s^2 + \left(\frac{\gamma - 1}{2}\right)\alpha^2 t^2 - (\gamma - 1)\,\alpha x . \tag{2.62}$$

(This equation, also, was first given by Stanyukovich[2.80].) The expressions for pressure, density, and temperature are then easily obtained by use of the isentropic relations for an ideal gas:

$$\left(\frac{a}{a_s}\right)^2 = \left(\frac{p}{p_s}\right)^{(\gamma-1)/\gamma} = \left(\frac{\rho}{\rho_s}\right)^{\gamma-1} = \frac{T}{T_s} . \tag{2.63}$$

Thus,

$$\frac{p}{p_s} = \left[1 + \left(\frac{\gamma - 1}{a_s^2}\right)\left(\frac{\alpha^2 t^2}{2} - \alpha x\right)\right]^{\gamma/(\gamma-1)} \tag{2.64}$$

and

$$\frac{\rho}{\rho_s} = \left[1 + \left(\frac{\gamma - 1}{a_s^2}\right)\left(\frac{\alpha^2 t^2}{2} - \alpha x\right)\right]^{1/(\gamma-1)} . \tag{2.65}$$

In this form it is readily seen that the gas conditions at any point depend only on the constants p_s, a_s, α, and γ, and on the distance from the point of interest to the projectile base, $x_s - x$ (since $\frac{1}{2}\alpha^2 t^2 - \alpha x = \alpha(x_s - x)$). The gas conditions are invariant with time *at a prescribed distance from the projectile base.* This is illustrated in the sketch shown in Figure 2.24.

It is convenient to nondimensionalize Equations (2.62) to (2.65) by referring all the variables to the constant acceleration and the quantities at the base of the projectile. Thus,

$$\bar{p} = \frac{p}{p_s}, \quad \bar{\rho} = \frac{\rho}{\rho_s}, \quad \bar{T} = \frac{T}{T_s}, \quad \bar{a} = \frac{a}{a_s},$$

$$\bar{t} = \frac{\alpha t}{a_s}, \qquad \bar{x} = \frac{\alpha x}{a_s^2}, \qquad \bar{u} = \frac{u}{a_s} = \bar{t}. \tag{2.66}$$

Hence, Equations (2.62), (2.64), and (2.65) become:

$$\bar{a}^2 = \bar{T} = 1 + (\gamma - 1)\left(\frac{\bar{t}^2}{2} - \bar{x}\right), \tag{2.67}$$

$$\bar{p} = \left[1 + (\gamma - 1)\left(\frac{\bar{t}^2}{2} - \bar{x}\right)\right]^{\gamma/(\gamma-1)}, \tag{2.68}$$

and

$$\bar{\rho} = \left[1 + (\gamma - 1)\left(\frac{\bar{t}^2}{2} - \bar{x}\right)\right]^{1/(\gamma-1)}. \tag{2.69}$$

These, then, express the manner in which the gas properties must vary along the length of the gas column behind the projectile in order to maintain a constant pressure at the base of the projectile.

Using the subscript e to denote the conditions at the entrance to the gun barrel, that is, for the position in the barrel where $x = \bar{x} = 0$, the preceding equations become:

$$\bar{a}_e^2 = \bar{T}_e = 1 + \left(\frac{\gamma - 1}{2}\right)\bar{t}_e^2, \tag{2.70}$$

$$\bar{p}_e = \left[1 + \left(\frac{\gamma - 1}{2}\right)\bar{t}_e^2\right]^{\gamma/(\gamma-1)}, \tag{2.71}$$

$$\bar{\rho}_e = \left[1 + \left(\frac{\gamma - 1}{2}\right)\bar{t}_e^2\right]^{1/(\gamma-1)}. \tag{2.72}$$

These relationships are shown in Figure 2.25, for both hydrogen and helium. It is seen that the pressure, p_e, must increase, at an ever-increasing rate, as the projectile traverses the barrel. The total length of travel over which constant acceleration is possible, then, is limited by the maximum pressure that can be withstood by the barrel. To maximize this length the pressure ratio must be minimized. Since $\bar{t}_e = \alpha t_e / a_s$, increasing the sound speed of the gas at the projectile base will result in lower required pressures as a function of time, for the same α and γ. Also, in the limit as $\gamma \to 1$, $p_e = e^{\bar{t}_e^2/2}$, which indicates that for values of $\bar{t}_e$ up to approximately 2.1 the pressure ratio required is minimized by minimizing γ. The desirability of maximizing the sound speed and minimizing the specific heat ratio is thus the same conclusion indicated in the analysis of isentropic expansion of a gas from a fixed reservoir.

It is of interest now to examine the equations of the characteristic lines for the case of uniform acceleration flow. As shown in Section 2.3.2, Equations (2.6) and (2.7) can be rewritten in the form

$$\frac{\partial}{\partial t}(u \pm \sigma) + (u \pm a)\frac{\partial}{\partial x}(u \pm \sigma) = 0, \tag{2.11 and 2.12}$$

where the Riemann invariants $u \pm \sigma$ are functions which remain constant along characteristic lines having slopes $dx/dt = u \pm a$, respectively. The equations for the characteristic lines, both for Eulerian and Lagrangian coordinate systems, have been derived and extensively discussed for uniform acceleration of ideal gases in References 2.28, 2.71, and 2.73. Herein, we will consider only the equations in the Eulerian coordinates.

Equations (2.58) and (2.62) give the relations for u and a:

$$u = \alpha t, \tag{2.58}$$

$$a^2 = a_s^2 + \left(\frac{\gamma - 1}{2}\right)\alpha^2 t^2 - (\gamma - 1)\,\alpha x \quad . \tag{2.62}$$

From Equations (2.24) and (2.25) of Section 2.3.2 we have:

$$u \pm a = u \pm \frac{2a}{\gamma - 1} = \text{constant along a characteristic} \quad . \tag{2.73}$$

Since $u = 0$ when $t = 0$ (Eq.(2.58)), letting $t = 0$ in Equation (2.62) provides the convenient parameter:

$$a_o^2 = a_s^2 - (\gamma - 1)\,\alpha x_o \quad . \tag{2.74}$$

(Note: a_o is simply the local speed of sound at a point on any characteristic when $u = t = 0$ and $x = x_o$) . Thus,

$$x_o = \frac{a_s^2 - a_o^2}{\alpha(\gamma - 1)} , \tag{2.75}$$

from Equation (2.74), is the x coordinate at which the characteristic line intersects the x-axis . Equation (2.73) can then be written as:

$$\frac{\gamma - 1}{2}\,u \pm a = \pm a_o \quad , \tag{2.76}$$

or

$$\left(\frac{\gamma - 1}{2}\,u \pm a_o\right)^2 = a^2 \quad . \tag{2.77}$$

Substitution of Equations (2.58) and (2.62) in the equation (2.77), and nondimensionalizing the terms by Equations (2.66), gives

$$\bar{x} = \frac{\bar{t}^2}{2} - \frac{\gamma - 1}{4}\left[\left(\bar{t} \mp \frac{2\bar{a}_o}{\gamma - 1}\right)^2 - \frac{4}{(\gamma - 1)^2}\right] , \tag{2.78}$$

as the general expression for the net of characteristic lines (negative sign used for $u + a$ characteristic, positive sign for the $u - a$ characteristic). *All* the characteristic lines are *identical parabolas*, having their major axes parallel to the x-axis. The locus of their vertices is given by

$$\bar{t}_v^2 = \frac{2}{3 - \gamma}\left[1 - (\gamma - 1)\bar{x}_v\right] , \tag{2.79}$$

which is also a parabola. Since at the vertex of any characteristic line $d\bar{x}/d\bar{t} = 0 = u \pm a$, so $u = \mp a$ at this point, Equation (2.79) is the path along which the flow conditions are sonic. Thus, sonic conditions are attained at the projectile base (where $\bar{x} = \bar{t}^2/2$) when $\bar{t} = \bar{t}^* = 1$ and at the barrel entrance ($\bar{x} = 0$) when $\bar{t}^* = \sqrt{\{2/(3 - \gamma)\}}$.

Equation (2.73) might also be written as

$$\frac{\gamma - 1}{2}\,u \pm a = \frac{\gamma - 1}{2}\,u_s \pm a_s \quad , \tag{2.80}$$

relating the characteristic lines to the point at which they meet the projectile path. Substitution of Equations (2.58), (2.62), and (2.66) as before, leads to the equations noted on the characteristics net shown in Figure 2.26. The segments of the characteristic lines of interest are most easily calculated from these equations, which are simply different forms of Equation (2.78).

Referring to Figure 2.26, it is evident that the $u - a$ characteristic lines intersect the $\bar{t}$-axis at a positive slope for $\bar{t} > \sqrt{\{2/(3-\gamma)\}}$. Since $d\bar{x}/d\bar{t} = u - a$ on these lines, the positive slope indicates that $u > a$, or the flow velocity must become supersonic at the barrel entrance. Theoretically this is allowable for a constant diameter (unchambered) gun, but it cannot be realized physically in a gun having chamberage. In the latter case, the flow velocity at the entrance to the launch tube cannot exceed the sonic velocity, since the flow becomes "choked" by the area transition from reservoir to launch tube. Hence, the constant base pressure solution, presented in Figure 2.26, sometimes called the "similarity solution", applies for all values of time and distance only to the constant diameter (unchambered) gun.

2.4.5.2 Uniform Acceleration in Chambered Gun

For $\bar{t} < \sqrt{\{2/(3-\gamma)\}}$ the flow velocity at the barrel entrance is subsonic, and the reservoir conditions required to produce a constant-base-pressure flow are readily obtained by applying the quasi-steady continuity and energy equations (see Figure 2.27 for notation):

$$a_r^2 = \frac{\gamma - 1}{2} u_e^2 + a_e^2 , \tag{2.81}$$

or, nondimensionalized,

$$\bar{a}_r^2 = \frac{\gamma - 1}{2} \bar{u}_e^2 + \bar{a}_e^2 . \tag{2.82}$$

With $\bar{u}_e = \bar{t}_e$ from Equations (2.66) and $\bar{a}_e^2 = 1 + \frac{1}{2}(\gamma - 1)\,\bar{t}_e^2$ from Equation (2.70),

$$\bar{a}_r^2 = 1 + (\gamma - 1)\bar{t}_e^2 = \bar{T}_r . \tag{2.83}$$

Using the isentropic relations previously noted,

$$\bar{p}_r = \left[1 + (\gamma - 1)\bar{t}_e^2\right]^{\gamma/(\gamma-1)} , \tag{2.84}$$

$$\bar{\rho}_r = \left[1 + (\gamma - 1)\bar{t}_e^2\right]^{1/(\gamma-1)} . \tag{2.85}$$

Equations (2.83) to (2.85) then define the reservoir conditions required until sonic flow is reached at the barrel entrance, at which time

$$\bar{t}_e = \bar{t}_e^* = \sqrt{\left(\frac{2}{3-\gamma}\right)}, \qquad \bar{p}_e^* = \left(\frac{2}{3-\gamma}\right)^{\gamma/(\gamma-1)}$$

from Equation (2.71), and

$$\bar{p}_r^* = \left(\frac{\gamma + 1}{3 - \gamma}\right)^{\gamma/(\gamma-1)} ,$$

from Equation (2.83).

At this point it is of interest to define that $u - a$ characteristic line which has its vertex on the $\bar{t}$-axis, that is, with $\bar{x}_v = 0$. This line is known as the "limiting characteristic" of the similarity solution on which sonic flow is reached at the barrel entrance. Substituting $\bar{x} = 0$ and $\bar{t} = \sqrt{\{2/(3-\gamma)\}}$ in Equation (2.78), one obtains $\bar{a}_o = \sqrt{\{(3-\gamma)/2\}}$. Using this value of $\bar{a}_o$ in Equation (2.78) then yields

$$\bar{x} = \tfrac{1}{2}\left[\sqrt{\left(\frac{3-\gamma}{2}\right)}\,\bar{t} - 1\right]^2 , \tag{2.86}$$

as the equation for the limiting characteristic. This is also shown in Figure 2.26.

Now for $\bar{t} > \sqrt{\{2/(3-\gamma)\}}$, the flow velocity at the barrel entrance must remain sonic ($\bar{u}_e = \bar{a}_e = \bar{t}_e$); hence, in the region between $\bar{x} = 0$ and the limiting characteristic, the $u - a$ characteristics are no longer parabolas and must become tangent to the $\bar{t}$-axis, as shown in Figure 2.28. However, as shown in References 2.71 and 2.28, the paths of the $u + a$ characteristics in this region, along the segment A - B in the sketch, may be assumed to be the same as those for an unchambered gun, at least in that portion of the region which can influence the conditions at the base of the projectile. (It has been verified by comparison with exact methods such as that of Reference 2.75 for $\gamma = 5/3$ (see also Reference 2.77) that this assumption results in negligible errors).

Again, along a $u + a$ characteristic, $u + \sigma$ is constant, so

$$u_e + \sigma_e = u_s + \sigma_s , \tag{2.87}$$

and thus for sonic flow at barrel entrance,

$$a_e + \frac{2}{\gamma - 1} a_e = at_s + \frac{2}{\gamma - 1} a_s , \tag{2.88}$$

or in nondimensional terms, using Equations (2.66),

$$\bar{a}_e^2 = \left[\frac{\gamma - 1}{\gamma + 1}\left(\bar{t}_s + \frac{2}{\gamma - 1}\right)\right]^2 . \tag{2.89}$$

The more general expression,

$$u + \sigma = u_s + \sigma_s , \tag{2.90}$$

gives:

$$\frac{\gamma - 1}{2}\,\bar{u} + \bar{a} = \frac{\gamma - 1}{2}\,\bar{u}_s + 1 . \tag{2.91}$$

Then, from Equations (2.66) and (2.67),

$$\frac{\gamma - 1}{2}\,\bar{t} + \left[1 + \frac{\gamma - 1}{2}\left(\bar{t}^2 - 2\bar{x}\right)\right]^{1/2} = \frac{\gamma - 1}{2}\,\bar{t}_s + 1 . \tag{2.92}$$

At $\bar{x} = 0$, $\bar{t} = \bar{t}_e$, and the above equation becomes

$$\bar{t}_s = \bar{t}_e + \frac{2}{\gamma - 1}\left[\left(1 + \frac{\gamma - 1}{2}\,\bar{t}_e^2\right)^{1/2} - 1\right] . \tag{2.93}$$

Substitution of this equation into Equation (2.89) gives

$$\bar{a}_e^2 = \left\{\frac{2}{\gamma + 1}\left[\frac{\gamma - 1}{2}\,\bar{t}_e + \left(1 + \frac{\gamma - 1}{2}\,\bar{t}_e^2\right)^{1/2}\right]\right\}^2 = \bar{T}_e , \tag{2.94}$$

$$\bar{p}_e = \left\{\frac{2}{\gamma + 1}\left[\frac{\gamma - 1}{2}\,\bar{t}_e + \left(1 + \frac{\gamma - 1}{2}\,\bar{t}_e^2\right)^{1/2}\right]\right\}^{2\gamma/(\gamma-1)} , \tag{2.95}$$

$$\bar{\rho}_e = \left\{\frac{2}{\gamma + 1}\left[\frac{\gamma - 1}{2}\,\bar{t}_e + \left(1 + \frac{\gamma - 1}{2}\,\bar{t}_e^2\right)^{1/2}\right]\right\}^{2/(\gamma-1)} . \tag{2.96}$$

From Equation (2.82), with $\bar{u}_e = \bar{a}_e$,

$$\bar{a}_r^2 = \frac{\gamma + 1}{2}\,\bar{a}_e^2 . \tag{2.97}$$

so, from Equation (2.94),

$$\bar{a}_r^2 = \left\{\left[\frac{2}{\gamma + 1}\right]^{1/2}\left[\frac{\gamma - 1}{2}\,\bar{t}_e + \left(1 + \frac{\gamma - 1}{2}\,\bar{t}_e^2\right)^{1/2}\right]\right\}^2 = \bar{T}_r , \tag{2.98}$$

$$\bar{p}_r = \left\{\left[\frac{2}{\gamma + 1}\right]^{1/2}\left[\frac{\gamma - 1}{2}\,\bar{t}_e + \left(1 + \frac{\gamma - 1}{2}\,\bar{t}_e^2\right)^{1/2}\right]\right\}^{2\gamma/(\gamma-1)} , \tag{2.99}$$

$$\bar{\rho}_r = \left\{\left[\frac{2}{\gamma + 1}\right]^{1/2}\left[\frac{\gamma - 1}{2}\,\bar{t}_e + \left(1 + \frac{\gamma - 1}{2}\,\bar{t}_e^2\right)^{1/2}\right]\right\}^{2/(\gamma-1)} . \tag{2.100}$$

Equations (2.94 - 2.96) and (2.98 - 2.100) thus define the gas conditions required at the barrel entrance (sonic flow) and in the reservoir, as a function of time ($\bar{t}_e > \sqrt{\{2/(3 - \gamma)\}}$) at the barrel entrance, to produce a uniformly accelerated flow of an ideal gas in a chambered gun. The pressure-time histories, from Equations (2.71) and (2.95) for $\bar{p}_e$, and Equations (2.84) and (2.99) for $\bar{p}_r$, are shown in Figure 2.29 for both hydrogen and helium. The symbols on this figure indicate the time at which sonic flow is reached at the barrel entrance.

Comparison of Figures 2.25 and 2.29 indicates that the pressures required at the barrel entrance ($\bar{p}_e$) of a chambered gun, due to the restriction to sonic flow at this point, are much higher, at times, $\bar{t}_e > \sqrt{\{2/(3 - \gamma)\}}$, than those for a gun with no chamberage.

2.4.6 Constant Base Pressure with Real-Gas Effects

All the solutions presented thus far have been based on the assumption that the gas is ideal and its properties can be related by the simple equation of state $pv = RT$ and the isentropic equation $pv^\gamma = \text{constant}$. These equations adequately predict the behavior of the gas for a certain range of temperatures and densities, within which

there is no change in the number of particles constituting the gas or in the number of degrees of freedon of motion of the particles, and no significant intermolecular forces (either attractive or repulsive) acting between particles because of their proximity to one another. If, however, the process to which the propellant is subjected results in sufficiently high temperatures and/or densities as is usual in the operation of high performance light-gas guns, the foregoing conditions no longer exist; the gas no longer behaves in accordance with the ideal-gas relations, and is said to exhibit nonidealities or to act as a real gas. These effects must be taken into account to predict accurately the performance of a given gun. Unfortunately, little experimental knowledge exists of the actual state properties of hydrogen at these elevated temperatures and densities. However, a number of estimates have been made of the behavior of hydrogen gas at high densities, and the effect of this behavior on gun performance. Several of these will be discussed in the following paragraphs.

One state equation often used in considering real-gas effects is the Able-Noble, or "covolume", equation,

$$p(v - b) = RT , \tag{2.101}$$

where the term b is a correction to the specific volume which accounts for the effective volume occupied by the gas molecules themselves, or in another sense, for the repulsive intermolecular forces occurring when the gas is at high densities. The Able-Noble equation is a reduced form of Van der Waal's equation of state

$$p = \frac{RT}{v - b} - \frac{a}{v^2} , \tag{2.102}$$

with the term containing the intermolecular attractive-force constant "a" considered to be negligible. The relation between p and v along an isentrope for this gas is

$$p(v - b)^{\gamma} = \text{constant} , \tag{2.103}$$

where the constant is a function only of the entropy. The sound speed is given by

$$a^2 = \frac{\gamma p v^2}{v - b} . \tag{2.104}$$

Seigel[2.28] has compared the expansion of an Able-Noble gas with that of an ideal gas, in constant-diameter and chambered guns, for both infinite and finite reservoir lengths. It is shown that the expression for the acoustic impedance, as a function of p along an isentrope of an Able-Noble gas,

$$a\rho = \left[\frac{\gamma p_o^2}{RT_o}\left(\frac{p}{p_o}\right)^{(\gamma+1)/\gamma}\right]^{1/2} , \tag{2.105}$$

is identical to that of the ideal gas, and hence, *in a constant-diameter gun*, the pressure-velocity histories for the expansion of the two gases will be identical, if started from the same initial temperature and pressure. There will be no difference in performance, even in guns having finite length reservoirs, so long as the ratio of propellant gas mass to projectile mass (G/m_s) is the same for both gases. The corresponding expressions for the densities as a function of pressure along the isentrope are not the same, however, for the two gases. For an ideal gas

$$\rho = \frac{p_o}{RT_o}\left(\frac{p}{p_o}\right)^{1/\gamma} , \tag{2.106}$$

whereas for the Able-Noble gas

$$\rho = \frac{\dfrac{p_o}{RT_o}\left(\dfrac{p}{p_o}\right)^{1/\gamma}}{1 + \dfrac{bp_o}{RT_o}\left(\dfrac{p}{p_o}\right)^{1/\gamma}} . \tag{2.107}$$

(Note: Equations (2.105) and (2.107) are easily derived from Equations (2.101), (2.103), and (2.104).) It is readily seen that, because of the covolume term b, the density as a function of pressure of the Able-Noble gas will be lower than that of the ideal gas for an expansion from the same initial conditions. As noted previously in Section 2.3.3.3, it is a low density as a function of pressure rather than a low acoustic impedance as a function of pressure which determines the relative merit of gases expanding through the transition section of a chambered gun. Hence, *in a chambered gun*, the pressure-velocity history of the expansion of an Able-Noble gas will be superior to that of the ideal gas. The performance of a chambered gun using a dense real gas in an effectively infinite-length reservoir will be better than that for an ideal gas, assuming both expansions proceed from the same initial conditions of pressure, temperature, and mass of gas.

Smith[2.70] applied the Able-Noble state and isentropic equations to the constant base pressure solution for a chambered gun. He observed that the sound speed of the Able-Noble gas is increased over that of the ideal gas when the molecular volume becomes significant (see Equation (2.104)), and hence that, when the initial propellant density is high, it is possible that sonic flow will not be attained at the barrel entrance for the real gas. His calculations show that in a chambered gun the real gas not only yields higher velocities, as compared to those produced using the same mass of ideal gas, but does so with lower required pressures in the reservoir and at the barrel entrance.

Another approximation for the behavior of dense real gases uses a semi-empirical entropic equation given below, which was first proposed by Seigel[2.81] as the following:

$$p^{(\beta-2)/\beta}\,(v - f) = k\,. \tag{2.108}$$

This equation has been fitted, in Reference 2.81, to match real-gas data for nitrogen and argon at high densities, and, in Reference 2.82, to match calculated data for real hydrogen at pressures up to 30.4 kilobars and temperatures up to 3500° K. The data of Reference 2.82 consists of an extrapolation of experimental data at lower densities obtained by Wooley, et al.[2.83]. This real gas data will be considered in some detail below. More recently calculations of hydrogen properties have been made by Baker, et al.[2.84] using a Rowlinson equation of state which accounts for molecular volume and two body intermolecular forces. The results, given in tabular form for densities from 1 to 2000 amagats and temperatures from 500 to 3000° K, are reported to be in close agreement with that of Reference 2.82 except at the highest densities.

In the following analysis of the effects of a real gas on the constant base pressure solution the real gas relations of Reference 2.80 will be considered. The quantities β, f, and k in Equation (2.108) are constants along a given isentrope, but vary as the entropy is changed. It is convenient to nondimentionalize Equation (2.108) by referring the variables to the ambient condition $T_a = 300^\circ$ K and $p_a = 1.013$ bars. Thus,

$$\frac{p}{p_a}^{(\beta-2)/\beta}\left(\frac{v}{v_a} - \frac{f}{v_a}\right) = \frac{k}{p_a^{(\beta-2)/\beta}\,v_a}\,. \tag{2.109}$$

If p in the above equation is chosen as $p = p_{ro}$, the pressure in the gas when it is expanded isentropically to rest at a temperature of 300° K, then the complete real hydrogen gas behavior is defined as a function of entropy by the data of Figures 2.30 and 2.31. The resulting pressure-volume diagram is shown in Figure 2.32, and a comparison of the real- and ideal-gas isentropes is presented in Figure 2.33. It may be noted that for compression to a given final pressure a higher specific volume (with a correspondingly lower temperature) is realized with real hydrogen.

The following equations are easily derived for the relation between p and v given by Equation (2.108):

Sound speed

$$a^2 = \left(\frac{\partial p}{\partial \rho}\right)_s = \frac{\beta}{\beta - 2}\,p\,\frac{v^2}{v^2 - f}\,, \tag{2.110}$$

Enthalpy

$$h - h_s = \int_{p_s}^{p}\left(\frac{dp}{\rho}\right)_s = \frac{\beta}{2}kp^{2/\beta} + fp - \left[\frac{\beta}{2}kp_s^{2/\beta} + fp_s\right], \tag{2.111}$$

Riemann function

$$\sigma = \int_0^p\left(\frac{dp}{\rho a}\right)_s = \{k\beta(\beta - 2)\}^{\frac{1}{2}}\,p^{1/\beta}\,, \tag{2.112}$$

So

$$\frac{\sigma}{\sigma_s} = \left(\frac{p}{p_s}\right)^{1/\beta}\,. \tag{2.113}$$

The foregoing equations have been applied to the constant base pressure solution (previously discussed in Section 2.4.5) in References 2.78 and 2.79. The derivation proceeds in the same manner as that shown for the ideal gas; hence, it will only be outlined here. Because of the change in the state equation, it is convenient to nondimensionalize some of the terms in a different fashion. Except for the following, the notation and nondimensional forms are as used previously for the ideal gas:

$$\left.\begin{aligned} \bar{x} &= \frac{p_s A_s}{m_s c_s^2}\, x \\ \bar{t} &= \frac{p_s A_s}{m_s c_s}\, t \\ \bar{u} &= \frac{u}{c_s}, \qquad \bar{a} = \frac{a}{c_s} \end{aligned}\right\} \quad \text{where} \quad c_s = \frac{(\beta - 2)a_s}{F + 1} \quad \text{and} \quad F = \frac{f}{v_a - f}. \tag{2.114}$$

For the real gas,

$$h_e - h_s = \frac{c_s \bar{t}_e^2}{2}, \tag{2.115}$$

and, with

$$\bar{u}_e = \bar{u}_e^\star = \bar{a}_e^\star = \bar{t}_e^\star, \tag{2.116}$$

when sonic conditions are attained at the barrel entrance, the equations providing the corresponding pressure and time are:

$$\bar{p}_e^{\star 2/\beta}\left[\bar{p}_e^{\star 2/\beta} - 1 + \frac{2F}{\beta}(\bar{p}_e^\star - 1)\right] = \frac{1}{\beta - 2}\left(F\bar{p}_e^\star + \bar{p}_e^{\star 2/\beta}\right)^2. \tag{2.117}$$

$$\bar{t}_e^\star = \frac{1}{\beta - 2}\bar{p}_e^{\star -1/\beta}\left(F\bar{p}_e^\star + \bar{p}_e^{\star 2/\beta}\right), \tag{2.118}$$

Note that $\bar{p}_e^\star$ and $\bar{t}_e^\star$ are functions of β and F, which depend on the entropy of the gas at the initial conditions. The manner in which $\bar{p}_e^\star$ and $\bar{t}_e^\star$ vary with projectile base pressure, for various initial reservoir pressures (p_{r_0} is also a function of entropy, Figure 2.30), is shown in Figure 2.34. The effects of the real gas are quite startling. Whereas $\bar{p}_e^\star$ and $\bar{t}_e^\star$ are constant values depending on γ for an ideal gas ($\bar{p}_e^\star = 2.18$, $\bar{t}_e^\star = 0.224$ for $\gamma = 1.4$), it is seen that for many combinations of initial reservoir pressure and projectile base pressure the constant base pressure solution for real hydrogen gas indicates that sonic conditions may be attained at the barrel entrance at two different pressures and times. This implies that in a constant diameter gun the flow at the barrel entrance may first accelerate to sonic conditions at one value of $\bar{p}_e^\star$ and $\bar{t}_e^\star$, then continue to accelerate to supersonic velocities, and because of the manner in which the sound speed varies, the flow subsequently reaches a *different* sonic condition at another value of $\bar{p}_e^\star$ and $\bar{t}_e^\star$. Moreover, for some values of initial reservoir pressure there is a maximum value of projectile base pressure which will produce sonic conditions at the barrel entrance. For any base pressure greater than this maximum, at these initial reservoir pressures, the flow at the barrel entrance will remain subsonic at all times, and thus can be completely defined, even for a chambered gun, by the "similarity" solution $u = \alpha t$.

The general equation for the characteristic lines for the real hydrogen gas, constant-base-pressure solution is

$$\bar{x} = \frac{\bar{t}^2}{2} - \frac{1}{\beta(\beta - 2)}\left\{\frac{\beta}{2}\left[(C \mp \bar{t})^2 - 1\right] + F\left[(C \mp \bar{t})^\beta - 1\right]\right\}, \tag{2.119}$$

where C is a constant, but a different value for each characteristic. As in the ideal-gas solution, this relationship applies at all times in the constant diameter gun, and at times less than $\bar{t}_e^\star$ in the chambered gun. Bixler and Seigel[2.79] have calculated the characteristic diagrams for flow in the constant diameter gun; these are compared with the ideal-gas solution in Figure 2.35. Again the real-gas effects produce startling results. The lines on which $u - \sigma$ is a constant, and $dx/dt = u - a$, in particular, are greatly changed in comparison with the ideal-gas characteristics, reversing direction twice and ultimately proceeding in a direction opposite to that for the ideal-gas characteristics. In accord with the discussion of the previous paragraph, there are two $u - a$ characteristics in Figure 2.35(b) having tangency points with the $\bar{x} = 0$ axis, corresponding to the two conditions for sonic flow at the barrel entrance when the initial reservoir pressure and projectile base pressure are appropriate. Similarly, as shown in Figure 2.35(c), when the base pressure exceeds that maximum value required to produce sonic flow at the barrel entrance for a given initial entropy, the $u - a$ lines have no tangency point along $\bar{x} = 0$ and all cross the $\bar{x}$-axis at a negative slope. Thus the flow at the barrel entrance in the latter case is subsonic at all times.

The equation for the real-hydrogen-gas pressure at the entrance to the barrel as a function of time, when the flow is not limited to sonic speed as for a constant diameter gun, is derived as

$$\bar{t}_e = \left\{\frac{2}{\beta(\beta - 2)}\left[\frac{\beta}{2}\left(\bar{p}_e^{\,2/\beta} - 1\right) + F\left(\bar{p}_e - 1\right)\right]\right\}^{1/2}. \tag{2.120}$$

For the chambered gun, in which sonic conditions at the barrel entrance are a necessary restriction, the same assumption is made regarding the path of the u + a characteristics as was made in the ideal-gas solution; namely, that they are the same, leading to the $\bar{p}_e - \bar{t}_e$ history for the real gas given by

$$\frac{\beta(\beta - 2)}{2} \bar{t}_e^2 = \frac{\beta}{2}\left[(\bar{t}_o - \bar{t}_e + 1)^2 - 1\right] + F\left[(\bar{t}_o - \bar{t}_e + 1)^\beta - 1\right], \tag{2.121}$$

where

$$\bar{t}_o = \frac{\bar{p}_e^{1/\beta}}{\beta - 2}\left(1 + F\bar{p}_e^{(\beta-2)/\beta}\right) + \bar{p}_e^{1/\beta} - 1 . \tag{2.122}$$

Similarly, consideration of the equations governing the expansion of the gas from the reservoir to barrel entrance leads to the following expressions for the required reservoir pressure as a function of time:

for the constant diameter gun,

$$\bar{t}_e = \left\{\frac{1}{\beta(\beta - 2)}\left[\frac{\beta}{2}(\bar{p}_r^{2/\beta} - 1) + F(\bar{p}_r - 1)\right]\right\}^{1/2} , \tag{2.123}$$

and for the chambered gun,

$$\frac{\beta}{2}\bar{p}_r^{2/\beta} + F\bar{p}_r = \frac{\beta}{2}\bar{p}_e^{2/\beta} + F\bar{p}_e + \frac{\beta}{2(\beta - 2)}\frac{(\bar{p}_e^{2/\beta} + F\bar{p}_e)^2}{\bar{p}_e^{2/\beta}} , \tag{2.124}$$

which must be solved in conjunction with Equations (2.121) and (2.122).

The foregoing equations have been solved by Bixler and Seigel for two values of projectile base pressure, 1.38 and 3.45 kilobars, over a range of initial reservoir pressure, and are compared with the ideal-gas solution in Figure 2.36. The effect of the real gas is to substantially reduce the differences between the pressure-histories required for the unchambered and chambered guns, both for $\bar{p}_e$ and $\bar{p}_r$. With increasing initial reservoir pressure (decreasing entropy) and model base pressure the solutions for the unchambered and chambered guns become, for all practical purposes, the same.

2.4.7 Piston Motion Required by Constant Base Pressure Solution

Having established in the preceding sections the required variation of pressure, density, and velocity with time (both at the entrance to the barrel and in the reservoir) for the constant base pressure solution, it is of interest to determine the pump piston motion necessary to satisfy these requirements. It should be noted that the constant-base-pressure solution does not consider the events occurring prior to the start of projectile motion at $t = 0$; it is assumed that the uniformly accelerated flow commences at time zero, with the desired gas conditions existant at the projectile base. This means that the gas conditions in the reservoir must also initially correspond to the desired base pressure conditions, requiring some form of compression or heating prior to this time. With the foregoing in mind, one may readily write the following relationships for piston motion for the ideal-gas case:

$$\begin{pmatrix}\text{Mass of gas}\\ \text{remaining in}\\ \text{reservoir at}\\ \text{time } t_e\end{pmatrix} = \begin{pmatrix}\text{Mass of gas}\\ \text{initially loaded}\\ \text{in reservoir}\end{pmatrix} - \begin{pmatrix}\text{Mass of gas}\\ \text{which was entered}\\ \text{barrel at}\\ \text{time } t_e\end{pmatrix}$$

or

$$\rho_r x_p A_r = \rho_s L_r A_r - \int_0^{t_e} \rho_e u_e A_s dt_e . \tag{2.125}$$

from which

$$\frac{x_p}{L_r} = \frac{\rho_s}{\rho_r}\left[1 - \frac{\int_0^{t_e} \rho_e u_e dt_e}{\rho_s \frac{A_r}{A_s} L_r}\right] , \tag{2.126}$$

where x_p is the distance between the front face of the piston and the end of the reservoir (or barrel entrance). Again nondimensionalizing terms, with

$$\left.\begin{aligned} \bar{x}_p &= \frac{p_s A_s x_p}{m_s a_s^2}, \qquad \bar{L}_r = \frac{p_s A_s L_r}{m_s a_s^2}, \qquad \bar{t}_e = \frac{p_s A_s}{m_s a_s} t_e, \\ \bar{\rho}_e &= \frac{\rho_e}{\rho_s}, \qquad \bar{u}_e = \frac{u_e}{a_s}, \qquad \bar{A}_r = \frac{A_r}{A_s}. \end{aligned}\right\} \tag{2.127}$$

So

$$\frac{\rho_s}{\rho_r} = \left(\frac{p_r}{p_s}\right)^{-1/\gamma} = \bar{p}_r^{-1/\gamma}, \tag{2.128}$$

and

$$\int_0^{t_e} \rho_e u_e dt_e = \frac{\gamma m_s}{A_s} \int_0^{\bar{t}_e} \bar{\rho}_e \bar{u}_e d\bar{t}_e, \tag{2.129}$$

and

$$\rho_s L_r = \frac{\gamma m_s}{A_s} \bar{L}_r. \tag{2.130}$$

Hence, Equation (2.126) becomes:

$$\frac{\bar{x}_p}{\bar{L}_r} = \bar{p}_r^{-1/\gamma} \left[1 - \frac{\int_0^{\bar{t}_e} \bar{\rho}_e \bar{u}_e d\bar{t}_e}{\bar{A}_r \bar{L}_r}\right], \tag{2.131}$$

where

$$\bar{A}_r \bar{L}_r = \frac{G}{\gamma m_s} = \bar{V}_{r_o} = \text{dimensionless initial reservoir volume (See Equation (2.52))}. \tag{2.132}$$

When $\bar{x}_p$ becomes 0, all of the gas in the reservoir will have entered the barrel; hence

$$\bar{V}_{r_o} = \int_0^{\bar{t}_{e_f}} \bar{\rho}_e \bar{u}_e d\bar{t}_e = \int_0^{\bar{t}_e^*} \bar{\rho}_e \bar{u}_e d\bar{t}_e + \int_{\bar{t}_e^*}^{\bar{t}_{e_f}} \bar{\rho}_e \bar{u}_e d\bar{t}_e, \tag{2.133}$$

where the first integral is for the subsonic portion of flow and the last integral is for sonic conditions at barrel entrance. That is:

For $0 < \bar{t}_e < \bar{t}_e^*$, the flow at the barrel entrance is subsonic; so $\bar{u}_e = \bar{t}_e$, and $\bar{\rho}_e$ is given by Equation (2.72).

For $\bar{t}_e^* < \bar{t}_e < \bar{t}_{e_f}$, the flow at the barrel entrance is sonic; so $\bar{u}_e = \bar{a}_e$ and is given by Equation (2.94), and $\bar{\rho}_e$ is given by Equation (2.96).

Also, $\bar{u}_s$ is related to $\bar{t}_{e_f}$ by Equation (2.93):

$$\bar{u}_s = \bar{t}_s = \bar{t}_{e_f} + \frac{2}{\gamma - 1}\left[\left(1 + \frac{\gamma - 1}{2}\bar{t}_{e_f}^2\right)^{1/2} - 1\right]. \tag{2.134}$$

Hence, Equation (2.133) becomes

$$\bar{V}_{r_o} = \int_0^{\bar{t}_e^*} \left[1 + \frac{\gamma - 1}{2}\bar{t}_e^2\right]^{1/(\gamma-1)} \bar{t}_e d\bar{t}_e + \int_{\bar{t}_e^*}^{\bar{t}_{e_f}} \left\{\frac{2}{\gamma + 1}\left[\frac{\gamma - 1}{2}\bar{t}_e + \left(1 + \frac{\gamma - 1}{2}\bar{t}_e^2\right)^{1/2}\right]\right\}^{(\gamma+1)/(\gamma-1)} d\bar{t}_e. \tag{2.135}$$

Equation (2.131) must also be evaluated in two steps, using $\bar{p}_r$ given by Equation (2.84) when $0 < \bar{t}_e < \bar{t}_e^*$, or Equation (2.99) when $\bar{t}_e^* < \bar{t}_e < \bar{t}_{e_f}$. Thus, for $0 < \bar{t}_e < \bar{t}_e^*$,

$$\frac{\bar{x}_p}{\bar{L}_r} = \left[1 + (\gamma - 1)\bar{t}_e^2\right]^{-1/(\gamma-1)} \left\{1 - \frac{1}{\bar{V}_{r_o}} \int_0^{\bar{t}_e} \left[1 + \frac{\gamma - 1}{2}\bar{t}_e^2\right]^{1/(\gamma-1)} \bar{t}_e d\bar{t}_e\right\}, \tag{2.136}$$

and for $\bar{t}_e^* < \bar{t}_e < \bar{t}_{e_f}$,

$$\frac{\bar{x}_p}{L_r} = \left\{\left[\frac{2}{\gamma+1}\right]^{1/2}\left[\frac{\gamma-1}{2}\bar{t}_e + \left(1+\frac{\gamma-1}{2}\bar{t}_e^2\right)^{1/2}\right]\right\}^{-2/(\gamma-1)}\left(1 - \frac{1}{\bar{V}_{r_o}}\int_0^{\bar{t}_e^*}\left[1+\frac{\gamma-1}{2}\bar{t}_e^2\right]^{1/(\gamma-1)}\bar{t}_e d\bar{t}_e\right.$$

$$\left. - \frac{1}{\bar{V}_{r_o}}\int_{\bar{t}_e^*}^{\bar{t}_e}\left\{\frac{2}{\gamma+1}\left[\frac{\gamma-1}{2}\bar{t}_e + \left(1+\frac{\gamma-1}{2}\bar{t}_e^2\right)^{1/2}\right]\right\}^{(\gamma+1)/(\gamma-1)} d\bar{t}_e\right). \qquad (2.137)$$

The pump-piston velocity-time history may then be obtained by differentiating Equations (2.136) and (2.137); that is,

$$\bar{u}_p = \frac{d\bar{x}_p}{d\bar{t}_e}. \qquad (2.138)$$

The authors are not aware that a complete solution of the above equations has yet appeared in the literature. Wilenius et al.[2,71] have presented an approximate solution in which only the first term of Equation (2.135) is integrated, with $\bar{t}_{ef}$ as the upper limit, to obtain $\bar{V}_{r_o}$, and only Equation (2.136) is solved (again with $\bar{t}_{ef}$ as the upper limit in the integral) to obtain the piston motion. From this the approximate base-pressure time history required for the pump piston was calculated using the relation

$$\bar{p}_b = \bar{p}_r - \frac{\bar{m}_p}{\bar{A}_r^2}\frac{d\bar{u}_p}{d\bar{t}_e}. \qquad (2.139)$$

While these are only approximate solutions, they are useful in illustrating qualitatively the following points concerning the achievement of a constant base pressure cycle of operation:

(1) In order that the base pressure be constant at the very beginning, the motion of the pump piston and projectile must commence simultaneously with both piston and projectile initially at rest. (This may be seen by differentiating Equation (2.136).)

(2) For an ideal gas, the maximum piston velocity is proportional to projectile velocity and is inversely dependent on the chamberage. When low chamberage ratios are used (e.g., less than diameter ratios of approximately 4), the maximum piston velocities become a very large fraction of the reservoir sound speed.

(3) Setting $\bar{x}_p = 0$ when all the reservoir gas has passed through the launch tube entrance (as assumed in the preceding derivation) requires that the pump piston have some final velocity (also strongly dependent on the chamberage) when it reaches the end of the reservoir.

(4) The base pressures required to drive the piston so as to produce the required piston motion are very high, almost as high as the reservoir pressure during the final stages of compression.

The preceding derivation of the piston motion has been shown, for simplicity, only for the ideal-gas case. A similar derivation can be made for the real-hydrogen-gas case, employing the relationships presented in Section 2.4.6. Although the magnitude of the piston velocities, accelerations, and base pressures would undoubtedly be different for the real- and ideal-gas cases, it is expected that the foregoing qualitative conclusions would remain unchanged.

It is apparent from the above requirements that constant-base-pressure flow cannot be precisely achieved but can only be approximated in the conventional two-stage free-piston gun. Smith's analysis[2,70] shows this quite clearly. He treats the mass-flow and reservoir-pressure requirements separately, and considers both the ideal gas and real (Able-Noble) hydrogen-gas cases. It is shown that matching of the mass-flow and pressure requirements in the later stages of the compression might be achieved by adjusting the mass of gas during compression. This can be accomplished in two ways, both of which start with an excess of gas in the reservoir. Either controlled leakage of some of the excess gas may be provided through bursting diaphragms in the reservoir or piston, or, portions of the excess gas may be progressively isolated (e.g., through ports which are subsequently covered by the piston) so as to remove it from the compression process. (This latter technique has also been studies by Winkler[2,74] in his analysis of the constant-base-pressure process.) However, in all cases shown by Smith, some mismatch between the mass-flow and pressure requirements must be accepted at the beginning of the launching cycle, even with later control of the gas mass.

In actual firings of present two-stage isentropic guns the ratios of maximum model base pressure to that pressure required for uniform acceleration (constant base pressure) to achieve the same velocity are frequently less than two when the guns are operated at conditions somewhat below maximum performance levels. However, at conditions used to obtain nearly maximum velocities this ratio may increase to values greater than five. The manner in which the individual variables can be adjusted to approach or approximate the constant-base-pressure process in conventional two-stage isentropic-compression guns is discussed more completely in Section 2.5.

2.4.8 General Computing Methods

Although the constant-base-pressure analyses may be applied to the selection of gun geometry and operating conditions in an effort to approach this desirable mode of operation, these analyses cannot be used to predict

actual gun performance when conditions deviate from the ideal, as is usually the case. Some general solution is necessary to predict performance over a wide range of gun geometries and loading conditions. A number of approximate methods have been developed (see, for example, References 2.19 and 2.28) which involve the numerical solution of a set of simultaneous equations using only a desk calculator. Predicted velocities compare well with experimental results at modest levels of performance, but these methods are limited to relatively low-performance levels and do not give necessary detailed information such as pressure histories. More accurate methods have been developed in which the nonlinear ordinary and partial differential equations of motion are numerically integrated by a high-speed digital computer.

Solutions may be readily obtained in this manner by writing the general equations in finite-difference form. The numerical scheme most widely used is based on the "q" method developed by von Neumann-Richtmyer (References 2.38 and 2.85). The quasi-one-dimensional hydrodynamic equations, valid within limits for changes in cross-sectional area, are most generally written in Lagrangian coordinates. The gun is divided into regions which may consist of the first-stage driver gas, piston, propellant gas, and model, each having a different equation of state. Each region is divided into a number of cells and mass points; the accuracy of this method is dependent, in part, on the number of cells chosen. The solution consists of numerical integration of the fluid dynamic equations over small intervals of time to determine the changes in pressure, density, internal energy, and velocity in each cell resulting from the influence of adjacent cells. The motion of these fluid elements and mass points, calculated with Newton's equation of motion, is determined by the pressure difference between adjacent cells. Stability requirements for the finite difference terms are given in Reference 2.85. An artificial viscosity term q (from which the "q" method derives its name) is added to the pressure term in the conservation equations and has the effect of spreading out the discontinuity at a shock wave to make the calculated variables continuous through the shock. An important feature of this method is that the presence and position of any shocks are known at each time interval and the overall effects of any shocks on the resulting performance are accounted for.

Equations for a two-stage gun analysis using the "q" method in Lagrangian coordinates are described by Piacesi, et al.[2.86] and Baer and Smith[2.87]. With numerical solutions of this type a real-gas equation of state can be used for the propellant gas, and estimates of the effects of friction and heat losses may also be readily included. A real-gas equation of state is used in Reference 2.78, which also includes calculations of friction and heat-transfer losses from an ideal gas to the gun walls. The "q" method computer program developed at the Naval Ordnance Laboratory has also been modified at Arnold Engineering and Development Center to include the effects of real gas, boundary layers, heat transfer, and piston friction. As shown in Reference 2.88, this program gives good results in comparison with experimental measurements. A numerical solution with equations written in Eulerian coordinates has been developed by Badhwar and Murphy[2.89, 2.90], with finite-differencing techniques given by Longley[2.91].

Digital machine programs have also been developed for analysis of the general two-stage gun problem using the method of characteristics. This method is readily adaptable to numerical solution with a digital computer for the case of isentropic flow of an ideal gas with friction and heat-transfer losses neglected. The use of this technique at Ames Research Center has provided results with good accuracy for isentropic-compression guns at velocities up to approximately 7.5 km/s. At higher levels of performance this particular program is inadequate, as are other methods which do not consider real-gas effects and losses.

When strong shocks must be considered, the method of characteristics becomes considerably more complex, although solutions can be obtained with the use of a third characteristic direction representing particle paths along which the entropy is constant (see Reference 2.27). A solution which might be adapted to the two-stage gun to handle shock waves is given in Reference 2.92.

2.5 ACTUAL GUN PERFORMANCE AND OPERATION

To aid in understanding the complex flow processes that occur during the operation of a light-gas gun so that performance can be optimized, it is expedient to explore, in a systematic manner, the many variables that influence performance. Virtually every ballistic-range laboratory has developed theoretical methods for this purpose. In most cases, the theories are based on ideal-gas relations and do not consider the various loss mechanisms such as fluid friction and heat transfer. These theories satisfactorily predict model velocities over a rather wide range of operating conditions, but, as the higher levels of performance are approached, where gas densities and temperatures rise to high values, the disparity between theory and the performance actually obtained becomes increasingly great. In some cases the results obtained experimentally actually contradict these theoretical predictions. To predict performance adequately under these conditions, real-gas effects and losses must be considered. More comprehensive theoretical treatments are being developed (see, for example, Seigel et al.[2.78] and Cable and DeWitt[2.88]) but, because of the complexity of the viscous flow processes and the lack of experimental data on the properties of hydrogen at high densities and temperatures, uncertainties exist which must be assessed experimentally.

Although extensive experimental studies have been made to determine the actual capabilities of light-gas guns, it would be an exceedingly ambitious task to attempt to optimize conditions experimentally for a wide range of velocities and model weights because of the interrelated effects of the large number of variables in gun geometry and loading conditions. These experimental studies have been of great value, however, in revealing, at the least, the basic trends of changes in variables, especially where the validity of theoretical predictions is uncertain. These efforts are aimed at obtaining a better understanding of the gas dynamics to aid in the final development of accurate computational methods.

A portion of the results of a systematic experimental study is presented in the following sections to illustrate the manner in which individual changes in the variables influence performance. The effects of changes in loading conditions for a two-stage isentropic-compression gun are given in Section 2.5.2 and changes in gun geometry are discussed in Section 2.5.3. The types of experimental measurements frequently made to determine gun performance are mentioned briefly in the following section.

2.5.1 Experimental Measurements

Measurements of maximum pressures generated in the first-stage driver gas are generally made to insure that the strength capabilities of the chamber are not exceeded. If gunpowder is used in the first stage, a time history of the chamber pressure is desirable to make certain that proper burning of the charge takes place. Pressure measurements are made most frequently with commercially available piezo-electric gages or with ballistic strain gages (for an example of the latter, see Reference 2.93).

Piston velocity, a primary factor in gun performance, is measured by means of simple wire probes inserted into the pump-tube bore at several positions along the length of the pump tube. A time measurement is obtained with electronic chronographs, as the electric probes are shorted by passage of the piston. Piston velocities given with the experimental data in the subsequent sections were obtained at a point somewhat before the start of the transition section, where the piston is near its peak velocity.

A time-resolved measurement of the reservoir gas pressure made at the point where the pressure becomes a maximum provides very important information for interior ballistic studies. Unfortunately this measurement is difficult to make with the use of standard gaging techniques without substantially reducing the strength of the gun in this critical area. Location of a pressure gage in the launch tube near the breech provides a convenient alternate position. The experimental data presented here do not include this measurement.

Perhaps the most meaningful diagnostic information is that obtained by measuring the position-time history of the projectile as it is being accelerated through the launch tube. This can be accomplished with a microwave reflectometer (see Chapter 10). With this information one can deduce the model acceleration-time history and thus obtain the resultant driving force acting on the model. If the friction between model and the wall of the barrel is neglected (a reasonable assumption for the plastic projectiles used) and if the barrel ahead of the model is evacuated, we then have a measure of the gas pressure acting on the model base throughout its travel in the barrel. One can then attempt to optimize loading conditions toward a constant base pressure. The measured base pressure history also provides additional important data with which to evaluate theoretical predictions. Comparison of measured muzzle velocities obtained in flight after launch with computed velocities is not sufficient to determine the accuracy of a theory. The final velocity is an integrated parameter of driving pressure and distance, and even though the calculated muzzle velocity may compare well with that measured, the pressure history (including maximum pressure) may be quite different. The model base pressure data presented in the following section were obtained by this microwave reflectometer technique as outlined in Reference 2.94.

Velocities are measured along the model trajectory from the muzzle of the gun. Most frequently this velocity is obtained by the standard techniques employing spark photography to measure distance and electronic chronographs to measure time (Chapter 6). To obtain an accurate value of muzzle velocity it is frequently necessary to account for the deceleration of the model occurring between the muzzle and the measurement stations.

Because of its ready accessibility to the authors, much of the experimental information presented herein was obtained with the Ames 7.1-, 25.4-, and 38.1-mm-bore-diameter guns, which are representative of the deformable-piston isentropic-compression gun. The dimensions of these guns, given in Table 2.2, are not considered to be optimum but are presented as examples of existing guns.

2.5.2 Effect of Loading Conditions

For any particular gun of fixed geometry the operating parameters or loading conditions that may be adjusted to achieve a desired velocity include:

1. Initial gas conditions
2. Piston velocity
3. Model release pressure
4. Piston mass
5. Model mass.

Large changes can be made in these conditions in various combinations to give the same velocity. However, the optimum condition that one would strive for is that of minimizing the maximum model base pressures to obtain the most uniform base pressure history possible and at the same time maintain gas reservoir pressures that are within the strength capabilities of the gun. Optimizing in this manner allows us, then, to test with a variety of models having the broadest range of strengths.

The reservoir pressure-time requirement for uniform base pressure is depicted by the dashed curve in Figure 2.37. A time history of reservoir pressure and base pressure representing conditions during firing is shown to indicate the manner in which these conditions might deviate from the desired conditions. (In this example, the effects of pressure gradients in the reservoir are neglected and thus the curves are a smoothed representation

of that actually encountered). The reservoir pressure depicted rises isentropically until it reaches the value at which the diaphragm ruptures, resulting in the start of model motion. For the case shown, the rate of rise of pressure (referred to as the pumping rate) is initially greater than the required ideal, with the result that the model base pressure then rises above that necessary for uniform acceleration. During the latter stages of compression, reservoir pressure drops rapidly as the piston decelerates to rest. However, this sudden decrease in pressure does not influence the model base pressure until later, because of the finite transmission speed of the expansion wave through the barrel. Thus the reservoir pressure need not be sustained for the full launch time.

The ideal pressure history shown applies for a particular model weight, but nondimensional similarity relationships can be used to account for changes in model weight. For uniform acceleration to the same velocity, an increase in model weight requires, with the same launch tube, a proportionate increase in base pressure, p_s, and model release pressure, p_R. From the constant-base-pressure equations (Section 2.4.5) it can be seen that an increase in base pressure necessitates a corresponding increase in reservoir pressure, p_r. By changing the initial loading pressure p_{r_o} (or gas mass G), in direct proportion, the pressure ratio p_r/p_{r_o} remains constant so that with ideal isentropic compression the same gas temperatures and sound speeds are maintained. With equal values of p_r/p_{r_o} the pressure rise time during launch will remain the same (as it must for equal acceleration to the same final velocity) if piston velocity is unchanged. Finally, the required adjustment in energy to compress the propellant gas is obtained by varying piston mass in direct proportion to gas mass. Ideally, then, the following similarity relationships can be used with a given gun to account for changes in model weight:

$$\left.\begin{array}{c}\text{For equal } U \text{ with } a = \text{constant} \\ p_s,\ p_R,\ p_{r_o},\ G,\ m_p \sim m_s \text{ with} \\ u_p \text{ unchanged.}\end{array}\right\} \qquad (2.140)$$

Real-gas effects encountered at high pressures, where sound speed is strongly influenced by density, will limit the region over which these relations apply. Further, the useful range of applicability is restricted because of the pressure limitations of both gun and model; for this reason a pump of fixed dimensions cannot be designed to achieve high performance over a wide range of model weights and strengths. If maximum performance is desired at relatively high model weights, the compressor size will, within limits, be made larger (to increase compression ratio) so that the gun can be operated more effectively at higher gas temperatures and sound speeds, within the given pressure restrictions.

The effects of variations in the gun-loading conditions are discussed in the following sections. It should be noted that the selection of the range of variables in the experimental data presented were made on the basis of other considerations and not specifically to test the validity of the similarity relationship for model weight noted above.

2.5.2.1 *Initial Gas Conditions*

When the choice is made of the propellant gas to be used, the ratio of specific heats, γ, and the molecular weight, M, are therefore specified, leaving two remaining gas variables to be adjusted; the gas mass, G, and the initial temperature, T_{r_o}. At this point we will consider only the effect of G (or p_{r_o}) and T_{r_o} will be taken to be ambient. The question of increasing the initial temperature by heating the gas prior to compression will be discussed in Section 2.5.2.6.

Rather than examining the complete set of equations for general gun performance, it is helpful, in understanding the way in which the initial gas pressure (and other variables) influences the subsequent reservoir-pressure history, to consider the simplified case of isentropic compression in a constant-diameter closed-end pump tube. For a piston traveling at velocity u_p with initial reservoir volume V_{r_o} one can obtain, using the isentropic relations for pressure and volume, the following expression for the time rate of change of pressure:

$$\frac{dp}{dt} = \frac{\gamma A u_p}{V_{r_o}} \left(\frac{p}{p_{r_o}}\right)^{1/\gamma} p \ . \qquad (2.141)$$

This expression is at least indicative of the rate of pressure rise existing in the initial phases of the launch cycle when the total model motion is small and when the mismatch between desired and actual reservoir pressure for constant-base-pressure flow tends to be greatest. From this equation it is seen that the pumping rate at a particular value of p and u_p is inversely proportional to $p_{r_o}^{1/\gamma}$; an increase in p_{r_o} by a factor of 2 decreases dp/dt by a factor of 0.61 for a γ of 1.4. The rate of rise of pressure is also a function of p, rising more rapidly as the pressure level increases, as shown in Figure 2.38.

The effect of initial loading pressure, p_{r_o}, on the resultant base pressure, p_s, experienced by a model during launch is seen in Figure 2.39. Base pressures were measured during firings of the Ames Research Center 7.1 mm/39 mm gun (7.1 mm-bore launch tube and 39 mm-bore pump tube). Except for initial pressure, the loading conditions are nearly the same for both cases. The higher base pressures developed with the low gas loading result in a higher model velocity, but the difference in velocity cannot be attributed entirely to the fact that the pumping rate is increased with a lower p_{r_o}. Another primary factor is that the effective compression ratio is increased by decreasing p_{r_o} resulting in higher gas temperatures which can also serve to increase performance.

The variation of the maximum base pressures developed with changes in initial loading pressure (using hydrogen), obtained for two model weights from firings of the Ames 7.1 mm/39 mm gun, is shown in Figure 2.40. The 0.16 and 0.65 gram models are, for this bore diameter, equivalent to plastic(polycarbonate) cylinders 1/2 and 2 calibers long, respectively. Piston mass, m_p, was held constant at 200 grams and diaphragm rupture (model release) pressure, p_R, at 690 bars. For constant values of piston velocity of 625 and 750 m/s it is seen that the maximum base pressures rise substantially as p_{r_o} is decreased, in accord with the increased pumping rate attendant with a decrease in p_{r_o}. This effect is much greater for the heavy model. With these test conditions, the maximum base pressures occurred shortly after diaphragm rupture when the model had moved only a short distance. The greater inertia of the heavy model results in a slower initial movement and because the pumping rate is high (particularly with low p_{r_o}) the base pressure rises to high values before a significant volume is opened behind the model.

The muzzle velocities achieved under these conditions are shown in Figure 2.41. It is seen again that the higher pressures and temperatures developed by reducing p_{r_o} result in increased model velocities. The rate of rise of velocity decreases as one approaches the lower tolerable limit of p_{r_o}, where the mass of gas becomes insufficient to maintain substantial base pressures for extended distances of model travel. As pointed out previously, the mass of gas required to supply constant base pressure is proportional to the model mass, so that higher initial loading pressures are required with increased model weight.

By cross-plotting the original data we obtain the variation of $p_{s_{max}}$ with p_{r_o} for a constant model velocity of 8 km/s with the light model and 6 km/s with the heavy model, as shown in Figure 2.42. Within the limits shown here one can reduce $p_{s_{max}}$ and yet achieve the same velocity by increasing p_{r_o} (u_p is increased simultaneously to maintain constant velocity).

Reservoir pressure histories were not measured during this test series, but to indicate the relation of maximum reservoir pressure, $p_{r_{max}}$, with changes in p_{r_o}, calculated values are presented in Figure 2.43. A reduction in p_{r_o} at constant piston mass and velocity produces an increase in $p_{r_{max}}$ in a manner similar to that seen for maximum base pressure $p_{s_{max}}$.

2.5.2.2 *Piston Velocity*

Piston velocity has a strong influence on the subsequent model base pressure history. The rate of rise of reservoir pressure is essentially a direct function of piston velocity (Eq.(2.141)) in the early stages of projectile motion when the mass-flow into the barrel is small.

Within limits, any desired piston velocity can be attained at one specified point in the compression cycle by proper selection of the powder charge. For example, the piston can be accelerated to the velocity required to give the desired pumping rate at the start of the model motion. There is, however, little control over the subsequent velocity history, except that the rate at which the piston decelerates during the latter part of compression may be varied by changing piston mass. In practice, as seen in Section 2.4.7, the piston velocity history cannot be matched to that required for constant base pressure for the full compression period. The actual velocity used, then, is that which will give the best overall match with the desired conditions.

The manner in which piston velocity influences the muzzle velocity attained is shown in Figures 2.44 and 2.45, for model weights of 0.16 and 0.65 gram, respectively. In this particular gun, piston velocity is determined at a position 1.5 m from the start of the transition section so that, depending upon the model release pressure, the piston will have decelerated somewhat before the start of the launching cycle. To examine the separate effects of changes in loading conditions, model release pressure and piston mass were held constant for both model weights, although the optimum requirements for each weight are necessarily different. Gas-loading pressure is presented as an independent variable and is expressed both in bars and as a ratio of gas-mass to model-mass, G/m_s. The latter is a classical nondimensional parameter of interest (see Section 2.3.3.3) - dependent upon the conditions desired, the required mass of gas is a function of the model mass and is useful in comparing guns of different sizes and configurations. The range of G/m_s (for ambient conditions) shown for the light model, Figure 2.44, is typical for this gun type but the same range was not covered for the heavy model. In this case piston mass, held constant for both model weights, was too low to provide the required energy for interest at the higher values of G/m_s. It is seen from both figures that, in general, model velocity increases rapidly with increasing piston velocity, along lines of constant p_{r_o}, but the rate of increase tapers off as u_p is raised. A combination of factors (which will be discussed in greater detail in following sections) may contribute to the gradual decrease in the slope of the U verses u_p curves at both high and low values of p_{r_o}; for example, as piston speed is increased to higher performance conditions, contamination of the propellant from erosion as well as other losses attendant with higher temperatures become increasingly significant (particularly at low values of p_{r_o}); at the lowest values of p_{r_o} there may be insufficient gas to provide substantial base pressures for an appreciable distance in the barrel; higher shock pressures generated as piston speed is increased may result in premature release of the model (this effect will be greater at high p_{r_o} and will have a larger influence on the velocity of the lighter model).

Maximum base pressures, $p_{s_{max}}$, measured for the test series shown in Figures 2.44 and 2.45, are correspondingly presented in Figures 2.46 and 2.47. Along lines of constant loading pressure the rate of rise of base pressure increases with increasing piston velocity. This effect is especially pronounced with the heavy model. For the test conditions and gun used, at high piston velocities the heavy model has moved, typically, less than 20 calibers at the time maximum base pressure is reached, indicating that the initial pumping rate at the start of the launch is much too high for these models.

When we add to Figures 2.46 and 2.47 the model velocities obtained for these conditions, in the form of lines of constant velocity, we obtain a most revealing picture. Within the limits of the test, the maximum base pressures are reduced by increasing, simultaneously, initial loading pressure and piston velocity. It is interesting to note that the model velocity can be maintained by moving in this direction even though the gas temperatures are steadily decreasing as p_{r_o} is increased. This may result, partly, from real-gas effects; that is, the reduction in sound speed with decreasing temperature may be partially offset by an increase in sound speed with increasing gas density at higher pressures (see Section 2.5.2.6). Secondly, the stronger shock waves produced with increasing piston velocity will enhance gas temperatures and pressures, although for these test conditions the shocks do not appear to produce a harmful rise in base pressure along the lines of constant model velocity.

In Figures 2.48 and 2.49 these data are plotted to show more clearly the variation of maximum base pressure with model velocity, for curves of constant p_{r_o}.

Shown in Figure 2.50 are two examples of the base-pressure time histories obtained using the microwave reflectometer, compared with corresponding theoretical calculations by the method of characteristics for an ideal gas. The curves in the upper portion of the figure represent the base pressure history of a 7.5-gm model accelerated to 7.63 km/s with a low value of initial pressure and piston speed in the Ames 25.4mm/102mm launcher. The improved pressure history shown in the lower portion of the figure resulted when the initial pressure and piston speed were both increased to obtain approximately the same model velocity, 7.32 km/s.

Calculated values of maximum reservoir pressure and the maximum pressure exerted by the piston on the wall of a 16^{o}-taper (included angle) transition section are given in Figure 2.51 as a function of piston velocity for several values of initial gas pressure, p_{r_o}. At the lowest piston velocities the maximum gas pressures are somewhat larger than the piston deformation pressures but the piston pressure becomes dominant at the higher piston velocities. With high initial gas loadings both gas and piston pressures are relatively low. At low loading pressures the reduced mass of gas has a smaller retarding effect on the piston so that the decelerating forces between the piston and the tapered wall rise rapidly, and at high piston velocities become much greater than the gas pressure. As will be seen later, the piston deformation forces can be reduced by decreasing the transition taper angle below the relatively high taper angle of this example.

2.5.2.3 *Model Release Pressure*

An additional important control over the model base pressure history is provided by varying the point in the compression cycle at which the model is released. This point is controlled by regulating the opening pressure of the valve isolating the pump from the model – in most cases this valve is simply a scored diaphragm and the pressure at which it ruptures is termed here, the model release pressure. Varying the release pressure changes not only the initial pressure felt by the model but the subsequent pressure history as well. From Equation (2.141) or Figure 2.38 it is seen that a reduction in release pressure results in a lower pumping rate at the start of model motion. The high base pressures experienced in the initial launching stage by the relatively heavy models (shown in Figure 2.47), which resulted from a pumping rate that was much greater than necessary to match the requirements for the initial motion of these heavy models, could thus be reduced by a reduction in model release pressure.

As stated previously, the reservoir and base pressures do not vary in the relatively smooth manner depicted in Figure 2.37. Instead, compression and expansion waves, generated by acceleration and deceleration of the piston, create pressure and velocity gradients which perturb the pressure curve predicted for isentropic compression. Strong shock waves generated at high piston speeds produce pressure gradients large enough to substantially change the time at which the diaphragm ruptures. The variation of reservoir pressure with time during compression, for a typical case, is shown in Figure 2.52. If the release pressure chosen was that occurring at time t_2 it is seen that a shock reaching the diaphragm at time t_1 would cause premature release of the model. Thus, the arrival of a shock at the diaphragm, of sufficient strength to cause diaphragm rupture, when the pumping rate is lower than desired, might then substantially affect the model base pressure and resultant velocity.

The effect of release pressure on the model base pressure history is shown in Figure 2.53 for two firings of the Ames 25.4mm/102mm gun. Release pressure was varied from 1.38 to 0.69 kilobars, with other loading conditions held constant. It can be seen that, even though the velocities obtained were approximately the same, a much more favorable base pressure history is obtained with the lower release pressure. In both cases base pressures rise very soon after start of model motion to substantially higher pressures than the release pressure, indicating that the pumping rate is greater than that required to match the model motion during the initial period of model travel.

The results of firings made with the 7.1mm/39mm gun to determine the influence of release pressure on the maximum base pressures developed for a wider variety of conditions are shown in Figure 2.54. The shots at the lowest value of rupture pressure were made without the use of a diaphragm. Some initial frictional restraint of the model, estimated to be of the order of 50 to 100 bars, was provided by making the models 0.2 to 0.3 mm larger than the bore diameter. A substantial decrease in maximum base pressure is generally noted with a decrease in rupture pressure. The data point for the 0.32 gram model at 0.3 kilobars showing a contrary trend is thought to be (for unexplained reasons) an unusual result peculiar to this particular shot and not representative of a normal round under these conditions.

The model velocities obtained for this test series are given in Figure 2.55. Except for one set of conditions with a light model, there is a surprisingly small variation in velocity over the full range of release pressures. The substantial loss in velocity incurred with decreasing release pressure with the 0.16 gram model and the lighter

piston is attributed to the following factors: the initial pressure, p_{r_o}, of 1.52 bars is relatively high for this light model in comparison with the other examples shown, resulting in a comparatively low pumping rate at the start. Movement of the model is too great during the initial stages to receive full benefit of the higher reservoir pressures eventually developed. (However, it is seen from Figure 2.54 that the peak pressures developed were very low). The low piston mass also resulted in more rapid piston deceleration. When p_{r_o} is lowered to 0.52 bars and piston mass increased to 200 grams, the variation in model velocity with rupture pressure becomes small. The heavy model test series resulted in essentially no change in model velocity. In this case, the initial acceleration of the higher inertia model is low enough so that the model travel is relatively small during the time that is required to reach an effectively high pumping rate. Within reasonable limits, then, the model velocity is relatively insensitive to changes in the timing of the diaphragm burst.

A final comparison of the effect of release pressure on normalized base pressure is given in Figure 2.56. Here, the base pressures presented in Figure 2.54 are normalized by dividing by the calculated effective constant base pressure necessary to achieve the measured velocities given in Figure 2.55. This ratio serves as a figure of merit for a particular firing, indicating how closely base pressure conditions approach the ideal, $p_{s_{max}}/p_{s_{avg}} = 1$. The advantage obtained by operating at relatively low release pressures for the loading conditions used in these tests is clearly evident. Although an appreciable reduction in velocity occurred with the light model at $p_{r_o} = 1.52$ bars, when release pressure was reduced to the minimum test value (see Figure 2.55), this firing approached most closely the desired constant base pressure conditions. In this case, as well as most of the other shots, lowering the release pressure resulted in a reduction in maximum base pressure that was proportionately greater than the reduction in velocity.

Operating with relatively low release pressures provides an effective means of reducing the high base pressures occurring in the early stages of model motion that result from a pumping rate that is too high to match the initial starting requirements. It should be noted, however, that for very light models which allow high initial pumping rates and models capable of withstanding high maximum pressures, the highest velocities are obtained with relatively high release pressures.

2.5.2.4 *Piston Mass*

In the type of gun under discussion, with the usual loading conditions, the piston reaches its maximum velocity prior to the start of the launching cycle. The first-stage driver gas, used to accelerate the piston, has by this time expanded to a low pressure and does not significantly contribute additional energy to the piston. Thus the major portion of the energy required to compress the propellant gas is supplied by the piston kinetic energy. The piston velocity, however, is specified by the pumping rate required to give the desired base pressure and so piston mass becomes an important variable in making up the energy requirement. Piston velocity must be reasonably matched to the pumping requirements during the early stages of model motion to limit a large initial pressure over-ride. Piston mass becomes an important factor in the later stages of compression in that it determines the rate at which the piston decelerates. A heavy piston maintains a higher pumping rate toward the end of the compression stroke, serving to maintain higher base pressures in the later stages of model travel. This effect can be seen in Figure 2.57, which shows the base pressure histories recorded during two launches with different piston masses. The less rapid deceleration of the heavier piston produces higher reservoir pressures which result, in this case, in higher base pressures throughout most of the launch. It should be noted that the 150 gram piston is comparatively light for the test conditions so that doubling piston mass in this case has a greater effect on the final velocity than would occur if the weights were closer to the optimum values.

The variation of model velocity with piston mass is presented in Figure 2.58 for several different launch conditions. With an initial pressure of 0.50 bars and a piston speed of 600 m/s a gain in muzzle velocity of 12% is realized for the 0.16 gram model when piston mass is increased from 150 to 300 grams. A further increase in mass shows no additional benefits. For the same change in piston mass but with an initial pressure of 1.52 bars and a piston velocity of 700 m/s a gain of approximately 40% in model velocity is realized for the 0.65 gram model. The larger increase in velocity obtained with the heavy model occurs because the 150 grams piston is farther from optimum conditions for this model than it is for the light model. The increased energy necessary to launch the heavy model with a greater gas mass requires a corresponding boost in piston mass. There is insufficient data to ascertain the optimum value of piston mass for these conditions but it appears that the primary gain has already been realized.

The curve identified by the square symbols, in Figure 2.58, is the result of a series of firings with the 0.16 gram model, made with powder charge mass held constant. Thus, as piston mass is increased, the piston velocity decreases, but the kinetic energy remains approximately constant. Actually, the resultant kinetic energy increased by 14% for the 250 gm piston and by 19% for the 350 gm piston. Even so, a continual loss in velocity occurred as piston mass was increased. The higher velocity realized with the 150 gram piston was obtained at the expense of greater maximum pressures (see Figure 2.59). It is seen in Figure 2.60 that a piston mass of 250 to 300 grams for the constant powder mass case gives the minimum ratio of maximum to average pressure. For the light model with constant piston velocity no improvement in normalized base pressure is shown by increasing piston mass above 150 grams.

The calculated effect of piston mass on the reservoir pressure and the pressure exerted by the piston on the tapered walls in decelerating to rest is shown as a function of piston velocity in Figure 2.61, for constant $p_{r_o} = 0.76$ bars and $m_s = 0.76$ gm. It should be noted that the transition-section taper angle for these data is 8.7 degrees - in contrast to the similar calculations for a 16-degree-taper transition section given in Figure 2.51 for the effect of initial loading pressure. Comparison of these two figures at the common condition of $p_{r_o} = 0.76$ bars and $m_p = 200$ gm shows that the maximum pressures generated are appreciably higher for the shorter (16^o) taper section, particularly so for the piston deceleration pressures.

2.5.2.5 *Model Mass*

It has been seen in a number of the foregoing discussions that variations in model mass have a significant effect on model performance. For example, the change in model velocity and base pressure occurring with two different model weights over a limited range of initial gas pressures was given in Figures 2.40 and 2.42. The effect of varying piston velocity for several model weights, while holding p_{r_0} constant is shown in Figures 2.62 to 2.64. One can see that, at a particular set of loading conditions, increasing model mass results in higher reservoir and base pressures with reduced velocities.

To achieve *equal velocities* with models of different mass (in a particular gun) by maintaining the same acceleration history requires that the model base pressure be increased in direct proportion to the increase in model mass. According to the similarity relations (Eq.2.140) discussed in the introduction to Section 2.5.2 this may be accomplished by a proportionate increase in release pressure, reservoir pressure, gas mass, and piston mass (with piston velocity history remaining the same). Unfortunately, the range of velocity and model mass over which these relations can be used may be quite restricted because of limitations in the tolerable model and reservoir pressures; or, interestingly, it can be stated in another way that, as the desired velocity is increased, the range of model mass over which constant base pressure conditions can be approximated becomes increasingly small.

In the operation of a conventional two-stage gun, the result is that with models of equal strength large deviations from the ideal are experienced at a lower velocity with the heavier model. Under these conditions, the above similarity relations cannot be used and the loading conditions must be, in effect, optimized for each model weight and velocity. In an effort to obtain high velocities with the high inertia models, the tendency frequently is to use loading conditions which result, initially, in a much greater pumping rate than that needed to match the required mass flow into the barrel at the start of model motion. In this situation, a reduction in model release pressure (contrary to that suggested by the similarity relations) provides a very effective method of lowering the initial pumping rate so that the base pressures at the start of launch can be kept within the strength of the model. Moreover, as seen in Section 2.5.3, reducing release pressure will not, for a relatively heavy model, result in a significant loss in velocity.

As mentioned previously, the experimental data given in this chapter are presented to indicate the manner in which individual changes in loading conditions influence performance, but the parameters have not been varied over the range required to optimize conditions for the spectrum of model weights and strengths normally encountered in ballistic-range tests. However, assuming that conditions are optimized, the best that can be achieved with models of *equal pressure capability*, as model weight is increased, is a reduction in velocity proportional to the square root of the increased mass. Unfortunately, the loss in velocity realized with models of increased weight may frequently be substantially greater than this, for in many tests, the heavier models tend to be complex configurations with less pressure capability than the simpler, lighter configurations.

To illustrate the relationship between velocity and model mass currently being achieved with light-gas guns, typical performance data from a number of laboratories in the United States, Canada, and England are given in Figure 2.65. Information from the VKF-Arnold Engineering Development Center has not been included because of internal security restrictions. Model velocity is plotted as a function of model mass, but to compare results of different size guns, the mass is divided by D_s^3 . These velocities are representative of those being achieved at the present time with a large assortment of models of widely varying strengths in a variety of guns having considerably different geometries. The velocities do not necessarily represent the optimum or maximum capabilities of each launcher. However, the envelope of the maximum velocities attained for various model weights illustrates how velocity is sacrificed as model weight is increased. It should be noted that, if one is concerned with achieving a high model kinetic energy rather than high velocity, model energy is increased with increasing weight; the kinetic energy of the heaviest model shown, for $m_s/D_s^3 = 4.0$ gm/cm^3 at 4.18 km/s , is 40 times that of the lightest model, with $m_s/D_s^3 = 0.26$ gm/cm^3 at 11.29 km/s .

The lowest mass model (0.26 gm/D_s^3) which achieved the highest velocity was a polyethylene plastic (specific gravity 0.95) cyclinder approximately 1/3-caliber long, about the minimum practical length that can be successfully launched. With lengths below 1/3 caliber, problems of attitude stability and gas leakage past the model during launch are enountered. Thus, further reductions in model weight to achieve higher velocities with comparable driving pressures can only be made with the use of lower-density materials having the necessary dynamic strength. (See Chapter 3 for further discussion of model materials). Often test requirements dictate the use of a high-density material such as steel, or tungsten, as a portion of the model, and in this case the relative launch weight may be reduced by making the test model small in relation to the bore size (termed a sub-caliber model) so that the weight of the sabot, constructed of appreciably lighter material, constitutes a large fraction of the total projectile weight. This requires the use of a larger bore gun, but may be necessary to achieve the desired velocity.

2.5.2.6 *Propellant Gas Temperature*

It was seen in the ideal equations presented in Section 2.3 (e.g., Equations (2.21) and (2.22)) that increasing the sound speed by increasing temperature will produce a gain in velocity. As has been stated previously, high temperatures can be achieved by using large volume pump tubes to obtain a high compression ratio. Other methods considered by many laboratories have been those of preheating the gas in some manner prior to compression or by increasing temperatures by chemical or electrical means during compression. The ideal equations show that the maximum gas temperature will be doubled if the initial temperature before compression is doubled. Numerous calculations have been made (see, e.g., References 2.63, 2.76, and 2.95 to 2.97) indicating that large gains in

velocity can be achieved by additional heating, but experimental tests made to verify these calculations have resulted in little or no gains. Stephenson and Anderson[2.96] report a 9% increase from 8.38 to 9.15 km/s when T_{r_0} was doubled. Swift and Baker[2.98], in conducting an extensive series of tests with several methods of heating, noted small gains in velocity when operating at moderate performance levels, but found essentially no increase in velocity with an increase in T_{r_0} from 290° to 1000° K when firing at higher levels of performance. Cable[2.47] reports no gain in velocity with preheating to 425° K. Berggren and Mitvalsky conducted a series of tests at Ames (unpublished) with similar results; in these tests the pump tube of a high-compression-ratio isentropic-compression gun was raised to 700° K by ohmic heating. A comprehensive parametric study was made to optimize conditions in an effort to increase the maximum performance. The results, however, produced no increase in velocity, and in many cases a degradation in performance was noted.

There may be a number of factors contributing to these disappointing results. Losses by heat transfer to the walls, for one, increase with temperature and result in increasing disparity between ideal calculated performance and that actually achieved, as temperature is raised; but this could be only partly responsible for the above results in that essentially no gain in velocity was noted. Serious erosion of the bore surfaces was noted with preheating in the Ames tests and it is thought that the resulting contamination of the propellant by metallic vapors, causing an increase in molecular weight, may have degraded performance. A most significant factor may be related to real-gas effects. For example, the influence of high gas density on the sound speed may override the effects of high temperature.

The real-gas temperatures produced during the later stages of compression in a light-gas gun are considerably below those computed for an ideal gas at comparable pressures. However, at these high pressures, strong intermolecular repulsive forces in the real gas serve to reduce the gas density, and this effect offsets the reduced temperature so that a net increase in the speed of sound is realized. Calculations were made using Seigel's semi-empirical entropic relation, Equation (2.108), for which the speed of sound is given by Equation (2.110). The results of these calculations, Figure 2.66, made for realistic gun conditions, show that: (1) the sound speed increases with increasing pressure faster than for the ideal case, and (2) the speed of sound increases more slowly, as the initial temperature of the gas is raised, than is predicted from ideal-gas behavior. In fact, if the real-gas curves in Figure 2.66 are extrapolated to higher pressures, they may actually cross over, resulting in a reduction of sound speed with increasing initial temperature. Such a "reversal" has been predicted by Swift and Baker[2.98] using a somewhat different real-gas model and occurred at a significantly lower pressure than an extrapolation of Figure 2.66 might predict.

The question of the effect of high temperatures at high densities in light-gas-gun operation can only be estimated at this point and will not be resolved until an experimentally verified equation of state is available. The discrepancy between the ideal predicted performance and that obtained experimentally with preheating serves, however, to point out the necessity of accounting for losses and real-gas effects in calculating performance.

2.5.2.7 *Powder Charge*

The quantity of gun powder used is that necessary to accelerate the piston of given mass to the desired velocity at a specified point in the compression cycle. If piston velocity is measured near this point, the relation between powder charge and velocity can be easily determined experimentally. An estimate of the powder pressure, p_c, developed during burning may be obtained with the following relation for a closed chamber (see Reference 2.13):

$$p_c V_c = m_c RT , \tag{2.142}$$

where m_c is powder charge mass and V_c is powder chamber volume. Powder burns at essentially constant temperature with the result that RT, for any particular powder, remains nearly constant. Depending on the ratio of the charge mass to chamber volume, typical values of RT for a nitrocellulose gun powder may vary from 5 to 11 kilobars cm^3/gm (the low values result when charge mass is small in relation to chamber volume). Equation (2.142) is valid if a relatively fast-burning powder is used so that burning is completed before the piston moves an appreciable distance. A fast powder may not always be desirable, however. To minimize peak powder pressures in a gun having a relatively small powder chamber volume it may be necessary to use a powder that burns more slowly and continues to burn as the piston moves, opening up additional volume. Maximum accelerations of the piston may thus be reduced by a slow-burning powder, minimizing the formation of shocks in the propellant gas ahead of the piston. Further considerations relating to the calculation of chamber-powder pressures and the powder-charge geometry are discussed in Section 2.5.3.5.

2.5.3 Effect Of Gun Geometry

The interrelation of the many variables of changing gun geometry and loading conditions on the resulting internal gas dynamics makes it difficult to pinpoint an optimum gun configuration – one which produces the desired launch velocities with the lowest resultant pressures. Further, a particular gun may be near optimum only for a limited range of model weights, and so, in many cases, the gun configuration chosen for general laboratory use to launch a large variety of models is at best a compromise.

Parametric studies made thus far have not been sufficiently broad in scope to enable one to select an optimum design. Theoretical parametric studies of the effect of gun geometry, which have been helpful in revealing trends, have been made using the ideal-gas relations (see, e.g., Reference 2.99). However, because of the uncertain effects of the various losses and gas non idealities at high temperature and density, in the following discussion of gun geometry we will rely as much as possible on experimental evidence obtained with existing guns.

Geometries representative of the two-stage guns in present use at a number of laboratories are given in Table 2.2 along with the velocities obtained for the typical loading conditions listed. Model velocities achieved with these guns were also plotted in Figure 2.65. Gun dimensions listed in Table 2.2 are defined in Figure 2.67. It is most interesting to note the extreme variance in the geometries of these guns. This is due, in part, to the differing test requirements of the various laboratories. However, there are also large differences in the relatively high-performance guns which have achieved velocities near the envelope of the curve of Figure 2.65. From the wide range in initial gas pressures and piston speeds shown in Table 2.2, one can deduce that there are considerable differences in the extent of shock heating; some guns operate with nearly isentropic compression while others, in varying degrees, approach the shock compression mode of operation.

2.5.3.1 *Launch-Tube Size*

Since the launch-tube bore diameter chosen establishes the overall size of the gun and its cost, this diameter is generally made no larger than necessary to fulfill the anticipated test requirements for model size. To obtain maximum velocities, the launch-tube length is determined, not by considerations of the maximum length over which a reasonable base pressure can be maintained constant, but instead, is made longer to take advantage of further expansion of the gas to low values. The point at which the driver gas expands to such a low value that its force no longer exceeds those due to bore friction and pressure ahead of the model depends on the pumping capabilities and loading conditions. A practical maximum length for existing guns has been determined by experience to be in the range of 300 to 400 calibers. The results of a test series performed at Ames Research Center (unpublished) with a 5.6-mm-bore launch tube and 45-mm diameter by 6.7-meters-long pump tube are shown in Figure 2.68. Of the four lengths tested, the highest velocities were obtained with a barrel 325 calibers long. These tests were conducted with loading conditions held constant at values normally used with a shorter barrel. To properly define a maximum limit, however, the loading conditions should be optimized for each launch tube length, requiring an increase in gas mass and piston energy as the length is extended. It is expected that, had this been done in this test series, the maximum velocity may have shifted to somewhat longer barrel lengths. Microwave reflectometer measurements of models during launch in the Ames 7.1-mm gun, which has a launch tube length of 357 calibers, show that in some cases the model is still accelerating, although at a low rate, as it reaches the muzzle. Thus, a longer length would give a slight increase in velocity. However, only a small percentage increase in velocity is obtained beyond lengths of approximately 250 calibers; barrels longer than this may not be warranted in instances where maximum velocities are not required.

2.5.3.2 *Pump-Tube Volume*

The ideal-gas relations show that for a specified mass of gas, increasing pump-tube volume to obtain an increase in compression ratio will result, without limit, in continually higher temperatures and sound speeds and, therefore, higher model velocities. However, as seen in Section 2.4.6, the reservoir requirements are changed when a real gas is considered. Because of the large intermolecular repulsive forces at high densities, the real gas has a higher enthalpy than the ideal gas when expanded from the same temperatures and pressures. The required temperatures and pressures calculated for a real gas are lower than for the ideal case, to maintain the same base pressure. An indication of the effect of this on the required pump-tube volume can be seen in Figure 2.69, taken from Reference 2.78. Model velocities are calculated for an ideal and real hydrogen gas as a function of pump-tube length. The results are presented for a 20-mm-bore launch tube, 6.86 m long, and a 102-mm-diameter pump tube. Maximum reservoir pressure was limited to 17.25 kilobars. With relatively short pump-tube lengths, substantially higher velocities are predicted for the real gas. A particularly significant result is that the rate of gain in velocity diminishes as length is increased for the real-gas case, and that at longer lengths little benefit is derived from increasing length.

There is substantial experimental evidence to show that pump-tube length (or volume) cannot be increased indefinitely to obtain further gains in velocity. Several examples to support this, as well as instances where an increase in pump-tube volume improved performance, are discussed below - with launcher dimensions listed in succeeding tabulations. (It should be noted that the ratio V_r/V_s, given in these tabulations, is a useful guide in comparing the relative reservoir volume of guns of different scale but its value becomes distorted and less meaningful when comparing guns having appreciably different launch-tube lengths (in terms of calibers); in practice, relatively small changes in performance result with changes in L_s/D_s for values greater than approximately 200.)

Launcher	D_s (mm)	D_r (mm)	L_r (m)	D_r/D_s	L_s/D_s	V_r/V_s
I_a	5.6	32.5	12.2	5.82	273	269
I_b	5.6	32.5	6.1	5.82	273	135
I_c	5.6	32.5	3.74	5.82	273	83
II_a	5.6	45.0	6.7	8.04	264	296
II_b	5.6	45.0	4.19	8.04	264	185

The 5.6mm/32.5mm isentropic-compression gun, listed as Launcher I_a, was constructed at Ames with an exceptionally large volume pump tube (12.2 m long) in an effort to obtain high performance. With this pump, a mass of gas five times the weight of 1/2-caliber-long plastic model required an initial loading pressure of 0.52 bars. Although extreme temperatures were developed during compression, as evidenced by the substantial erosion that

occurred during each firing, the launch velocities obtained were no higher than those achieved with several other lower-compression-ratio guns at the laboratory. To reduce the intolerably high erosion, the pump-tube length was decreased to 6.1 m (listed as Launcher I_b), then finally to 3.74 m (Launcher I_c). An appreciable reduction in erosion was noted with each decrease in length. (The temperatures calculated for isentropic compression of a perfect gas to 13.8 kilobars from an initial pressure of 0.52 bars in the 12.2-m tube, and for the same mass of gas in the 3.74-m tube, are 5400° K and 3920° K, respectively). In spite of the large reduction in temperature,, there was no discernible decrease in the velocities attained; in fact, the 3.74-m configuration has produced, with a light (0.045 gm) model, the highest velocity (11.3 km/s) yet achieved with a conventional two-stage light-gas gun. Because of the serious erosion encountered with the longest pump tube, it is reasoned that the inability to obtain higher performance with this configuration may be due, at least in part, to greater contamination of the hydrogen by the vaporized or molten metallic particles.

A 5.6mm/45mm gun at Ames (Launcher II_a), having a pump tube 6.7 m long, was also modified by shortening the pump to 4.19 m (Launcher II_b). The maximum velocities obtained after modification, with the light models generally used, are at least as high under comparable conditions as those achieved with the longer pump. It should be noted that although the compression ratio for Launcher II_a was somewhat greater than that for I_a the erosion occurring at the entrance to the launch tube was much less severe for II_a (not sufficient to present a significant operational problem) than for I_a. Reasons for this difference, which may be attributable to a difference in chambrage, are discussed in Section 2.5.3.3.

Both guns I_a and II_a appear to be, however, beyond the limit for which an increase in pump-tube volume will produce an increase in performance at the model masses of interest. Yet, with appreciably smaller volume pumps, experience has shown that an improvement in performance is obtained with an increase in reservoir volume. For example, a 5.6-mm gun at Ames gave an increase in velocity from 7.3 to 8.5 km/s for a particular saboted model configuration when the pump-tube-volume ratio (V_r/V_s) was increased from 58 (Launcher III_a) to 98 (Launcher III_b).

Launcher	D_s (mm)	D_r (mm)	L_r (m)	D_r/D_s	L_s/D_s	V_r/V_s
III_a	5.6	20	5.54	3.58	218	58
III_b	5.6	32.5	3.51	5.68	218	98
IV_a	6.35	25.4	1.52	4.00	200	19
IV_b	6.35	25.4	6.1	4.00	200	77
V_a	7.1	39.3	10.7	5.53	357	129
V_b	7.1	39.3	5.8	5.53	357	70

It should be noted that for Launcher III, volume was increased by an increase in chambrage and a decrease in pump-tube length. RARDE reported a gain in performance (Reference 2.47) with a 6.35mm/25.4mm gun when the pump-tube volume ratio (V_r/V_s) was increased from 19 to 77 by quadrupling pump length (Launchers IV_a and IV_b). A 350% increase in reservoir volume made by increasing both pump-tube length and diameter in a 12.7-mm launcher at the AEDC made possible an improved mode of operation whereby 30% heavier models are launched to the same velocity with a 50% reduction in peak base pressure. Gun dimensions for this case may be obtained from Reference 2.100.

A very limited study of the effect of pump-tube volume was made with the Ames 7.1mm/39.3mm gun by shortening the pump tube from 10.7 m to 5.8 m long (Launchers V_a and V_b). The effect on model velocity of the change in length, with mass of gas held constant for both cases, is shown in Figure 2.70. A gain in velocity was obtained with the shortened pump although the difference diminishes at the higher piston speeds. Attendant with this gain in velocity is a substantial increase in maximum model base pressure, Figure 2.71. At values of G/m_s of 2.5 and 3.8, the models broke up during launch in the shortened gun; the base pressures shown are values measured prior to model failure. The increase in base pressure is due, at least in part, to a difference in pumping rate for equal piston speed and gas mass that results when volume is changed. From Equation (2.141) of Section 2.5.2, it was seen that dp/dt is inversley proportional to V_{ro} and $p_{ro}^{1/\gamma}$, resulting in a pumping rate for the short tube approximately 1.2 times that of the longer pump. The decrease in maximum pressure noted for the short gun at the highest piston velocity may be due to premature diaphragm rupture (because of higher shock pressures developed with an increase in initial pressure). Normalized maximum base pressure, $p_{s_{max}}/p_{s_{avg}}$, is plotted in Figure 2.72, as a function of model velocity to indicate the relative efficiency of launch for the two gun configurations. Although the apparant scatter or lack of consistent trend would make any fairing of the data questionable, it can be seen that the longer pump tube definitely provides the more favourable launch conditions in these tests.

An examination of Table 2.2 will reveal that there is a large variation in pump-tube geometry, even with the guns which have achieved velocities near the envelope of the velocity curve given in Figure 2.65. High velocities have been obtained with both the small volume pumps operating with relatively higher gas densities and the large compressors which generate considerably higher temperatures. The parameters lacking to make a meaningful comparison between these guns are the reservoir and base pressures produced in each case to obtain a given velocity.

2.5.3.3 Chambrage

From theoretical considerations (ideal gas) discussed in Section 2.3 it is indicated that a gain in performance is realized from chambrage when the pump-tube diameter is increased to three to four times the launch-tube diameter. However, the computations of Reference 2.79 indicate that with real hydrogen gas the difference in reservoir conditions for the chambered and unchambered gun, to maintain constant base pressure, is for high-performance conditions, not large enough to be of practical significance. Other considerations, then, can be used to determine a suitable value of D_r/D_s. For example, lack of laboratory space may limit pump-tube length, requiring a relatively large diameter tube to provide the desired reservoir volume. Because of space limitations, guns having diameter ratios up to at least 10 have been used with good results.

As the diameter is increased for a pump-tube of specified volume, with mass of gas held constant, piston velocity must be decreased to maintain the same pumping rate; that is

$$\frac{u_{p_1}}{u_{p_2}} = \left(\frac{D_{r_2}}{D_{r_1}}\right)^2 . \tag{2.143}$$

The slower piston in a larger diameter pump will generate weaker shock waves and thus compress the gas in a more nearly isentropic manner. Further, with a larger-diameter, shorter pump the piston can be accelerated from rest to the proper velocity with a lower value of acceleration. This is significant in that the time required for compression waves to form shocks is a function of the piston acceleration (See, e.g., Rudinger, Reference 2.101). The fact that the piston acceleration is directly related to the pump-tube length can be reasoned as follows. If the piston is accelerated uniformly to the desired peak velocity, the acceleration will vary directly as the velocity squared and inversely with distance traveled; that is,

$$\frac{\alpha_1}{\alpha_2} = \left(\frac{u_{p_1}}{u_{p_2}}\right)^2 \frac{x_{p_2}}{x_{p_1}} . \tag{2.144}$$

To maintain the same pumping rate, piston velocity must vary inversely with distance traveled, or

$$\frac{u_{p_1}}{u_{p_2}} = \frac{A_2}{A_1} = \frac{x_{p_1}}{x_{p_2}} , \tag{2.145}$$

(for equal pump-tube volumes). Thus the piston acceleration is proportional to pump-tube length, or

$$\frac{\alpha_1}{\alpha_2} = \frac{x_{p_1}}{x_{p_2}} = \frac{L_{r_1}}{L_{r_2}} . \tag{2.146}$$

It is of interest to compare further two 5.6-mm-bore guns in use at Ames (Launchers I_a and II_a) having approximately the same pump-tube volume but different values of chambrage. It was stated that the erosion occurring with the smaller diameter pump was far beyond acceptable limits, while that experienced with the other was not sufficient to be of concern. Having approximately equal compression ratios, the two guns would, with isentropic compression, produce the same gas temperature. Considering that the surface area to volume ratio is greater for the smaller diameter pump it would be predicted that the attendant convective losses would be greater and the mean gas temperature somewhat lower than with the large diameter pump. The greater erosion associated with the small bore pump is thought to be due, at least in part, to its higher piston velocity (approximately 700 to 900 m/s, as compared to 350 to 450 m/s) with greater shock heating. Further evidence of greater shock compression in the smaller bore gun is indicated by the slightly higher maximum velocities attainable in this gun with simple models capable of withstanding the higher peak pressures generated.

Consider again that piston velocity varies inversely as the square of the pump-tube diameter if volume, gas mass, and pumping rate are held constant. To provide the same piston energy, then, the mass of the piston must vary as the fourth power of the diameter ratio,

$$\frac{m_{p_2}}{m_{p_1}} = \left(\frac{D_{r_2}}{D_{r_1}}\right)^4 , \tag{2.147}$$

with the result that as diameter is increased piston mass ultimately becomes impractically high. The effects of pump-tube to launch-tube diameter ratio (D_r/D_s), piston velocity, and piston mass on the stresses developed at the end of the pump when the piston decelerates to rest must also be considered. The pressure at the wall of a tapered transition section increases with an increase in D_r/D_s and is proportional to the piston mass and the square of the piston impact velocity. The pressure relationships for this case are developed in Reference 2.102.

Average values of D_r/D_s, used in current guns, can be seen from Table 2.2 to be in the range of 4 to 5.

2.5.3.4 Pump-Tube to Launch-Tube Transition

The guns listed in Table 2.2 include a number that have a square-ended or abrupt transition section between the pump and launch tube, but the majority have a slender tapered transition of 15° (included angle) or less. The function of the tapered transition was discussed in Section 2.4.4.

Tests made at several laboratories have shown that with the use of a deformable piston and a slender tapered transition the maximum velocity can be substantially increased over that attainable with a gun having an abrupt transition (in which additional gas is used as a buffer to prevent damage to the end of the pump). RARDE tests (Reference 2.47) obtained (for a limited range of loading conditions) an increase of approximately 760 m/s when taper angle was changed from 60 to 16 degrees. Examination of the available firing results plotted in Figure 2.65 for the guns listed in Table 2.2 reveals that the highest velocities, that is, those within 1000 m/s of the envelope, were (with one exception) obtained using guns having taper angles less than 15°. The exception, at $m_s/D_s^3 = 1.74$ and a velocity of 7000 km/s, was obtained with a 60° taper utilizing an expendable transition section.

Although the slender-taper deformable-piston gun has achieved the best performance with present methods, the question arises as to whether there is an optimum angle for this slender taper. Calculations for isentropic compression of an ideal gas (Reference 2.76) indicate that an increase in velocity is obtained as taper angle is increased from approximately 3° to 11° (included angle). At angles from 11° to 16° a rapid decrease in velocity is noted. The predicted pressure exerted on the walls increases slowly at small angles as taper angle is increased, but rises rapidly at angles above approximately 8°. In experimental tests, Curtis[2.65] noted, for a limited range of test conditions, a slight increase in velocity (370 m/s) when taper angle was increased from 5.4° to 7.4°. The RARDE results at higher angles show no appreciable velocity difference between 9° and 16°. Additional tests at Ames at included angles of 8.7°, 12.4°, and 16° also show no essential difference in model base pressure as well as velocity for a variety of different model weights and loading conditions (see Figures 2.73 and 2.74).

Since there is seen to be no gain in performance at angles above approximately 8°, and that piston deformation pressures increase rapidly at angles above this value, it may be concluded that 8° included angle (or possibly slightly lower) is a suitable angle for the deformable piston gun.

2.5.3.5 Powder Chamber

With the typical mode of operation of a two-stage isentropic compression gun the sole function of the first stage is to accelerate a pump piston of given mass to a specified velocity at the start of the launch. Ideally, for isentropic compression, the first-stage pressure-time history should be such that the piston is accelerated relatively smoothly to minimize shock formation in the second-stage propellant. With gunpowder as the first-stage propellant, the kinetic energy of the piston is determined by the mass of the charge. For a specified charge mass, pressures generated during combustion can be limited (to minimize peak piston base pressure) by making the volume of the powder chamber large in relation to the charge volume. The relation between peak powder pressure and chamber volume for a fast-burning powder which burns completely before the piston moves appreciably can be estimated by Equation (2.142) of Section 2.5.2.7. As noted there, a more uniform piston acceleration history is obtained with a slow-burning powder which continues to burn as the piston travels through a substantial part of the pump tube. The volume opened up by the motion of the piston serves as additional chamber volume so that the initial chamber need not be as large. The motion of the piston may be calculated using the conventional propellant interior ballistics solutions of References 2.13, 2.14, or 2.103 (see also Wilenius, et al.[2.71]).

Powder-chamber volumes for the guns in current use are listed in Table 2.2, expressed as the ratio of powder-chamber volume to launch-tube volume V_c/V_s. Launch-tube volume is considered a meaningful parameter with which to normalize chamber volume (to compare guns of different sizes) since powder chamber volume is determined by the required powder charge mass, which depends on the mass of light gas to be energized, which in turn is a function of model mass, and which, finally, may be related to launch-tube size. A wide variation in V_c/V_s is noted in the table. The two guns listed at the RARDE facility use compressed helium as a first-stage driver gas and should be exempted from this comparison. Values of V_c/V_s range typically from 3 to 8 but a number of cases differ widely from these values. With two 5.6-mm Ames guns having a V_c/V_s of 45.4 and 49.6 the pump piston can be satisfactorily accelerated to the required velocity with relatively low peak accelerations but the chamber volumes are considered to be unnecessarily large. The maximum density of loading (ratio of charge mass to chamber volume) for these guns is approximately 0.12 gm/cm^3. The Ames 25.4-mm and 38.1-mm guns, on the other hand, are considered to have undesirably small chamber volumes ($V_c/V_s = 1.8$, and maximum $m_c/V_c \sim 0.25$ gm/cm^3). A somewhat larger volume would reduce the need for the close control of the powder burning rates presently required with changes in charge mass and piston weight.

Variations in shape of the charge will produce changes in the burning rate and the peak pressures developed. This effect is more pronounced at high loading densities (Reference 2.13). For reproducible results it is necessary that the charge geometry be approximately the same for each firing. An example of the charge geometry used in light-gas guns is shown in Figure 2.75. The main charge is contained in a paper or cardboard tube and is ignited by an electrical primer. To provide uniform ignition when the charge is large in relation to the primer, it is sometimes desirable to use a booster consisting of a core of fast-burning powder extending through the length of the charge. A charge of relatively high fineness ratio, extending over a large fraction of the chamber length, is preferable to a compact charge located at the breech end of the chamber. The compact charge provides a greater distance for compression waves generated during combustion to form shocks which may affect the piston motion and add to the generation of shocks in the second-stage gas (see Reference 2.104).

2.5.3.6 Effects of Scale

From Equation (2.5), Section 2.3.1, it is seen that the velocity attainable under ideal conditions is:

$$U = \left[\frac{2\tilde{\rho}_s}{\rho_s}\frac{L_s/D_s}{l_s/D_s}\right]^{1/2} . \qquad (2.5)$$

A given velocity may be obtained with guns of different size by maintaining the same average propelling pressure, model density, and launch tube and model lengths expressed in units of the model diameter. The volume of gas required to produce the same base-pressure history must increase in direct proportion to the increase in the launch-tube volume. The required increase in volume is provided if pump-tube dimensions are also scaled up in direct proportion to the increase in launch-tube-bore diameter. Thus equal velocities may be achieved with guns of different size if all gun dimensions (including model and pump piston) are changed by the ratio of launch-tube diameters.

The motion of the model is determined by

$$\frac{du_s}{dt} = \frac{p_s A_s}{\rho_s A_s l_s} = \frac{p_s}{\rho_s l_s} ,$$

which shows that an increase in model length results in a proportionate decrease in acceleration. Therefore, for the same final velocity, the launch time will vary directly with changes in gun size. With a proportionate change in outside gun dimensions and wall thicknesses, equal stresses will result from operation at the same pressures.

To summarize, the same performance obtained from a gun of bore diameter D_{s_1} will be realized with a larger gun of diameter D_{s_2} if:

1. Gun dimensions are increased by D_{s_2}/D_{s_1}
2. Mass of model and piston are increased by $(D_{s_2}/D_{s_1})^3$
3. Mass of gas and powder charge are increased by $(D_{s_2}/D_{s_1})^3$,

with the result that:

1. Acceleration of piston and model will decrease by D_{s_1}/D_{s_2}
2. Time scale will increase by D_{s_2}/D_{s_1}
3. Pressures, stresses, velocities remain the same.

Because one can obtain (ideally) the same performance with guns of different sizes, small scale or pilot guns have been used to develop and proof larger more costly guns. Additional considerations regarding scaling, including experimental comparisons, are contained in References 2.77 and 2.88.

The range of gun sizes over which these scaling relations can be used with reasonable accuracy depends on the extent of possible nonscalable losses. Because of the complex nature of the nonsteady flow processes in guns, calculations of boundary layer and heat-transfer losses (influenced in a nonlinear manner by Reynolds number) made thus far have not been sufficiently rigorous to establish the effect of scale. In practice, the highest velocities have been obtained with small-bore guns, but this may be due principally to the added caution used in operation of large-bore guns and the reluctance to press the more expensive and potentially more dangerous equipment to the limits imposed on the smaller guns.

2.6 MECHANICAL DESIGN CONSIDERATIONS

2.6.1 Powder Chamber and Pump Tube – Low-Pressure Sections

The design of many of the various components making up a light-gas gun involves only application of standard practice. In those areas of the gun where the pressure loadings are relatively light, such as the powder chamber and most of the pump tube, the design is straightforward, primarily involving selection of tube-wall thicknesses and attention to joint details. Joints in these areas may be sealed by standard neoprene "O"-rings in accordance with practices recommended by their manufacturers. These seals are preferably located on journals or shoulders which serve to maintain concentricity of adjoining parts and permit some axial strain of joint retaining members without loss of seal effectiveness. One nonstandard seal arrangement which has proven particularly reliable is sketched in Figure 2.76.

Straightness of the pump tube is not a critical factor, since pump-piston speeds are relatively low, but it is desirable to have a reasonably smooth, honed, uniform-diameter bore, with no offsets or other discontinuities, throughout the length of the tube.

2.6.2 Pump Tube - High-Pressure Section

Since the performance of the gun is limited in part by the pressure capability of the high-pressure end of the pump tube, this section is designed to have maximum strength consistent with acceptable costs of construction. Of the several types of construction in general use the simplest is the single piece or monobloc thick-wall cylinder. The pressure at which local yielding is first reached at the inner wall is given by:

$$p_y = \frac{\sigma_y}{\sqrt{3}}\left(\frac{w^2 - 1}{w^2}\right), \tag{2.148}$$

where w = wall ratio = $\dfrac{\text{outer diameter of cylinder}}{\text{inner diameter of cylinder}}$

and σ_y = yield stress. This relation is developed from the maximum distortion energy theory of Von Mises, which is reported in Reference 2.105 to be the most appropriate of the various failure criteria for this application. Very little increase in pressure capability is realized for wall ratios greater than 5, but even with an infinite wall ratio the pressure at which yielding occurs is only 0.58 σ_y. If operation is limited to completely elastic conditions, the maximum pressures for ductile high-strength steels must be restricted to values of the order of 7.0 kilobars. For the high-pressure section of a light-gas gun, this is, however, an unnecessary restriction and the bore is allowed to yield to obtain an increase in operating pressure. When a cylinder is subjected to internal pressures greater than that required to produce yielding, plastic flow of the material begins at the bore and progresses toward the outside diameter as pressure is increased. Release of the pressure then results in residual tensile hoop stresses in the elastic outer fibers and compressive stresses in the inner fibers near the bore. In subsequent loadings, as pressure is increased, this compressive stress is first reduced to zero before a tensile stress is induced, and thus, the chamber can be pressurized elastically to the previous value at which the chamber has been prestressed before again reaching the tensile yield strength. This prestressing process, termed "autofrettage" (See References 2.106 to 2.109), is finally limited for elastic operation by the compressive yield strength of the material at the bore; auto frettaging beyond this limit results in reverse yielding at the bore. For cylinders having wall ratios greater than 2.2 (see Reference 2.110) this pressure is approximately twice the value given by Equation (2.148), or:

$$p_y = \frac{2\sigma_y}{\sqrt{3}}\left(\frac{w^2 - 1}{w^2}\right). \tag{2.149}$$

A further increase in maximum pressure can be made if reverse yielding at the bore is accepted. The pressure at which yielding has progressed to the outside wall in a monobloc cylinder (for all wall ratios), so that the cylinder is fully plasitc, is given by Equation (2.150). This relation can be used to obtain an estimate of the bursting pressure, although the actual bursting pressure will be somewhat higher because the ultimate material strength is not considered.

$$p_{max} = \frac{2}{\sqrt{3}}\sigma_y \log_e w\ , \tag{2.150}$$

Although cylinders are frequently auto frettaged during construction, this operation is commonly performed, in effect, in light-gas guns by subjecting the chamber to the actual pressures developed during firing.

Because of its relative simplicity, the monobloc is widely used in light-gas-gun construction. To allow extensive plastic flow the cylinders are made massive with wall ratios commonly in the range of 3.5 to 6.0. These ratios are based on the pump-tube diameter ahead of the tapered transition section if such a section is used. With a slender taper and relatively high-compression-ratio pump, peak pressures generally occur towards the small end of the taper where the wall ratios are much greater. Operation of this section under conditions producing extensive yielding requires the use of a highly ductile material. AISI 4340 (heat-treated to Rockwell C-38 to C-40) has proven to be an excellent high-strength steel of high ductility and good harden ability and is generally used in this application.

Although the slender taper transition section provides a means for decelerating the piston without severe damage during each firing, there is a gradual deterioration at the bore from high-performance shots with this configuration. Continued operation at conditions producing extreme gas and piston pressures results in local cracking of the bore material and the section is discarded when this cracking becomes pronounced. To minimize the hazard resulting from a possible complete failure, a thick-plate shield is sometimes placed over this section.

Another method of construction whereby a favorable residual stress distribution is induced in the pressure vessel to increase the maximum operating pressure consists of the assembly of two or more concentric cylinders having interference fits. The shrink-fit of an outer cylinder or jacket upon an inner cylinder or liner generates tensile hoop stresses in the jacket and compressive stresses in the liner. Relations for shrink-fit pressures and the stress distributions induced by this method can be obtained in standard design texts such as Reference 2.111. As with the auto frettage process, the maximum operating pressure for elastic operation, determined by the compressive yield strength of the bore material, is given by Equation (2.149). Again the pressure capability can be increased substantially if a portion of the cylinder is allowed to reach the plastic state. This may be accomplished by stressing the chamber during normal usage or by a separate auto frettaging procedure after construction, or by an alternate method wherein the cylinders are auto frettaged separately before assembly. An example of a compound structure of two cylinders is given by Cloutier in Reference 2.112,

in which the liner is considered to be three-quarters plastic and the jacket one-half plastic. With a wall ratio of five for the duplex structure and three for the liner, and a yield strength of 10.4 and 17.3 kilobars for the jacket and liner, respectively, the design pressure capability is computed to be 25.9 kilobars. In this case a high-strength steel, such as a maraging steel, is chosen for the liner material and a conventional gun steel for the jacket. Herein lies an advantage of compound construction - the possibility exists of using a costly, ultra-high-strength steel for the liner that may not be practical in a large monobloc cylinder. Further, a more uniform hardness can be achieved with heat treatment of the separate pieces used in a compound cylinder than can be obtained in the thick-wall monobloc. The greater complexity of the compound cylinder, requiring additional machining to close-tolerance interference fits and a shrink-fit operation, add to the initial cost of the unit. This may be partially offset by the fact that replacement of the cylinder, which may be necessary because of failure at the bore from high-performance firings, may require renewal of only the inner liner.

2.6.3 Launch Tube

Several factors other than a high-pressure capability dictate the design of the launch tube. To maintain proper stability of the model in the barrel (the model is often relatively short) and to insure an effective gas seal between the model and the wall, the launch-tube bore must be smooth and continuous. The high model velocities and relatively low model strengths also require that the bore be exceedingly straight, and because the launch tubes are frequently very long in relation to the bore diameter, it is difficult to produce barrels with the necessary straightness. The straightness requirement frequently specified for launch-tube construction, but often not attained, is that the bore shall not deviate from a mean centerline more than 1 part in 10^4 units of length. For many applications this is an unnecessarily stringent specification.

Gun barrels are typically machined from a solid forging using special deep-hole-drilling techniques to produce a relatively straight bore. If necessary, the barrels are mechanically straightened after the drilling operation.

The erosion encountered at the breech of the launch tube necessitates periodic replacement of the barrel. Failure and breakup of the model frequently produces sufficient damage to the bore (even with simple plastic models) to also require replacement of the barrel, unless some local repair can be made. It is desirable then, that the launch-tube construction be such that replacement can be made with minimum cost and effort.

One launch-tube design, made to satisfy the requirements for straightness and economical replacement can be seen in Figures 2.77 and 2.78. The design consists of a thin-wall seamless-tube liner supported externally by a heavy, split, rectangular block clamped by a double row of bolts. This bolted construction is sufficient to withstand the gas pressures except in the region of highest pressure at the breech end of the tube where a thick-walled jacket approximately 30 calibers long is used.

Jacket and split-clamp housing are generally constructed of AISI 4340 steel heat-treated to Rockwell C-40, and the liner is a commercially available seamless tube of an annealed alloy such as AISI 4130. A planing operation is used to machine the split clamp, including the semi circular groove in the separate halves which form the bore of the housing upon assembly. It is this operation, made possible with the split construction, that produces a straight bore launch tube; while it is difficult to bore or drill a long straight hole, it is relatively easy to machine an exceptionally straight groove on a planer if proper precautions are taken. With the larger launch tubes the bolts are tightened during assembly with a hydraulic bolt tensioner, which makes possible uniform loading of all bolts to nearly the yield point. A slight interference fit between the liner and both the jacket and split housing prevents movement of the liner during firing. The liners are purchased slightly oversized, in quantity lots from the same mill run to insure uniformity, and are sized to the precise outside diameter, if necessary, by a simple external honing operation. With a spare jacket and liner assembly held in reserve, replacement of a damaged gun liner can be made in a very short time and at a cost which is only a small fraction of the replacement cost of a conventional one-piece barrel. The fact that launch tubes can be rapidly and economically replaced leads to greater freedom in the selection of models - one can attempt to launch models of marginal strength at high-performance conditions without fear of substantial penalties in cost in the event of model failure.

This design has been used successfully at Ames Research Center in a range of gun sizes having bore diameters from 5.6 mm to 38.1 mm.

2.6.4 Coupling of Launch Tube to Pump Tube

Generally, the design of the joint between the pump and launch tubes entails the provision for three items:

(a) a quick-opening valve that will release the high-pressure gas, at a prescribed pressure, from the pump tube to the projectile base,

(b) an adequate seal to prevent escape of the hot, high-pressure gas through the joint, and

(c) external structural members to couple the launch and pump tubes together and carry the axial pressure and inertia loads developed when the gun is fired.

Although other types of quick-opening valves have been used successfully in the past, such as discs which fail in shear or members which part in half in tensile failure under the applied gas-pressure loadings, the petaling-diaphragm type valve is now in most general use. These diaphragms are made thick enough that they will not fail in direct shear, are prescored to provide a four-petal opening configuration which bursts at a pressure

dependent on the remaining depth at the scored section, and are machined from annealed type 304 stainless steel, which is sufficiently ductile that the petals will usually not tear off during the opening, or bursting, process. Their design is relatively straightforward and is detailed in Reference 2.113.

The problem of providing a seal at the critical joint between the pump and launch tubes, where the pressures and temperatures of the gas are near a maximum, has been a difficult one. Early attempts to employ neoprene "O"-rings at this joint met with only limited success. Some leakage nearly always occurred, with consequent erosion of areas adjacent to the seals, and in some cases the "O"-rings were completely extruded into the joint making it very difficult to disassemble the gun after firing. One successful solution has been to use a low-carbon steel ring as a seal, machined to size in the form sketched in Figure 2.79. The O.D. and I.D. of the seal ring have small clearance with the respective journals on the heat-treated pump and launch tubes so that the pieces readily assemble until the outer corners of the seal come to bear against the adjoining faces. The slant height of the seal cross section is made sifficiently long so that when an axial load is applied bringing the pump and launch tubes together, the seal is upset and will develop its yield strength in compression against the mating journals. The diameters of the seal ring and journals with which it mates must be precisely controlled, but when the parts are machined and assembled properly, it provides a very effective seal.

The structural coupling of the launch and pump tubes may be accomplished in several different ways. For smaller guns, either bolted flanges or threaded nuts, as sketched in Figure 2.80, are generally sufficient. Inherent in the bolted flange design is the disadvantage that many bolts are required to carry the pressure and inertia loads developed when the gun is fired, with consequent time-consuming assembly operations. The interrupted-thread nut is a good, simple design, but for large guns, the nut may be cumbersome to handle and difficult to torque when substantial preload forces are required to minimize axial separation of the joint for proper sealing. In this case, at the expense of additional complexity, mechanical or hydraulic torque multipliers may be used with the nut to provide the necessary preload.

A satisfactory method of joining pump tube to launch tube for larger guns, which allows quick and easy assembly and disassembly, employs a hydraulically constrained coupling, as shown in Figure 2.81. With this system hydraulic preload forces greater than the axial separating forces can readily be applied. The outer nut and retaining ring assembly threaded on the high-pressure end of the pump tube contains a hydraulic piston having an internal interrepted shoulder (like a spline in appearance). The shoulder nut threaded on the launch-tube breech has a mating external segmented shoulder. During assembly the launch tube and pump tube are brought together with the shoulder segments on the soulder nut aligned to slip between those on the piston. The outer nut and piston assembly is then rotated until the interrupted shoulder on the piston opposes the shoulder segment on the launch-tube nut. Application of hydraulic pressure between the piston and retaining ring moves the piston against the shoulder nut, forcing it and the launch tube into firing position against the pump-tube face. The joint is restrained hydraulically in this manner during firing without the use of any secondary mechanical backup. Disassembly of the coupling involves simply the release of the hydraulic pressure, return of the piston to its start position, a slight rotation of the shoulder nut to realign the interrupted faces, and finally, the withdrawl of the launch-tube assembly through the piston. This particular design has been used successfully on guns having launch-tube bores up to 38.1 mm diameter.

A general consideration concerns the use of AISI 4340 steel, frequently chosen for gun structural members. Experience has shown that with mating parts of this same steel there is a tendency towards galling and seizing, with relative motion of the parts under high local contact pressures. For this reason, highly loaded threaded joints requiring many threads with large heavy nuts are preferably constructed with interrupted, rather than continuous threads. Such a joint can be assembled with rapidity and ease, and with a minimum of sliding motion between mating threads. The use of an anti-seizing lubricant is also helpful in reducing this tendency towards galling.

2.6.5 Mounting

The mounting structure used in the support and restraint of the gun will be dictated, in part, by the method chosen for moving and handling the separate gun components during disassembly, cleaning, and assembly operations. Separation and movement of components may be accomplished in a variety of ways: with launch tube or pump tube kept stationary and other (or all) components moved axially and/or laterally to provide clearance for cleaning and for assembly of expendable parts.

It is frequently expedient to provide vertical and horizontal adjustment at individual support points so that the bore of long tubes can be readily aligned with regard to direction and straightness, eliminating in many cases the requirement that the outside tube diameter be made concentric with the inside diameter, as well as reducing the precision required in machining and locating mounts and supports.

The methods successfully used to restrain the gun members during firing vary from that of rigid restraint, allowing essentially no gun motion, to that of no restraint in which components are allowed to slide freely. With the highly restrained system the most effective point to provide this restraint is in the vicinity of the high-pressure transition section, where the highest peak axial loads are developed, so that these high loads need not be carried through the tubes and joints of other gun members. However, except perhaps for small guns, a rigid restraint system is undesirable because of the high peak loads developed in the support structure. These loads may be reduced with the use of a flexible support system with, for example, torsion bars, which act to temporarily store strain energy. The support structure loads may be reduced to moderate values by allowing greater motion of the gun with a system that applies some frictional restraint through clamped supports. Going a step beyond this, many two-stage guns, both large and small, are fired satisfactorily with essentially no

restraint other than the friction resulting from the weight of the gun. During operation, as a consequence of the free piston, an end load is first applied at the powder chamber accelerating the gun rearward, but this is counteracted later, for the most part, by the impulse imparted by the piston to the high pressure end. Although the net impulse is not zero the momentum of the model and light gas is generally small compared to the piston momentum, and, because the inertia of the complete gun is relatively high, the total excursion of the gun is reasonably small. It should be noted that, in such a system where the gun is allowed to move, the tubes and joints must be designed to handle the additional inertia loads developed.

2.7 PROSPECTS FOR HIGHER PERFORMANCE

The need in certain types of studies for velocities higher than presently attainable in the laboratory leads one to speculate about future possibilities for substantially increasing speeds. Techniques employing electrostatic acceleration, explosively formed jets, explosively driven plates, acceleration by drag forces, and others (see Reference 2.114) show promise, and, as noted in the Introduction, have achieved velocities well above 20 km/s. However, in most cases the particles accelerated are restricted in size, shape, and material. What are the prospects for accelerating the variety of aerodynamic models that are now launched primarily with guns? Very large gains in velocity have been made with the light-gas gun during the last decade but the rate of gain has of late slowed appreciably. Further increases in velocity with the conventional two-stage light-gas gun are becoming increasingly difficult to achieve. This is not meant to imply that the limits of capability of this launcher have been reached. Higher performance will surely be realized with an improved understanding of the internal ballistics of guns so that loading conditions and gun geometry can be better optimized to produce more nearly constant base pressure conditions. Further gains would result with improvements in the strength of gun and model materials. Perhaps the most significant increases in performance will result from the technological development of new concepts.

One of the basic limitations of the conventional gun is related to the fact that the propellant gas is expanded from a fixed reservoir. Extreme reservoir pressures are required to maintain an effective base pressure as the distance between the projectile and the chamber becomes large. The large expansion ratios required could be decreased if: the reservoir of gas were made to follow behind the model in some manner; or, the pressure and temperature of the gas were enhanced in some other fashion, in the region directly behind the model. A number of attempts have been made to achieve these conditions but in most cases without notable success.

One exception which promises to give substantially higher speeds is a new concept developed by Godfrey and Moore employing an explosive lensing technique (see Figure 2.82 taken from Reference 2.26). This launcher is a form of light-gas gun in which the model is accelerated in two stages. The function of the first stage is to accelerate the projectile and a reservoir of gas from rest to at least some minimum velocity (greater than approximately 5 km/s) required for operation of the second stage. The first stage used for this purpose has been a linear explosive driver consisting of a reservoir of helium contained in a metal tube surrounded by a high explosive. The tube is collapsed inward by detonation of the explosive, producing, in effect, a conical piston which travels progressively toward the projectile at a constant velocity equal to the detonation velocity of the explosive. The model, and driver gas energized by shock compression, are accelerated into the second stage, and when a sufficient quantity of gas at the proper conditions of pressure and temperatures have been introduced, operation of this stage is started. Employing a unique explosive lens, which also generates a conical piston, the second stage then further accelerates the projectile to the desired final velocity. The lens consists of two explosives having different detonation rates - a thin layer of fast explosive surrounds the slow explosive placed contiguous to the barrel. The difference in detonation speeds results in a detonation front that is inclined to the axis of the barrel. The smaller the angle of inclination, the higher the speed at which the collapse point (acting as a piston) proceeds along the barrel. By proper selection of detonation rates and lens geometry the "virtual piston" can be programmed to accelerate at various prescribed rates to speeds well above the highest explosive detonation velocity. The "piston" motion can be tailored to accelerate the reservoir gas in a manner to maintain a high and reasonably constant base pressure for an appreciable distance. Upon completion of the detonation phase a small further increase in velocity is obtained by expansion of the reservoir gas. Velocities as high as 12.2 km/s (with a 0.17-gm model, 6.4 mm in diameter) have been obtained with this technique - the highest velocity yet achieved with a light-gas gun - and projections indicate that velocities in the 15 to 20 km/s range are feasible.

Techniques such as this which do not depend on launching a model from a fixed reservoir, or other schemes in which the driver gas can be further energized in the region behind the model to sustain a high base pressure, may provide the means for launching laboratory test models to substantially higher velocities than presently attainable.

REFERENCES

2.1 Robins, B. — *New Principles of Gunnery.* James Wilson, MD, London, 1742.

2.2 (Lagrange, Joseph-Louis) Poisson, M.D. — *Mouvement de Poulet dans l'Intérieur de Canon.* Extraites des Manuscripts de Lagrange. J. d'Ecole Polytech., Vol.21, 1832.

2.3 Résal, — *Recherches sur le Mouvement des Projectiles dans les Armes à Feu.* Paris, 1864.

2.4 Hélie, — *Balistique Expérimentale.* Paris, 1865.

2.5 Sarrau, — *Recherches Théoriques sur la Chargement des Bouches à Feu.* Paris, 1882.

2.6 Moisson, — *Pyrodynamique.* Paris, 1887.

2.7 Hugoniot, — J. d'Ecole Polytech, Paris, 1889.

2.8 Gossot, Liouville — Mém. Poudres 1905, 1914.

2.9 Charbonnier, — *Balistique Intérieure.* Paris, 1908.

2.10 Röggla, — Mitt. Gegenstände d.Artill. u. Genie-wesens, 1914.

2.11 Love, A.E.H. Pidduck, F.B. — *Lagrange's Ballistic Problem.* Phil. Trans. of the Royal Society, Series A, Vol.222, 1922.

2.12 Cranz, — *Lehrbuch der Ballistik.* Berlin, 1926.

2.13 Corner, J. — *Theory of the Interior Ballistics of Guns.* John Wiley & Sons, 1950.

2.14 Thornhill, C.K. — *A New Special Solution to the Complete Problem of the Internal Ballistics of Guns.* AGARD Report 550, 1966.

2.15 Hunt, F.R.W. — *Internal Ballistics.* Her Majesty's Stationery Office, London, 1951.

2.16 Nelson, W.C. — *Selected Topics on Ballistics.* Pergamon Press, New York, 1959.

2.17 Fowler, R.H. Gallop, E.G. Lock, C.W.H. Richmond, H.W. — *The Aerodynamics of a Spinning Shell.* Phil. Trans. of the Royal Society, London, 1920.

2.18 Crozier, W.D. Hume, W. — *High-Velocity Light-Gas Gun.* J. Applied Physics, Vol.28, 1957.

2.19 Charters, A.C. Denardo, B.P. Rossow, V.J. — *Development of a Piston-Compressor Type Light-Gas Gun for the Launching of Free-Flight Models at High Velocity.* NACA TN 4143, 1957. (originally issued as RM A55G11, 1955).

2.20 Slawsky, Z.I. — *Survey of NOL Hyperballistics Research.* NOL Report 1238, 1959.

2.21 Seigel, A.E. Slawsky, Z.I. — *A Hypervelocity Gun Using a Shock-Compressed Steam-Heated Propellant.* NAVORD Report 4345, 1956.

2.22 Scully, C.N. Escallier, E.A. Rosen, F.D. O'Keefe, J.D. — *Electrothermal Gun for Hypervelocity Ballistics Research.* Proceedings of the Seventh Hypervelocity Impact Symposium, 1965.

2.23 Friichtenicht, J.F. Slattery, J.C. Hansen, D.O. — *Electrostatic Accelerators - Experimental Techniques.* Proceedings of the Seventh Hypervelocity Impact Symposium, 1965.

2.24 Kronman, S. Kineke, J.H. Jr — *Explosive Devices for Projecting Hypervelocity Pellets up to 21.0 Km/Sec.* Proceedings of the Fifth Hypervelocity Impact Symposium, 1962.

2.25 Howell, W.G. Orr, W.R. — *Results of Developmental Research on an Augmentation Technique for a Light-Gas Gun.* Proceedings of the Fifth Hypervelocity Techniques Symposium, 1967.

2.26 Moore, E.T. Jr — *Explosive Hypervelocity Launchers.* Physics International Co. NASA Contractor Report CR-982, 1968. Also, Physics International Final Report-051, 1967.

2.27 Courant, R. Friedrichs, K.O. — *Supersonic Flow and Shock Waves.* Interscience Publishers, New York, 1948.

2.28 Seigel, A.E. — *The Theory of High Speed Guns.* NATO AGARDograph 91, 1965.

2.29 Seigel, A.E. — *The Rapid Expansion of Compressed Gases Behind a Piston.* Ph.D. thesis, University of Amsterdam, 1952.

2.30 Heybey, W. — *A Solution of Lagrange's Problem of Interior Ballistics by Means of Its Characteristics Lines.* NOL Memorandum 10819, 1950.

2.31 Kent, R.H. — *The Motion of the Powder Gas. I. A Special Solution for the Case of an Imperfect Gas.* Aberdeen Report No.36, 1936.

2.32 Seigel, A.E. — *The Effect of Optimum Chambrage on the Muzzle Velocity of Guns with a Qualitative Description of the Fundamental Phenomena Occurring During Gun Firing.* NAVORD Report 2691, 1952.

2.33 Seigel, A.E. — *The Influence of Chamber Diameter on the Muzzle Velocity of a Gun with an Effectively Infinite Length Chamber.* NAVORD Report 3635, 1954.

2.34 Seigel, A.E. Dawson, V.C.D. — *Results of Chambrage Experiments on Guns with Effectively Infinite Length Chambers.* NAVORD Report 3636, 1954.

2.35 Stephenson, W.B. — *Theoretical Light-Gas Gun Performance.* Arnold Engineering Development Center, AEDC-TR-61-1, 1961.

2.36 Vasiliu, J. — *Analysis of Chambered, Finite Length Hypervelocity Launchers by the Method of Characteristics. A Complete Solution.* Republic Aviation Corp., Report RAC 1617, 1963.

2.37 Zondek, B. — *A Computing Program for the Interior Ballistics of a Hypervelocity Gun.* US Naval Weapons Lab. Report 1743, 1964.

2.38 von Neumann, I. Richtmyer, R.D. — *A Method for the Numerical Calculation of Hydrodynamic Shocks.* J. of Applied Physics, Vol.21, 1932.

2.39 Swift, H.F. Porter, C.D. Condon, J.J. Baker, J.R. — *NRL Hypervelocity Accelerator Development.* Proceedings of the Sixth Hypervelocity Impact Symposium, Vol.1, 1963.

2.40 Kovitz, H.E. — *An Electrically Heated Light Gas Gun for Wake Ionization Studies and Preliminary Results.* AVCO Everett Research Note 201, 1960.

2.41 Glass, I.I. — *Hypervelocity Launchers. Part 1: Simple Launchers.* University of Toronto, UTIAS Review No.22, 1962.

2.42 Glass, I.I. — *Hypervelocity Launchers. Part 2: Compound Launchers - Driving Techniques.* University of Toronto Institute for Aerospace Studies, Review No.26, 1965.

2.43 Glass, I.I. — *Shock and Combustion-Wave Dynamics in an Implosion-Driven Hypervelocity Launcher.* University of Toronto Institute for Aerospace Studies, Review No.25, 1965.

2.44 Sevray, P.A.L. — *Performance Analysis of UTIAS Implosion-Driven Hypervelocity Launcher.* University of Toronto Institute for Aerospace Studies, TN-121, January 1968.

2.45 Crosby, J.K. Gill, S.P. — *Feasibility Study of an Explosive Gun.* Stanford Research Institute Final Report No.2. Prepared for Ames Research Center under Contract NAS2-1361, 1966.

2.46 Moore, E.T. Godfrey, C.S. Waldron, H.F. — *Recent Developments in the Use of Chemical Explosives for Hypervelocity Test Devices.* Proceedings of the Fifth Hypervelocity Techniques Symposium, University of Denver, 1967.

2.47 Cable, A.J. — *The Performance of the RARDE 1/4-In. Calibre Hypervelocity Launcher.* RARDE Memorandum 14/64, 1964.

2.48 Waldron, H.F. McMahon, H.M. Letarte, M. — *Free Flight Facilities and Aerodynamic Studies at CARDE.* IAS Preprint No.60-90, 1960.

2.49 Liepmann, H.W. Roshko, A. — *Elements of Gasdynamics.* John Wiley & Sons, Inc., 1957.

2.50 Bradley, J.N. — *Shock Waves in Chemistry and Physics.* John Wiley & Sons, Inc., 1962.

2.51 Glass, I.I. Hall, J.G. — *Shock Tubes.* Handbook of Supersonic Aerodynamics, Section 18, NAVORD Report 1488, Vol.6, 1959.

2.52 Evans, C. Evans, F. — *Shock Compression of a Perfect Gas.* J. of Fluid Mechanics, Vol.1, Part 4, 1956.

2.53 Watson, J.D. Godfrey, C.S. — *An Investigation of Projectile Integrity Using Computer Techniques.* Proceedings of the Fifth Hypervelocity Techniques Symposium, University of Denver, 1967.

2.54 Baker, J.R. — *A Comparison of Shock and Isentropic Heating in Light-Gas Gun Compression.* US Naval Research Lab. Report 6063, 1964.

2.55 Stollery, J.L. Maull, D.J. — *A Note on the Compression of Air Through Repeated Shock Waves.* J. of Fluid Mechanics, Vol.4, Part 6, 1958.

2.56 Bioletti, C. Cunningham, B.E. — *A High Velocity Gas Employing a Shock Compressed Light Gas.* NASA TN D-307, 1960.

2.57 Lord, M.E. — *Performance of a 40-mm, Combustion Heated, Light Gas Gun Launcher.* AEDC-TN-60-176, 1960.

2.58 Knystautas, R. Leftheris, B. — *An Analysis of the Double Shock Compression Light Gas Gun Cycle.* CARDE TR 516/65, 1965.

2.59 Winter, D.F.T. — *Multiple Shock Compression Using a Piston of Finite Weight.* J. of Fluid Mechanics, Vol.8, Part 2, 1960.

2.60 Bull, G.V. — *Hypervelocity Research in the CARDE Free Flight Ranges.* Galbraith Building Opening Ceremonies, University of Toronto, 1961.

2.61 Stephenson, W.B. Anderson, D.E. — *Design of a Large, Two-Stage, Light-Gas Model Launcher.* AEDC TR-61-6, 1961.

2.62 Lukasiewicz, J. Stephenson, W.B. Clemens, P.L. Anderson, D.E. — *Development of Hypervelocity Range Techniques at Arnold Engineering Development Center.* AEDC TR-61-9, 1961.

2.63 Stephenson, W.B. Knapp, R.E. — *Performance of a Two-Stage Launcher Using Hydrogen.* AEDC TDR-62-32, 1962.

2.64 Lemcke, B. — *An Investigation of the Performance of a Compression Heater for Use with Gun Tunnels or Hypervelocity Launchers.* Aeroelastic and Structures Research Lab. MIT Report 1010, 1963.

2.65 Curtis, J.S. — *An Accelerated Reservoir Light-Gas Gun.* NASA TN D-1144, 1962.

2.66 Bird, C.A. — *The Effect of Wall Shape on the Degree of Reinforcement of a Shock Wave Moving into a Converging Channel.* J. of Fluid Mechanics, Vol.5, Part 1, 1959.

2.67 Laporte, O. — *On the Interaction of a Shock with a Constriction.* Los Alamos Scientific Lab., University of California, LA-1740, 1954.

2.68 Charters, A.C. — *The Free-Flight Range. A Tool for Research in the Physics of High Speed Flight.* ARS Preprint 1984-61, 1961.

2.69 Wilenius, G.P.T. — *Slow Piston Gun Development at CARDE.* ARPA, CARDE, ARGMA Symposium on Aeroballistic Ranges. CARDE TM-Q-646/61, 1961.

2.70 Smith, F. — *Theory of a Two-Stage Hypervelocity Launcher to Give Constant Driving Pressure at the Model.* RARDE Report (B) 5/63, 1963.

2.71 Wilenius, G.P.T. Cloutier, M. Cowen, P.L. — *A Theoretical Analysis of a Constant Base Pressure Light-Gas Gun.* CARDE TN 703/62, 1962.

2.72 Curtis, J.S. — *An Analysis of the Interior Ballistics of the Constant Base Pressure Gun.* Proceedings of the Third Hypervelocity Techniques Symposium, Denver, 1964.

2.73 Winkler, E.H. — *The Presentation of the Propellant Flow in a Constant Acceleration Gun by the Method of Characteristics.* NOL TR 64-69, 1964.

2.74 Winkler, E.H. — *The Constant Acceleration Gas Gun Problem.* NOL TR 64-111, 1964.

2.75 Somes, J. — *Analytical Solution of a Special Gun Problem.* Naval Weapons Lab. TM K-45/64, 1964.

2.76 Charters, A.C.; Curtis, J.S. — *High Velocity Guns for Free Flight Ranges. The High Temperature Aspects of Hypervelocity Flow.* AGARDograph 68, 1964. Also, General Motors Corp., Defense Research Lab. TM62-207, 1962.

2.77 Lukasiewicz, J. — *Constant Acceleration Flows and Applications to High-Speed Guns.* AEDC-TR-66-181, 1966.

2.78 Seigel, A.E.; Piacesi, R.; Bixler, D.N. — *Wall Friction, Heat Transfer, and Real-Gas Propellant Effects in High Speed Guns.* Proceedings of the Fourth Hypervelocity Techniques Symposium, Tullahoma, 1965.

2.79 Bixler, D.N.; Seigel, A.E. — *Calculations of the Flow Conditions in a Constant Base Pressure Launcher with a Real Hydrogen Gas Propellant.* NOL TR 66-157, 1966.

2.80 Stanyukovich, K. — *Unsteady Motion of Continuous Media.* Pergamon Press, London, 1960, pp.605-607.

2.81 Seigel, A.E. — *A Convenient and Accurate Semi-Empirical Entropic Equation for Use in Internal Ballistic Calculations.* NAVORD Report 2695, 1953.

2.82 Bixler, D.N.; Piacesi, R.; Seigel, A.E. — *Calculated Thermodynamic Properties of Real Hydrogen up to 30,000 Atmospheres and 3500° K.* NOL TR 65-209, 1965.

2.83 Wooley, H.W.; Scott, R.B.; Brickwedde, F.G. — *Complication of Thermal Properties of Hydrogen in its Various Isotopic and Ortho-Para Modifications.* National Bureau of Standards Research Paper RP1932, Vol.41, 1948.

2.84 Baker, J.R.; Geatches, W.H.; Swift, H.F. — *Theoretical Theromodynamic Properties of Gases at High Temperatures and Densities with Numerical Results for Hydrogen.* NRL Report 6675, September 27, 1968.

2.85 Richtmyer, R.D. — *Difference Methods for Initial Value Problems.* Interscience Publishers, Inc., New York, 1957.

2.86 Piacesi, R.; Gates, D.F.; Seigel, A.E. — *Computer Analysis of Two-Stage Hypervelocity Model Launchers.* NOL TR 62-87, 1963.

2.87 Baer, P.G.; Smith, H.C. — *Experimental and Theoretical Studies on the Interior Ballistics of Light Gas Guns.* Sixth Symposium on Hypervelocity Impact, Cleveland, Ohio, 1963.

2.88 Cable, A.J.; DeWitt, J.R. — *Optimizing and Scaling of Hypervelocity Launchers and Comparison with Measured Data.* AEDC TR-67-82, 1967.

2.89 Badhwar, L.K.; Murphy, J.R.B. — *A New Interior Ballistics Computation System for Light Gas Guns.* Computing Devices of Canada, Report 9825/R1, 1965.

2.90 Murphy, J.R.B.; Badhwar, L.K.; Lavoie, G.A. — *Interior Ballistics Calculations Systems for Light Gas Guns and Conventional Guns.* The Fluid Dynamic Aspects of Ballistics, AGARD Conference Proceedings No.10, 1966.

2.91 Longley, H.J. — *Methods of Differencing in Eulerian Hydrodynamics.* Los Alamos Scientific Lab., University of California, LAMS-2379, 1960.

2.92 Vasiliu, J. — *Piston Motion and Shock Wave Formation in a Free-Piston Cycle – A Computer Solution.* Republic Aviation Corp., Report RAC 2553, 1964.

2.93 Dimeff, J.; Carson, J.A.; Charters, A.C. — *A Piston-Type Strain Gage for Measuring Pressures in Interior Ballistics Research.* Review of Scientific Research, September 1955.

2.94 Hruby, R.J.
Sander, R.C.
Berggren, R.E.
Microwave Technique for Measuring Projectile Time History in Light-Gas Guns. IEEE Second International Congress on Instrumentation in Aerospace Simulation Facilities. Stanford University, August 1966.

2.95 Anderson, D.E.
Prince, M.D.
Design of Light-Gas Model Launchers for Hypervelocity Research. AEDC-TDR-62-97. 1962.

2.96 Stephenson, W.B.
Anderson, D.E.
Performance of Two-Stage Light-Gas Model Launchers. IAS Thirtieth Annual Meeting, New York, January 1962.

2.97 Eckerman, J.
McKay, W.L.
Performance of a Three-Stage Arc Heated Light Gas Gun. Proceedings of the Sixth Symposium on Hypervelocity Impact, Cleveland, Ohio, Vol.1, August 1963.

2.98 Swift, H.F.
Baker, J.R.
Hypervelocity Capability and Impact Effect Program. Final Report, NRL Memorandum Report 1677, 1966.

2.99 Collins, D.J.
Charters, A.C.
Christman, D.R.
Sangster, D.K.
Parametric Studies of Light-Gas Guns. Fifth Hypervelocity Techniques Symposium, University of Denver, March 1967.

2.100 Cable, A.J.
DeWitt, J.R.
Lukasiewicz, J.
Prepared Comments on the Calculation and Measurement of the Performance of Hypervelocity Launchers. Fifth Hypervelocity Techniques Symposium, University of Denver, 1967.

2.101 Rudinger, George
Wave Diagrams for Nonsteady Flow in Ducts. D. van Nostrand Co., New York, 1955.

2.102 Leech, C.
Piston Extrusion in Light-Gas Guns. CARDE TR 580/67, 1967.

2.103 Fleming, D.
Williams, R.
An Interior Ballistics System for a Propellant Driven Piston. CARDE TM 626/61, 1961.

2.104 Johnson, R.
Shock Phenomenon in Gas Gun Propellant Chambers as a Function of Charge Length. CARDE TN 1605/64, 1964.

2.105 Brooks, P.N.
A Comparative Review of Strength Criteria. CARDE TN 1583/63, 1963.

2.106 Davidson, T.E.
Barton, C.S.
Reiner, A.N.
Kendall, D.P.
The Autofrettage Principle as Applied to High Strength Light Weight Gun Tubes. Watervliet Arsenal WVT-RI-5907, 1959.

2.107 Dawson, V.C.D.
Seigel, A.E.
Reverse Yielding of Fully Autofrettaged Tube of Large Wall Ratio. NOL TR 63-123, 1963.

2.108 Dawson, V.C.D.
Limitations of the Autofrettage Process for High Strength Guns. Proceedings of the Third Hypervelocity Techniques Symposium, March 1964.

2.109 Dawson, V.C.D.
Residual Bore Stress in an Autofrettaged Cylinder Constructed of a Strain Hardening Material. NOL TR 64-25, 1964.

2.110 Dawson, V.C.D.
Seigel, A.E.
High Pressure Chamber Design. NOL TR 67-121, 1967.

2.111 Timoshenko, S.
Strength of Materials. Part II, 3rd edition, D. van Nostrand Co., New York, 1956.

2.112 Cloutier, M.
Design of High-Pressure Sections for Light-Gas Guns. CARDE TR 529/65, 1965.

2.113 Rast, J.J.
The Design of Flat Scored High Pressure Diaphragms for Use in Shock Tunnels and Gas Guns. NOL Report 6865, 1961.

2.114
Proceedings of the Seventh Hypervelocity Impact Techniques Symposium, Tampa, Florida, February 1965.

TABLE 2.1

Properties of Propellant Gases

Gas	p *(bars)*	γ	ρ *(kg/m^3)*	a *(m/s)*	ρa *(kg/m^{2}s)*	a/γ *(m/s)*	C_p *(kJ/kg°K)*	C_v *(kJ/kg°K)*	C_pT *(kJ/kg)*
Hydrogen	1*	1.40	0.0887	1,260	1.12×10^2	899	14.3	10.2	3,910
	2,000†	1.40	20.2	3,730	7.53×10^4	2,660	14.3	10.2	34,200
Helium	1*	1.67	0.176	971	1.71×10^2	583	5.19	3.11	1,420
	2,000†	1.67	16.8	4,440	7.46×10^4	2,660	5.19	3.11	29,700
Air	1*	1.40	1.27	330	4.19×10^2	236	1.01	0.722	274
	2,000†	1.40	291.	974	2.83×10^5	695	1.01	0.722	2,400
Gun Powder	1*	~1.25	1.23	318	3.91×10^2	254	1.48	1.18	405
	2,000†	~1.25	542.	681	3.69×10^5	545	1.48	1.18	1,850

*At T = 273° K.

†Isentropic compression neglecting caloric and thermal imperfections and intermolecular forces.

TABLE 2.2

Dimensions and Performance of Representative Laboratory Guns

Facility (1)	D_s *(mm)*	$\frac{L_s}{D_s}$	$\frac{D_r}{D_s}$	$\frac{L_r}{D_r}$	$\frac{V_r}{V_s}$	$\frac{V_r}{V_c}$	$\frac{V_c}{V_s}$	*Transition angle (included) (deg)*	p_{r_0} *(bars hydrogen)*	m_s *(gm)*	$\frac{G}{m_s}$	m_p *(kgm)*	u_p *(m/s)*	U *(km/s)*
Ames	5.6	273	5.82	115	82.90	1.67	49.60	14.6	2.76	0.0453	15.60	0.10	–	11.30
	[2]5.6	273	5.82	115	82.90	1.67	49.60	14.6	2.76	[3].0756	9.35	0.10	–	9.84
	5.6	264	8.04	93	184.50	4.06	45.40	11.8	1.59	0.0520	16.76	0.34	–	10.84
	5.6	264	8.04	93	184.50	4.06	45.40	11.8	1.03	0.0568	10.03	0.34	–	10.41
	7.1	357	5.53	273	129.20	36.80	3.51	8.6	0.50	0.1625	3.36	0.15	817	9.24
	7.1	357	5.53	273	129.20	36.80	3.51	8.6	1.03	0.5016	2.23	0.15	983	7.35
	12.7	300	5.07	246	105.00	27.50	3.82	8.6	0.69	0.9407	3.12	0.89	823	9.46
	12.7	300	5.07	246	105.00	27.50	3.82	8.6	1.03	3.170	1.39	0.89	879	6.72
	25.4	288	4.00	244	54.38	30.50	1.78	8.6	2.07	7.418	4.65	5.58	763	8.44
	38.1	256	4.15	208	58.30	31.90	1.83	8.6	2.07	15.205	7.30	22.70	786	9.07
	38.1	256	4.15	208	58.30	31.90	1.83	8.6	2.07	27.412	4.05	22.70	789	8.50
CARDE	38.1	312	2.67	95	5.77	6.34	0.91	14.2	[4]23.79	[3]50.0	6.17	9.08	869	5.21
	38.1	312	2.67	40	2.45	3.10	0.79	14.2	[4]59.65	[3]72.0	4.55	9.08	731	4.57
	101.6	207	2.67	41	3.10	6.60	0.47	33.4	[4]56.55	[3]1251.0	3.95	90.80	716	4.57
Douglas	7.6	200	5.13	182	124.00	3.57	34.70	11.8	1.72	0.21	5.86	0.30	731	8.84
	7.6	200	5.13	182	124.00	3.57	34.70	11.8	2.41	0.84	2.05	0.30	610	7.01
	12.7	200	4.00	120	40.15	4.64	8.65	3.6	3.45	1.00	3.69	0.40	762	9.14
	12.7	200	4.00	120	40.15	4.64	8.65	3.6	4.14	4.00	1.11	0.40	610	6.10
	19.1	240	4.67	100	43.60	10.00	4.36	6.6	6.90	[3]10.00	3.24	4.50	671	7.62
	19.1	240	4.67	100	43.60	10.00	4.36	6.6	9.66	14.00	3.24	4.50	610	6.40
	31.8	144	2.80	100	15.75	10.00	1.57	5.4	6.90	10.00	2.42	4.50	671	7.92
	31.8	144	2.80	100	15.75	10.00	1.57	5.4	9.66	[3]25.00	1.29	6.00	610	7.31
GM	5.6	200	4.53	145	67.60	1.70	39.80	7.5	4.00	0.0533	11.61	0.10	1050	10.80
	5.6	200	4.53	145	67.60	1.70	39.80	7.5	–	0.0822	–	–	–	10.30
	20.0	380	4.45	148	34.40	7.97	4.32	7.8	–	3.73	–	–	–	9.90
	20.0	380	4.45	148	34.40	7.97	4.32	7.8	4.70	[3]11.04	2.90	10.40	522	7.50
	60.0	382	4.23	141	28.10	8.27	3.40	7.7	–	87.0	–	–	–	8.90
	60.0	382	4.23	141	28.10	8.27	3.40	7.7	6.20	[3]500.0	1.89	252.00	436	5.90
NOL	12.7	480	4.00	60	8.06	1.02	7.90	41.2	28.62	[3]1.30	11.34	0.20	–	8.17
	12.7	480	4.00	60	8.06	1.02	7.90	41.2	28.62	[3]1.66	8.88	0.20	–	7.30
	12.7	168	2.50	134	12.50	1.79	6.98	14.3	6.55	0.90	2.04	0.20	–	7.62
	12.7	168	2.50	134	12.50	1.79	6.98	14.3	7.93	[3]4.00	0.56	0.30	–	6.10
	32.0	338	3.17	128	12.30	21.70	0.57	8.7	20.00	[3]73.0	2.42	11.00	671	5.55
	32.0	338	3.17	128	12.30	21.70	0.57	8.7	21.72	[3]95.0	2.02	11.00	661	5.18
	50.8	480	4.00	129	17.50	17.60	0.99	9.5	14.83	[3]82.0	13.47	45.40	792	6.89
	50.8	480	4.00	129	17.50	17.60	0.99	9.5	18.28	[3]220.0	6.19	143.01	610	6.40
	50.8	480	4.00	89	17.50	17.60	0.99	9.5	18.28	[3]108.0	8.36	52.66	792	7.74
	50.8	480	4.00	89	17.50	17.60	0.99	9.5	28.62	[3]250.0	5.65	102.15	671	6.61
NRL	7.6	160	3.81	68	23.78	7.35	3.23	23.6	15.50	0.41	4.15	0.30	1000	9.20
	7.6	160	3.81	68	23.78	7.35	3.23	23.6	17.10	[3]0.72	2.60	0.35	600	7.00
	21.0	205	3.93	74	21.98	8.80	2.50	62.0	18.00	5.20	9.39	4.09	–	8.00
	21.0	205	3.93	74	21.98	8.80	2.50	62.0	15.10	[3]16.20	2.53	4.09	–	7.00
	63.5	161	3.28	81	19.04	6.66	2.86	3.0	[4]20.00	253.0	4.03	43.00	–	6.16
	63.5	161	3.28	81	19.04	6.66	2.86	3.0	[4]20.00	[3]447.0	2.28	43.00	–	4.85
RARDE	6.4	200	4.00	204	65.40	[5]0.24	269.00	74.0	7.91	0.08	21.51	0.03	1097	9.20
	6.4	200	4.00	204	65.40	[5]0.24	269.00	74.0	13.08	[3]1.36	2.09	0.07	1036	3.05
	25.4	96	5.00	55	71.87	[5]0.37	193.00	180.0	7.93	14.0	21.07	1.61	792	5.18
	25.4	96	5.00	55	71.87	[5]0.37	193.00	180.0	7.93	28.0	10.53	1.62	777	3.66

[1] Facility title and address given in Table 1.1

[2] Rifled launch tube

[3] Saboted model

[4] Helium propellant gas

[5] Helium first-stage driver gas

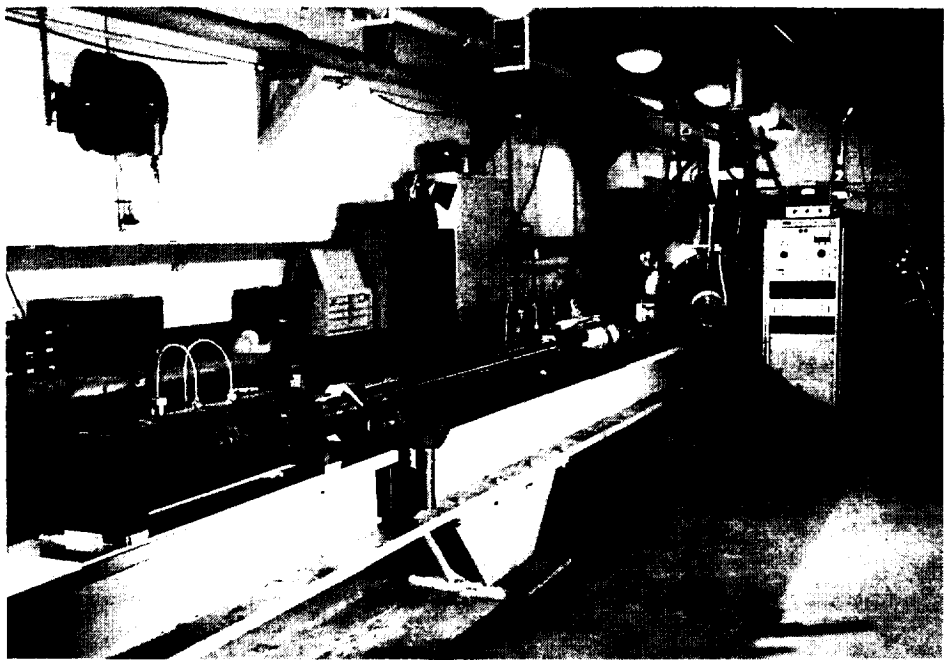

2.1 US Naval Ordnance Laboratory 12.7mm/50.8mm two-stage light gas gun

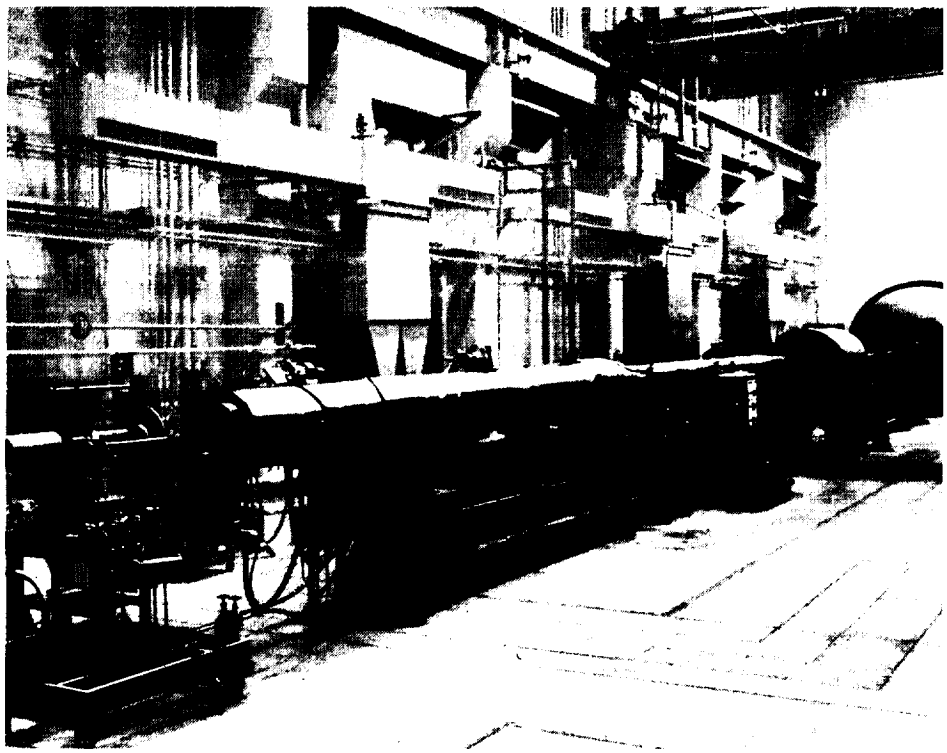

2.2 von Kármán Facility - Arnold Engineering Development Center 63.5mm/203mm two-stage light-gas gun

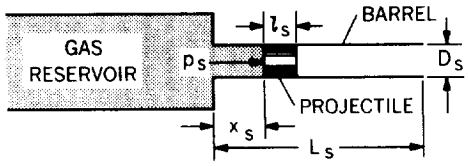

2.3 Simple light-gas gun

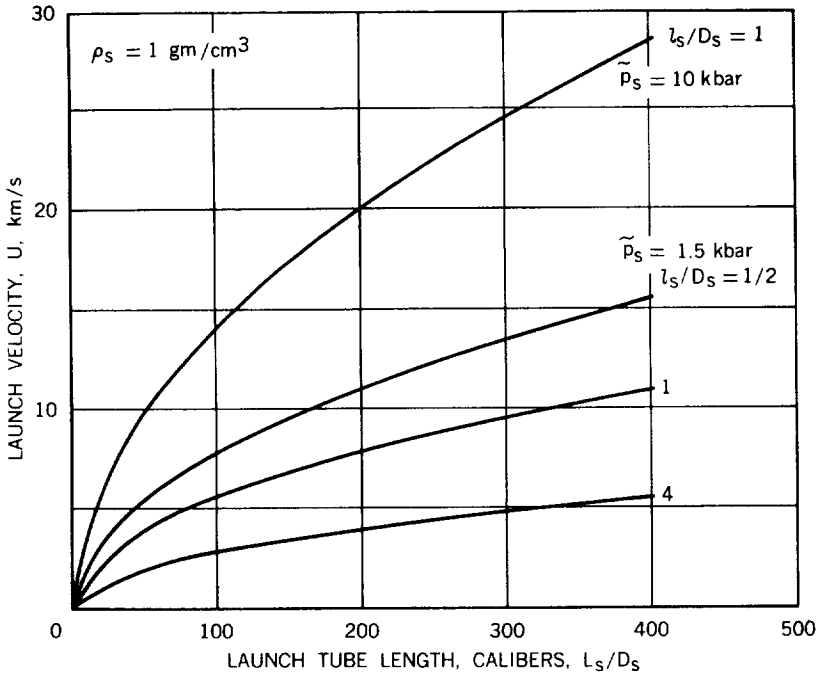

2.4 Maximum launch velocity as a function of launch-tube length for several values of base pressure and model mass

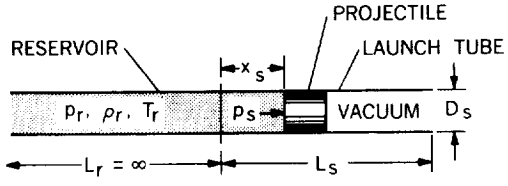

2.5 Simple constant-diameter gun

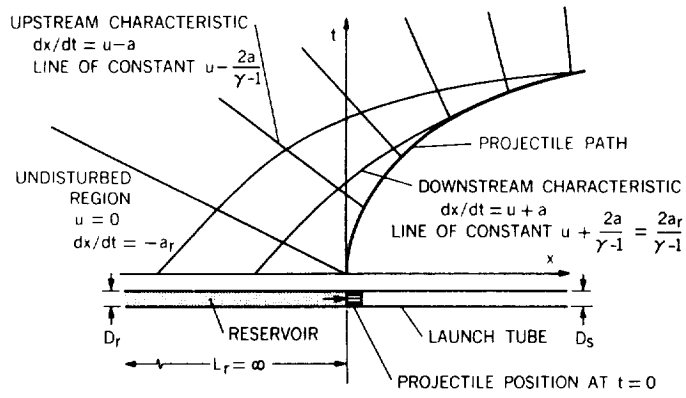

2.6 Acoustic waves in constant-diameter launcher with infinite-length reservoir

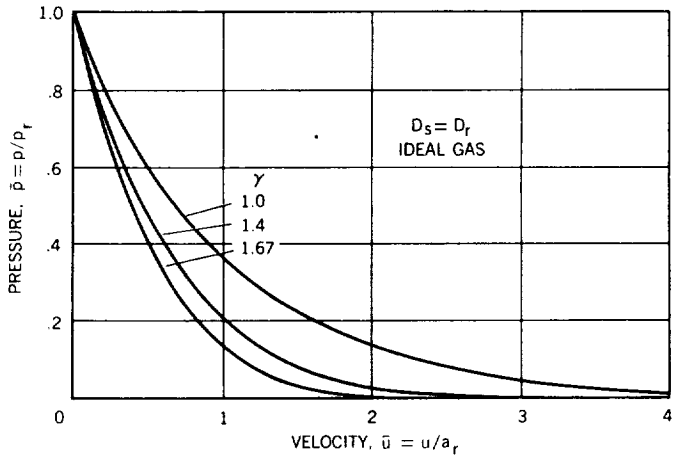

2.7 Variation of nondimensional pressure with velocity during expansion of an ideal gas in an infinitely long tube of constant diameter

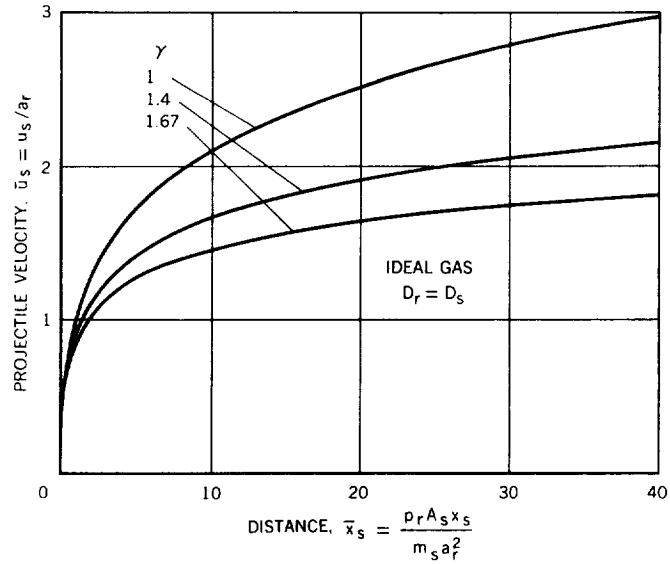

2.8 Variation of nondimensional projectile velocity with distance for the expansion of an ideal gas in an infinitely long tube of constant diameter

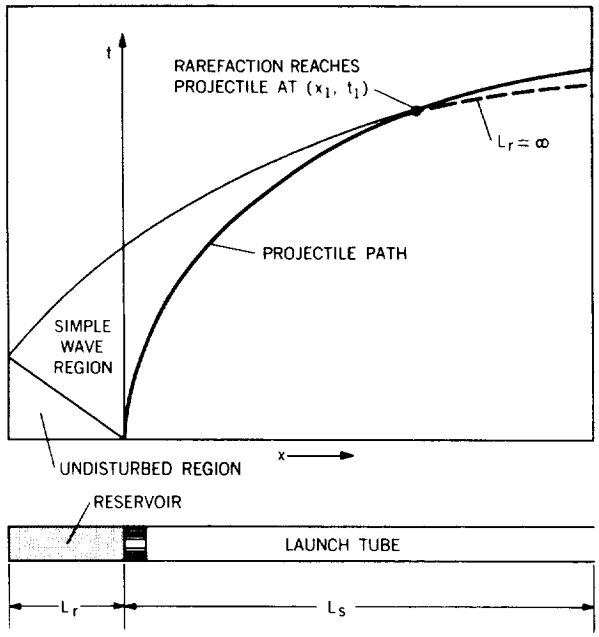

2.9 Acoustic waves in constant-diameter launcher with finite-length reservoir

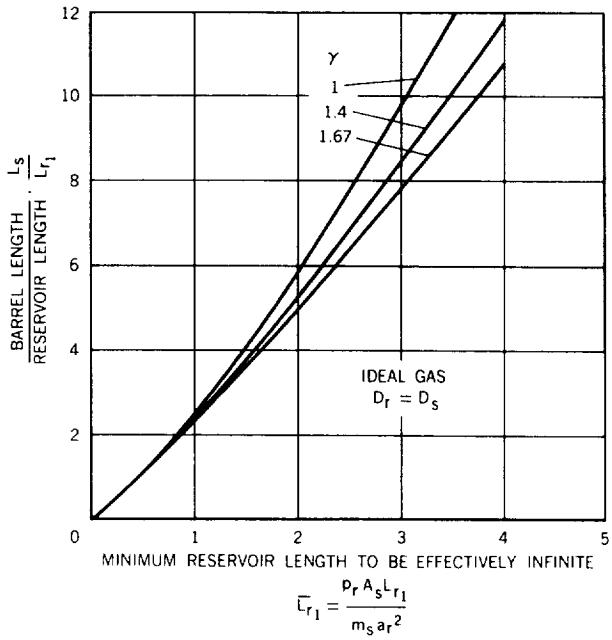

2.10 Minimum reservoir length to be effectively infinite as a function of normalized barrel length

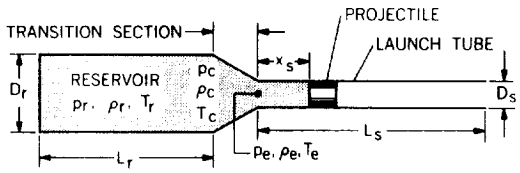

2.11 Simple light-gas gun with chambrage

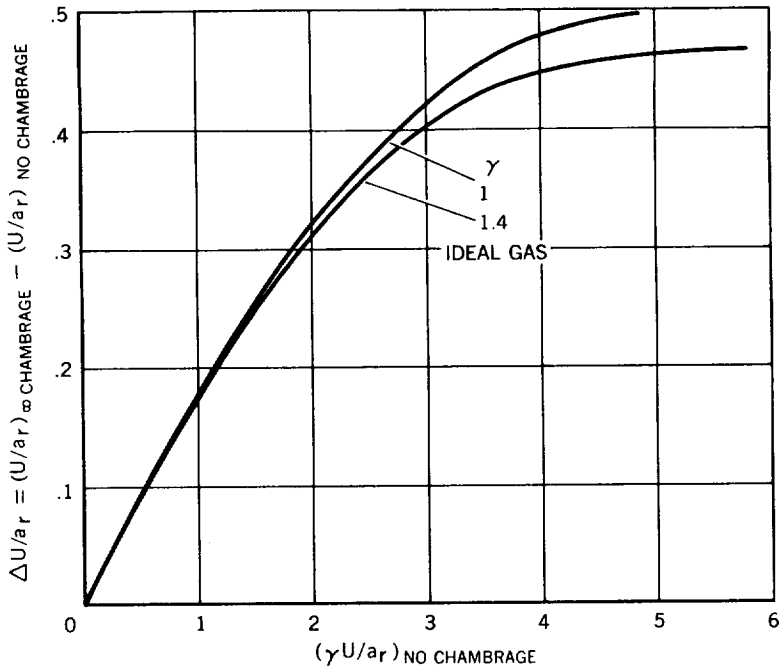

2.12 Increase in velocity due to chambrage for guns having infinite-length reservoirs. (From Seigel, Ref. 2.28)

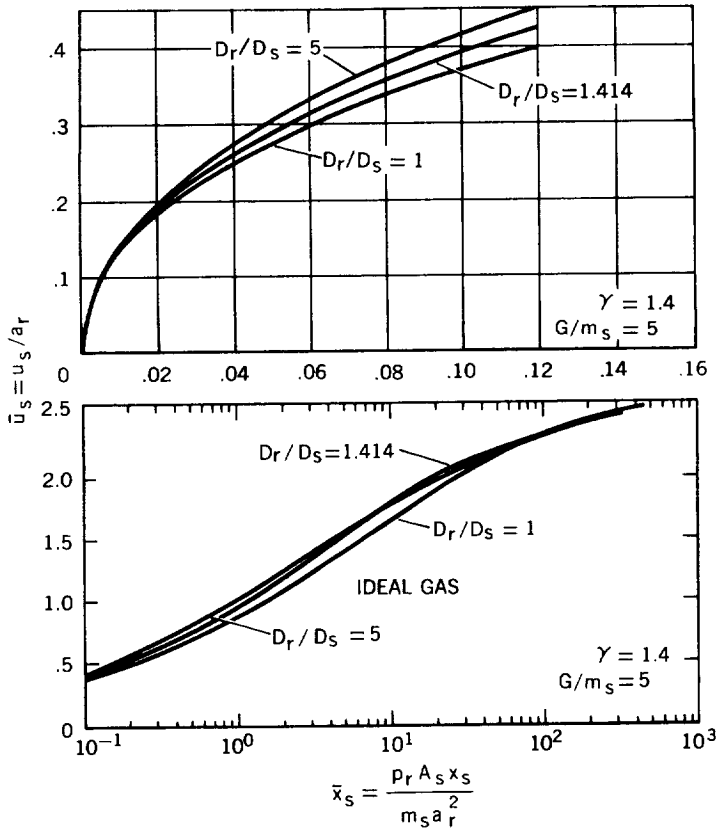

2.13 The effect of chambrage on the calculated performance of a gun with finite-length reservoir, for $\gamma = 1.4$ and gas-mass ratio, $G/m_s = 5$. (Data taken from Seigel, Ref. 2.28)

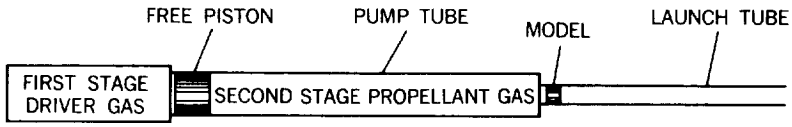

2.14 Two-stage light-gas gun

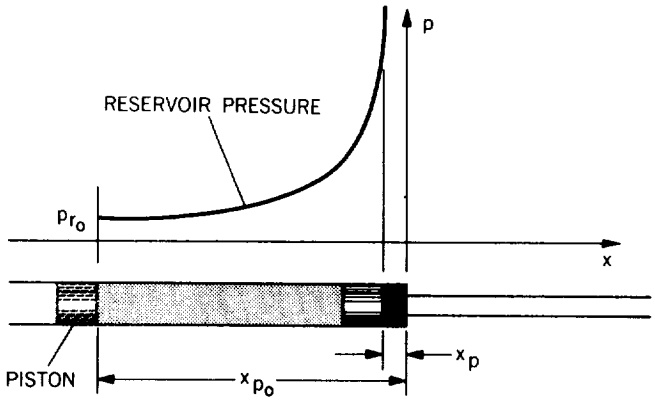

2.15 Reservoir-pressure history with isentropic compression of ideal gas

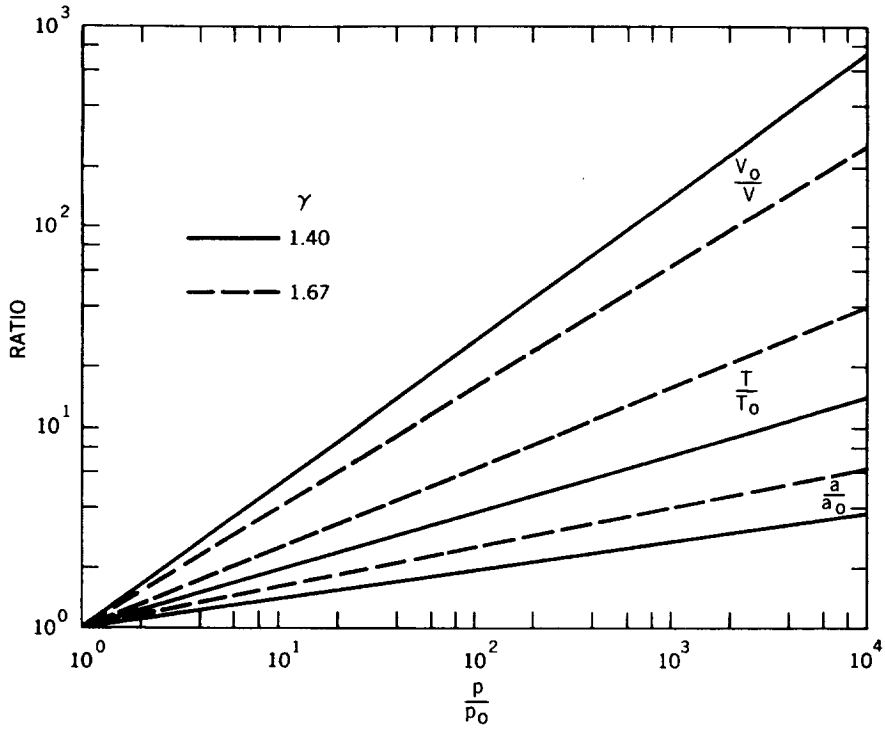

2.16 Variation of thermodynamic properties with isentropic compression

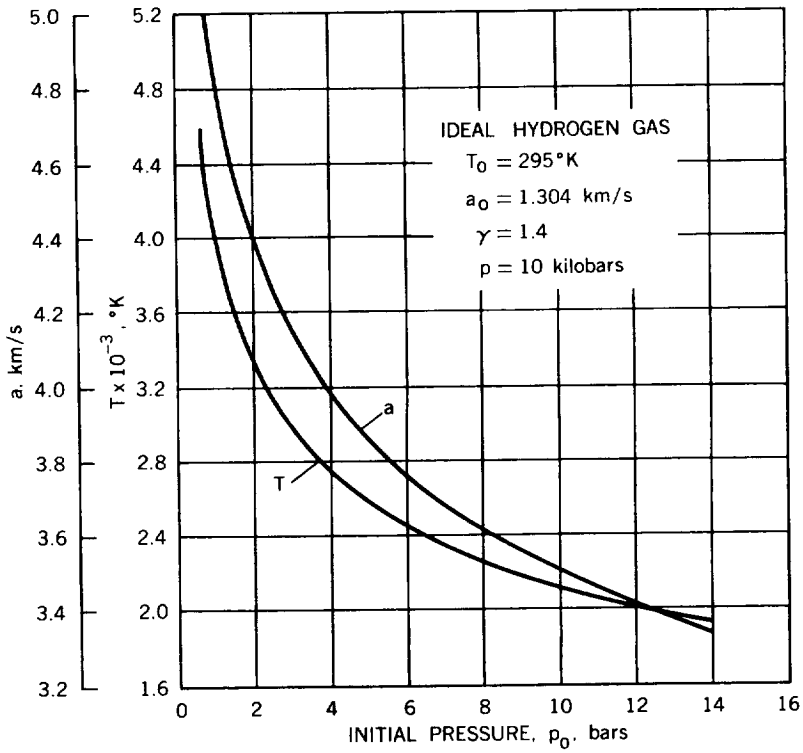

2.17 Isentropic compression of ideal hydrogen gas from initial pressure to 10 kilobars

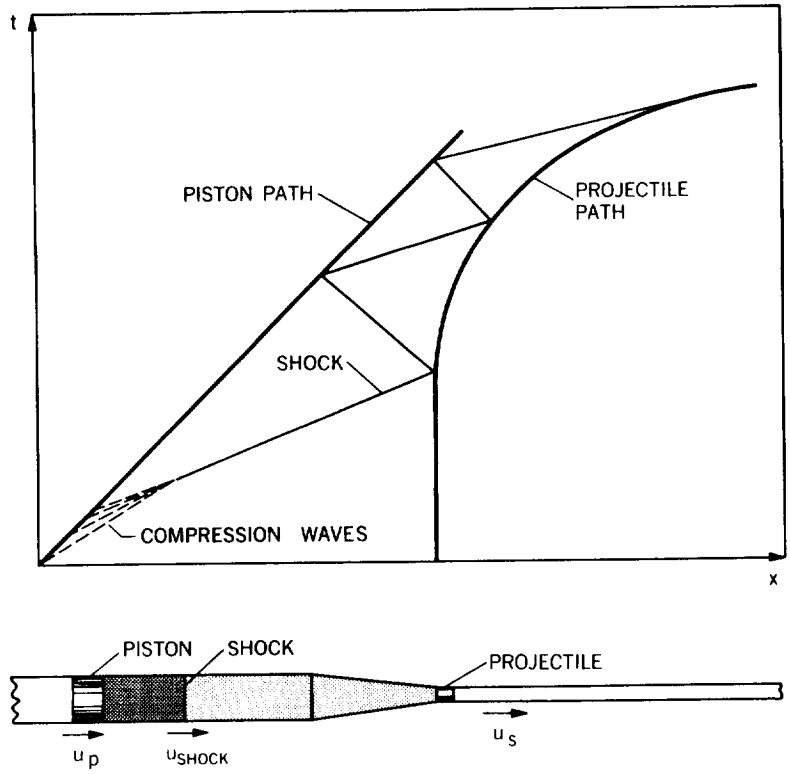

2.18 Acceleration of model by shock compression

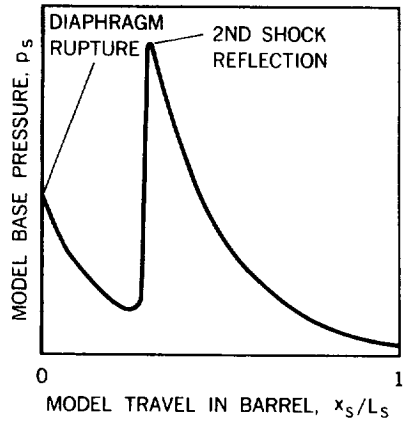

2.19 Example of model base pressure with shock compression

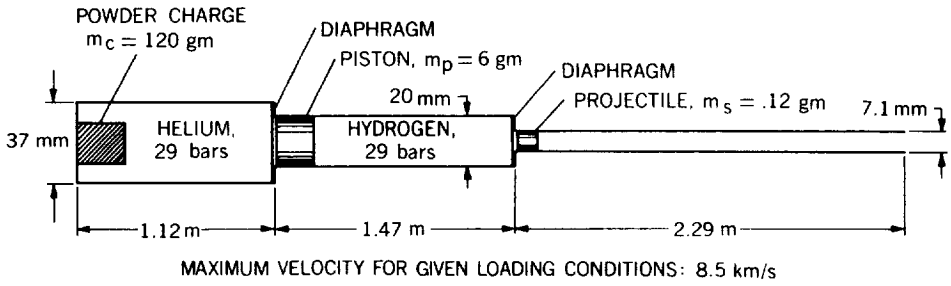

2.20 Ames Research Center 7.1 mm/20 mm two-stage shock-compression gun

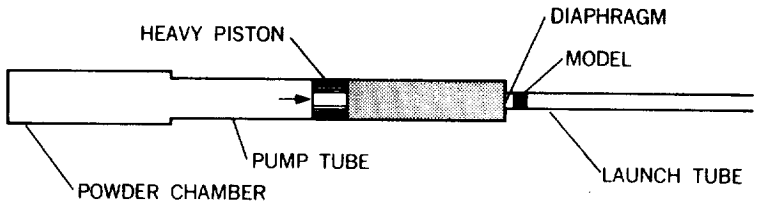

2.21 Two-stage isentropic-compression gun

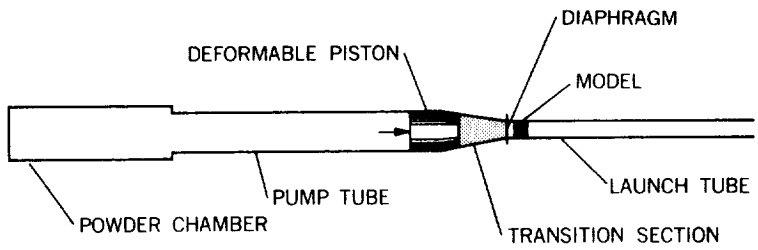

2.22 Deformable-piston isentropic-compression gun

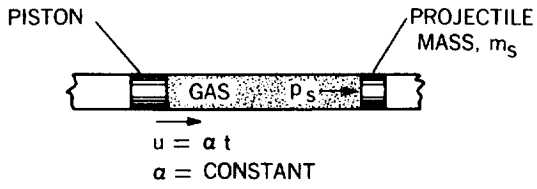

2.23 Uniform acceleration in constant-diameter tube

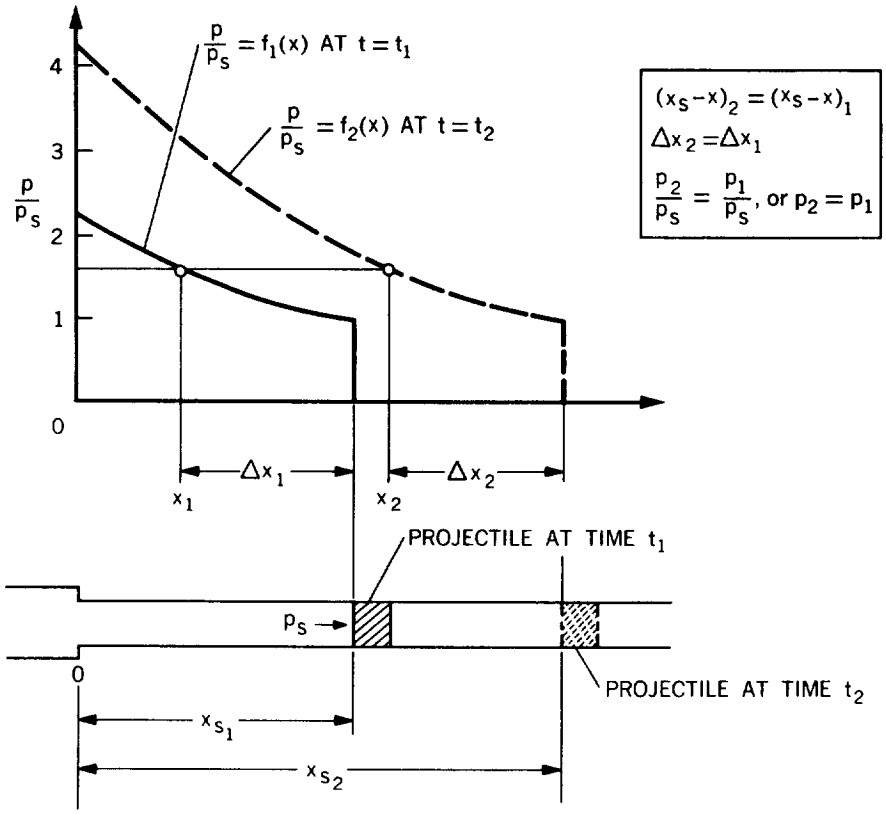

2.24 Constancy, with time, of pressure ratio, p/p_s, at a prescribed distance from the projectile base for constant-base-pressure flow

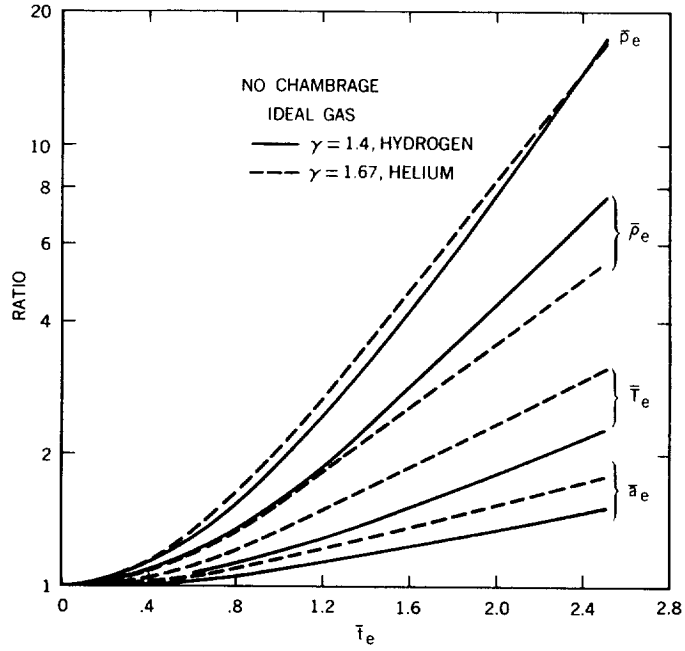

2.25 Gas conditions at entrance to barrel, as a function of time, as required by constant-base-pressure solution with isentropic compression

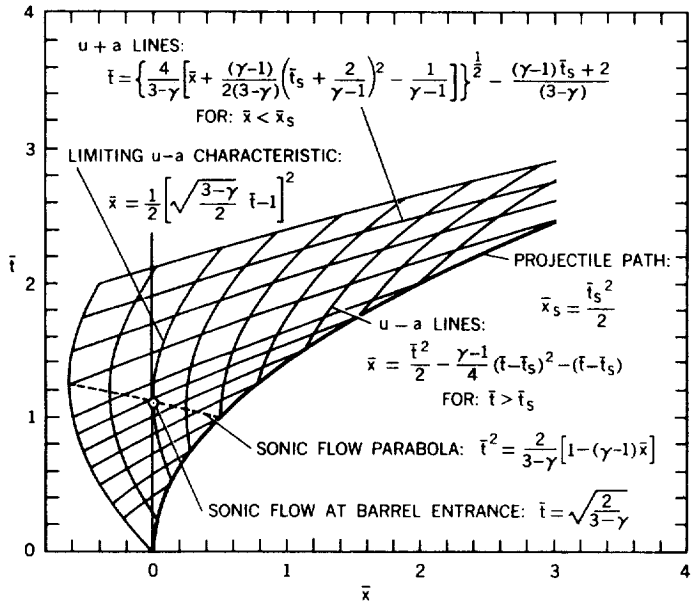

2.26 Characteristic lines for constant-base-pressure flow in an unchambered gun, γ = 1.4

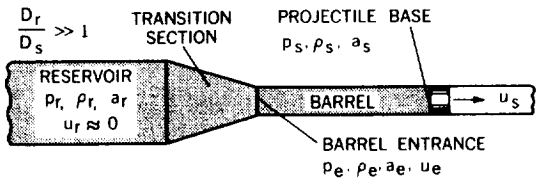

2.27 Flow parameters in chambered gun

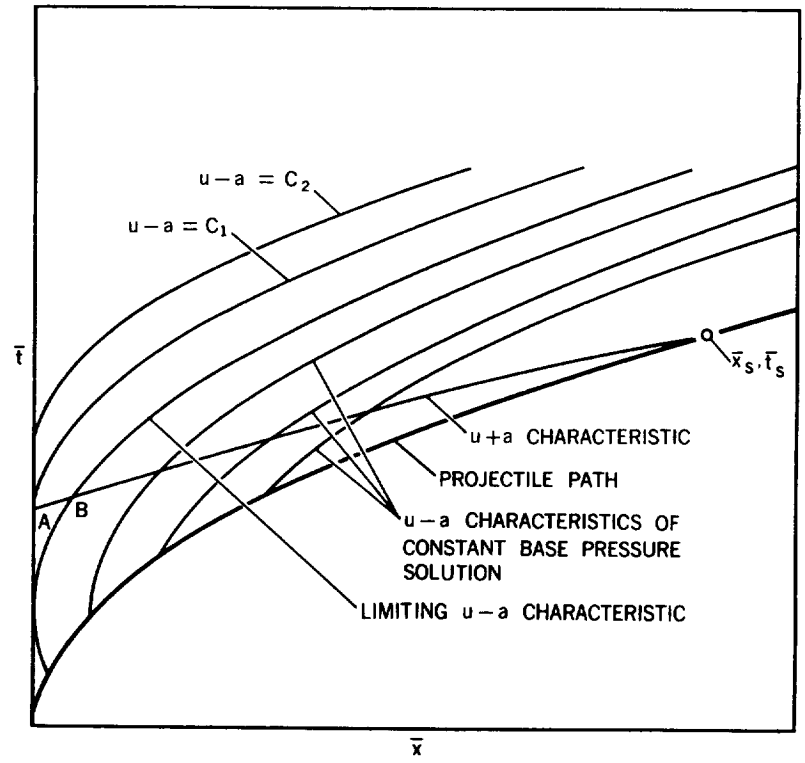

2.28 Characteristic lines for constant-base-pressure flow in a chambered gun

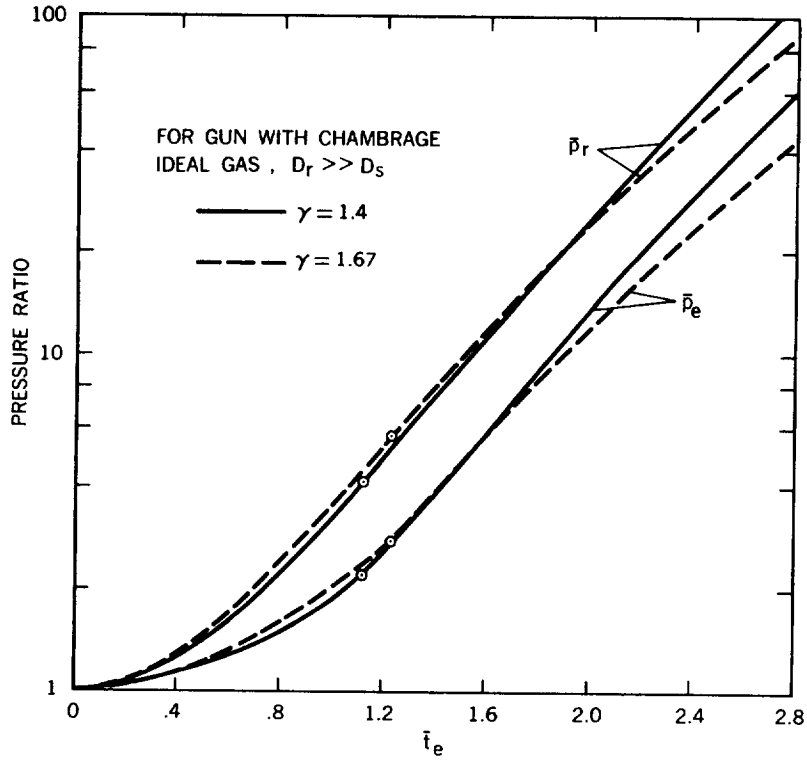

2.29 Pressure ratios in reservoir and at barrel entrance as a function of time, required by constant-base-pressure solution for a chambered gun

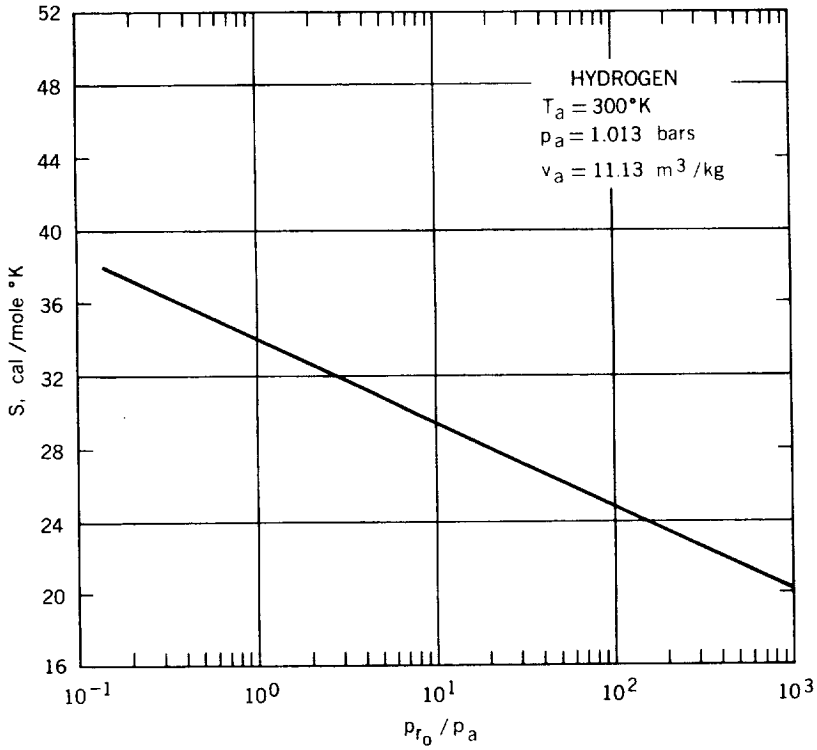

2.30 Entropy as a function of initial reservoir pressure at ambient conditions. (Data from Bixler, Piacesi, and Seigel, US Naval Ordnance Laboratory, Ref. 2.82)

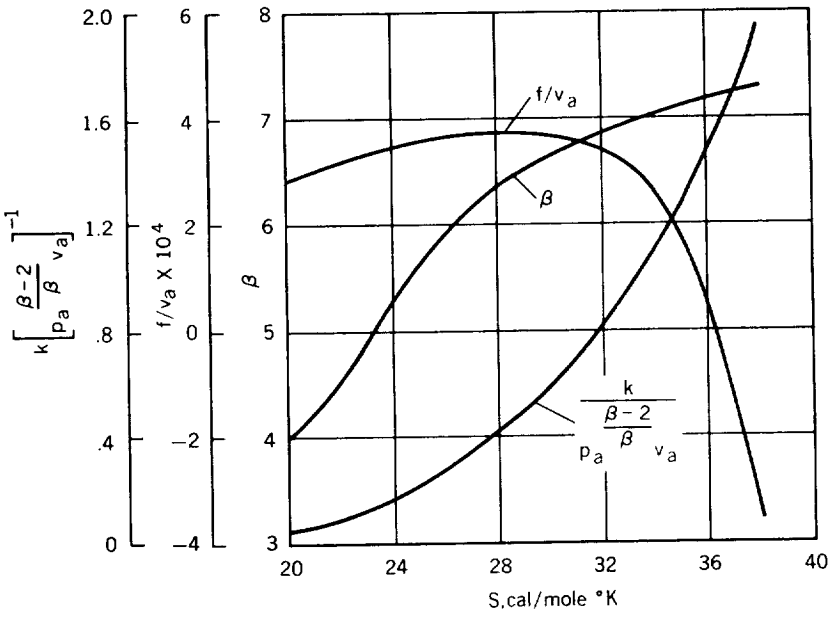

2.31 Constants in entropic equation which define behavior of real hydrogen gas. (From Bixler, Piacesi, and Seigel, US Naval Ordnance Laboratory, Ref. 2.82)

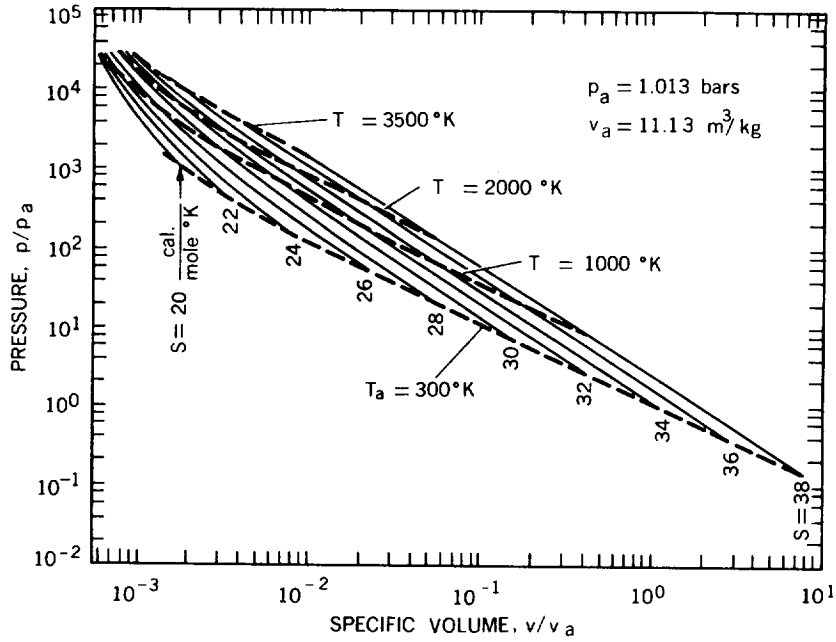

2.32 PV diagram for real hydrogen. (From Bixler, Piacesi, and Seigel, US Naval Ordnance Laboratory, Ref. 2.82)

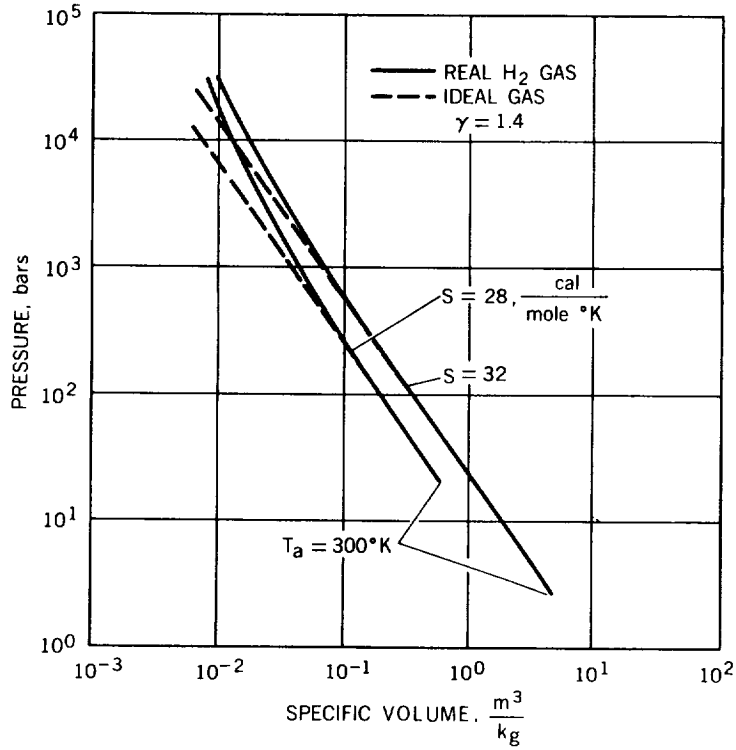

2.33 Comparison of real-gas and ideal-gas isentropes for hydrogen. (From Seigel, Piacesi, and Bixler, US Naval Ordnance Laboratory, Ref. 2.78)

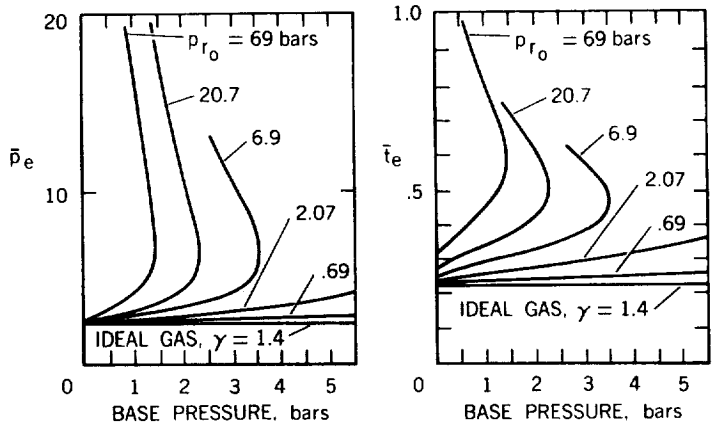

2.34 Pressure and time when flow at entrance of barrel reaches sonic speed; real hydrogen gas. (From Bixler and Seigel, US Naval Ordnance Laboratory, Ref. 2.79)

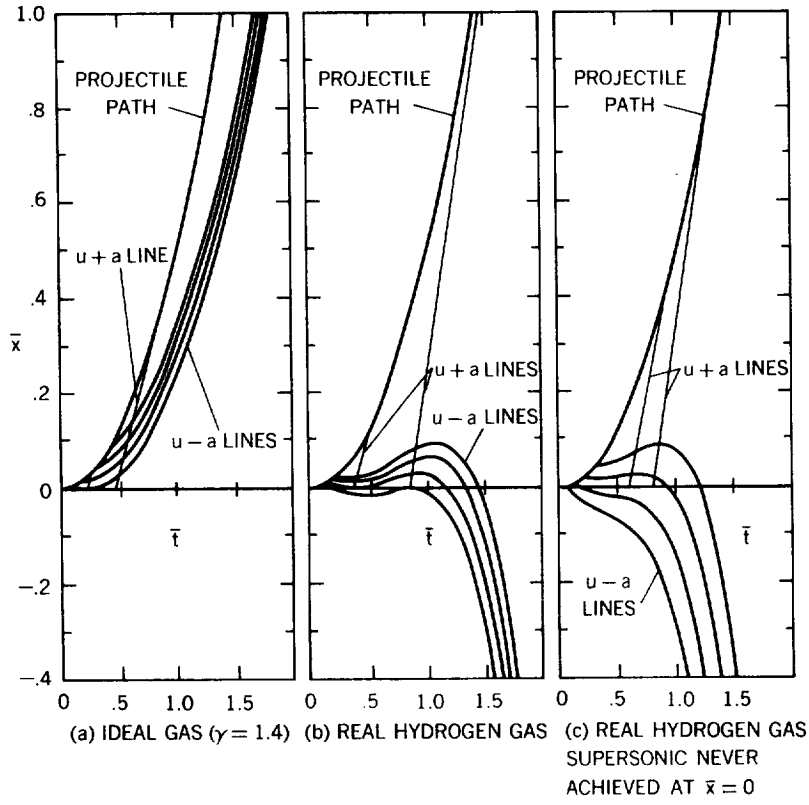

2.35 Characteristics diagram for a constant-base-pressure process in a straight tube. (From Bixler and Seigel, US Naval Ordnance Laboratory, Ref. 2.79)

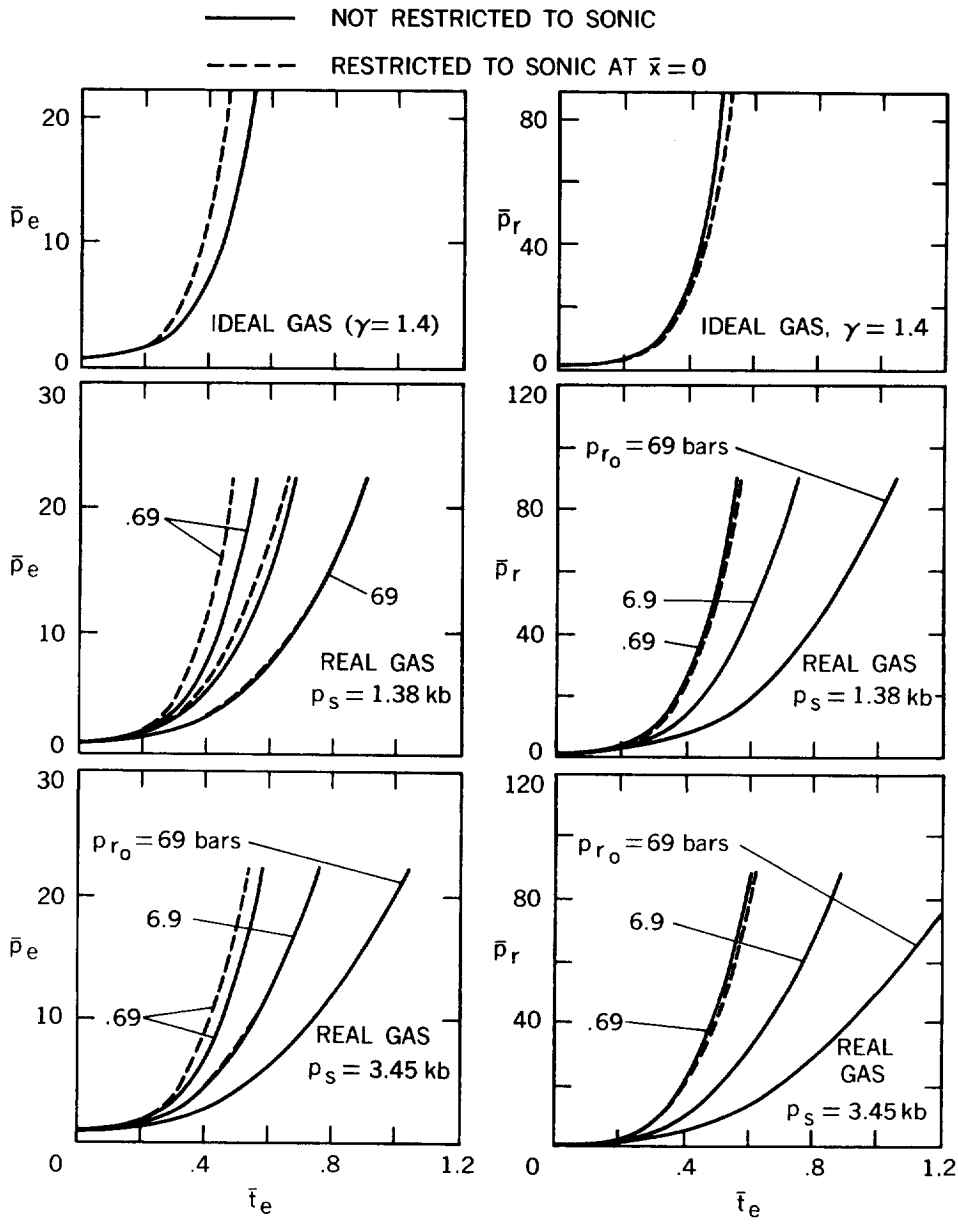

2.36 Pressure histories at the barrel entrance and reservoir in a constant-base-pressure solution for hydrogen gas. (From Bixler and Seigel, US Naval Ordnance Laboratory, Ref. 2.79)

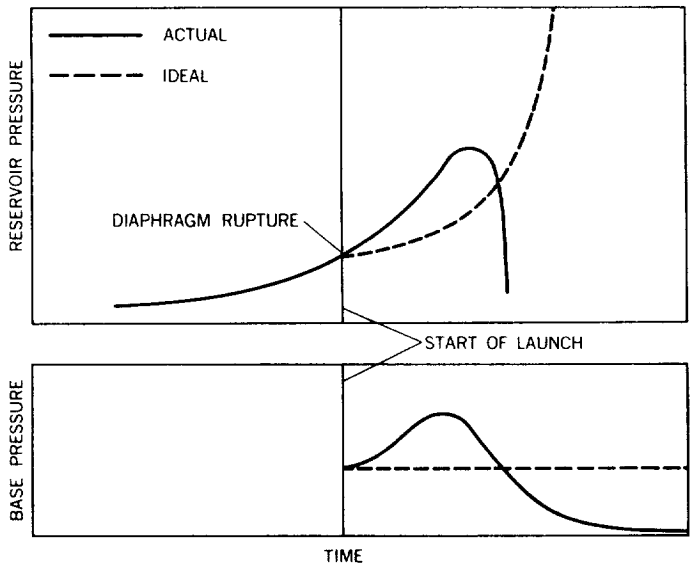

2.37 Example of actual reservoir- and base-pressure variation compared with ideal behavior

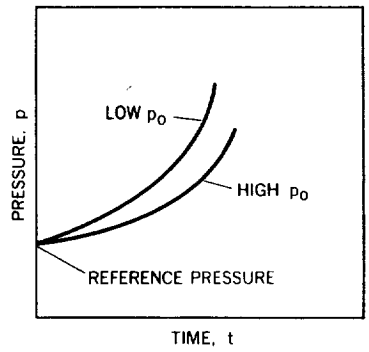

2.38 Effect of initial loading pressure on the rate-of-rise of pressure with isentropic compression, shown from some reference pressure

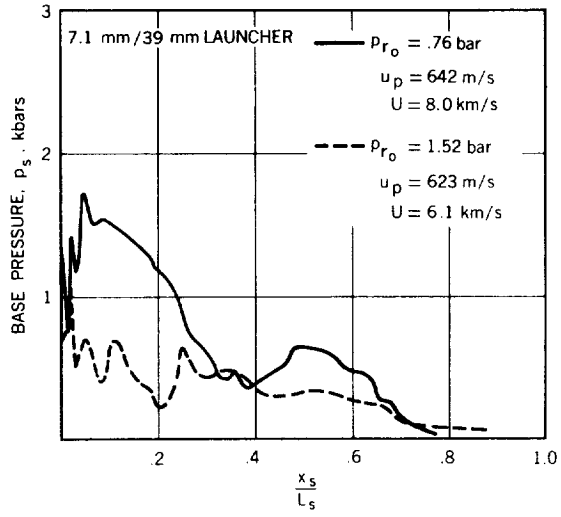

2.39 Effect of initial loading pressure on model base pressure during launch (experimental)

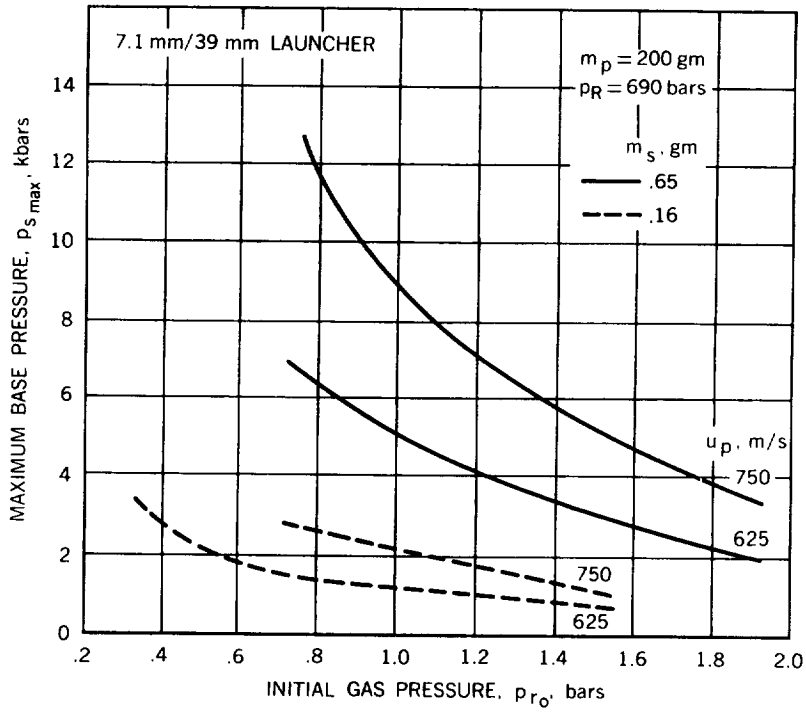

2.40 Effect of initial hydrogen pressure on maximum model base pressure, for two values of piston velocity and model weight (experimental)

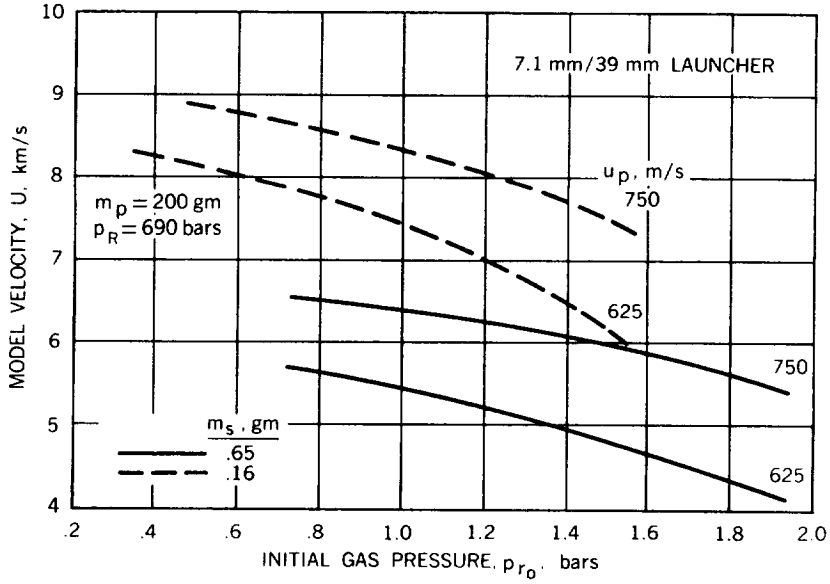

2.41 Variation of model velocity with initial hydrogen pressure, for two values of piston velocity and model weight (experimental)

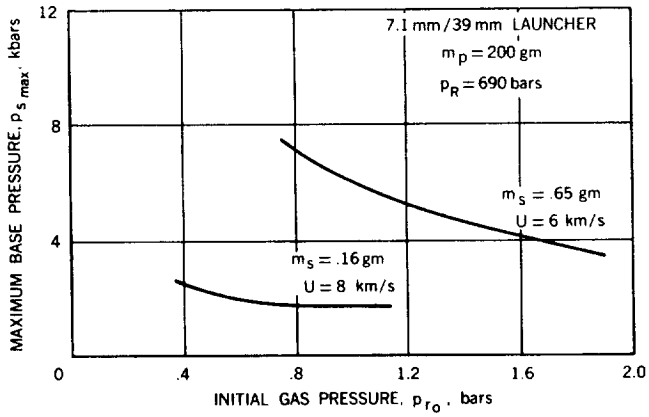

2.42 Effect of initial hydrogen pressure on the resultant maximum base pressure, at constant model velocity (experimental)

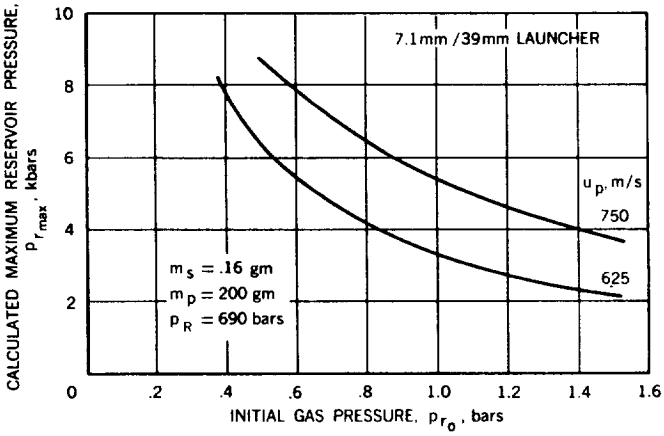

2.43 Variation of calculated maximum reservoir pressure with initial hydrogen pressure, at constant piston velocity

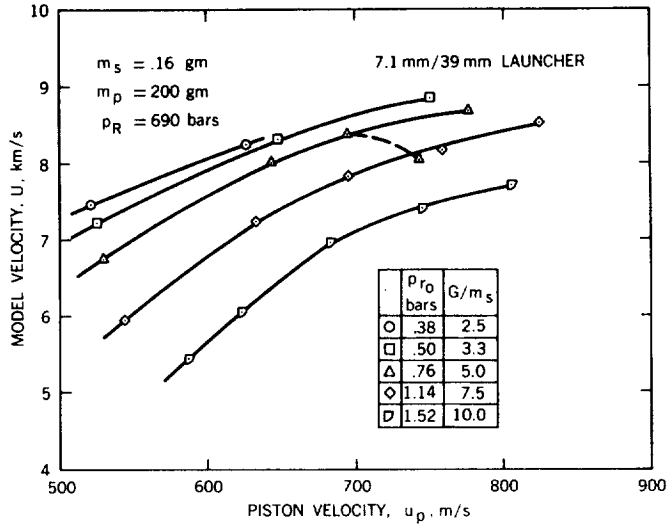

2.44 Variation of model velocity with piston velocity at constant values of initial hydrogen pressure, for a relatively light model (experimental)

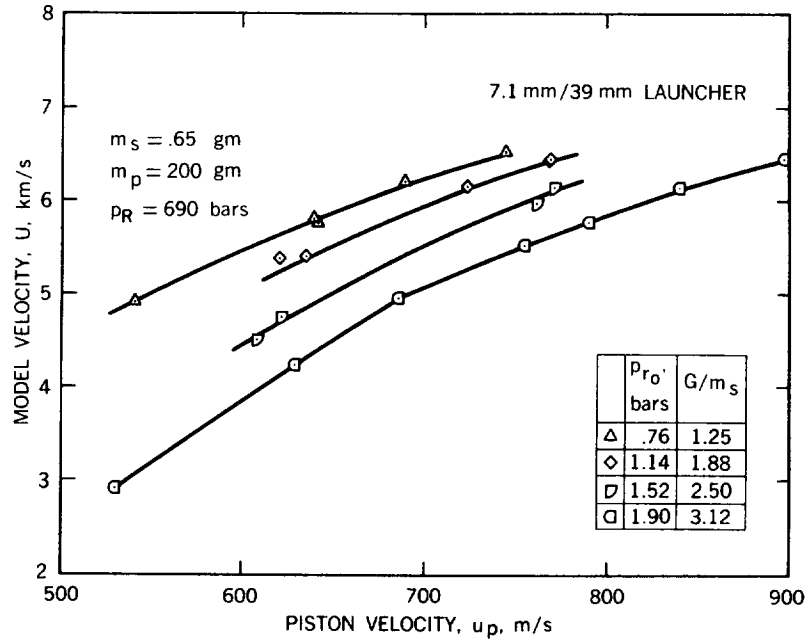

2.45 Variation of model velocity with piston velocity at constant values of initial hydrogen pressure, for a relatively heavy model (experimental)

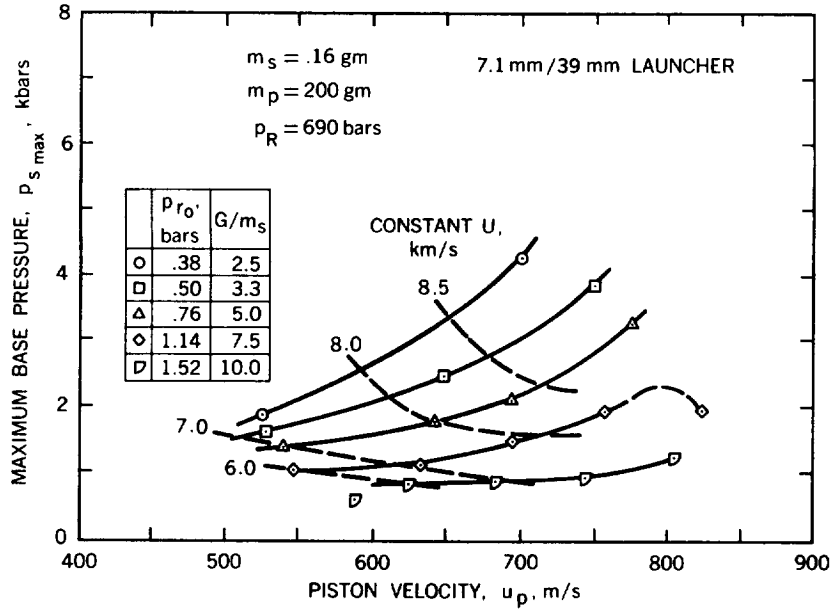

2.46 Variation of maximum base pressure with piston velocity at constant values of initial hydrogen pressure, for a relatively light model (experimental)

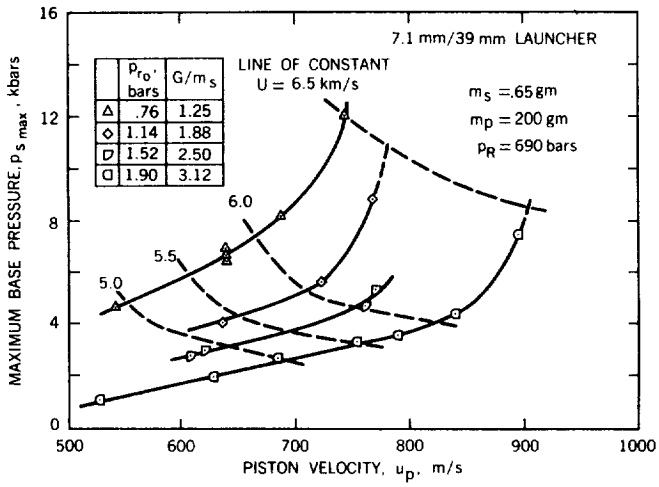

2.47 Variation of maximum base pressure with piston velocity at constant values of initial hydrogen pressure, for a relatively heavy model (experimental)

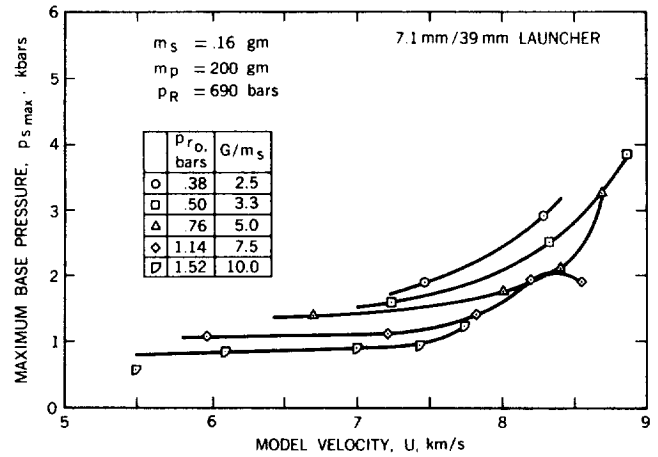

2.48 Variation of maximum base pressure with model velocity at constant values of initial hydrogen pressure, for a relatively light model (experimental)

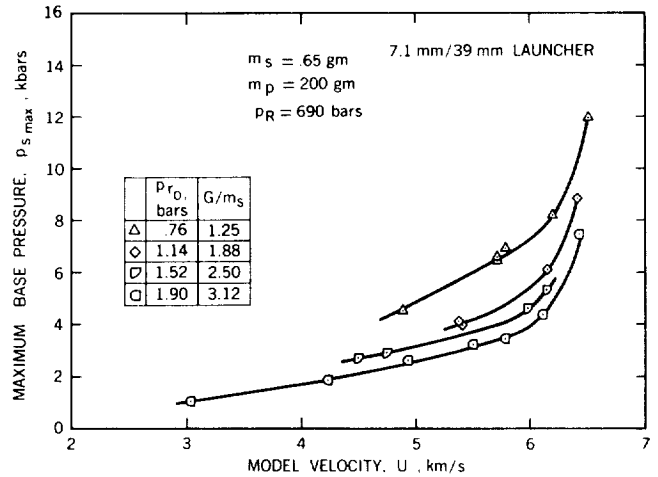

2.49 Variation of maximum base pressure with model velocity at constant values of initial hydrogen pressure, for a relatively heavy model (experimental)

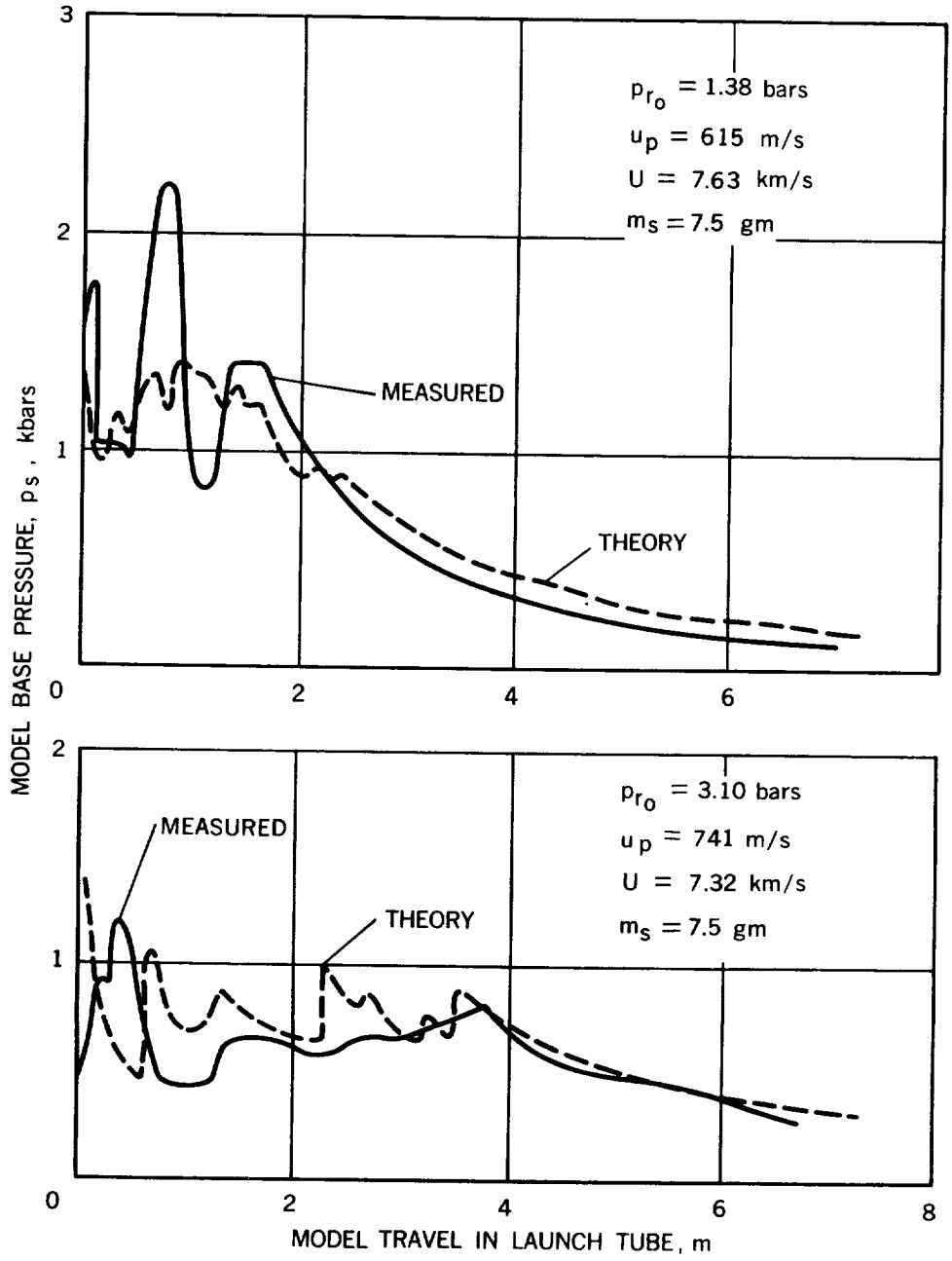

2.50 Example of base-pressure histories for two different initial reservoir pressures and piston velocities which give approximately the same model velocity; 25.4 mm/102 mm launcher

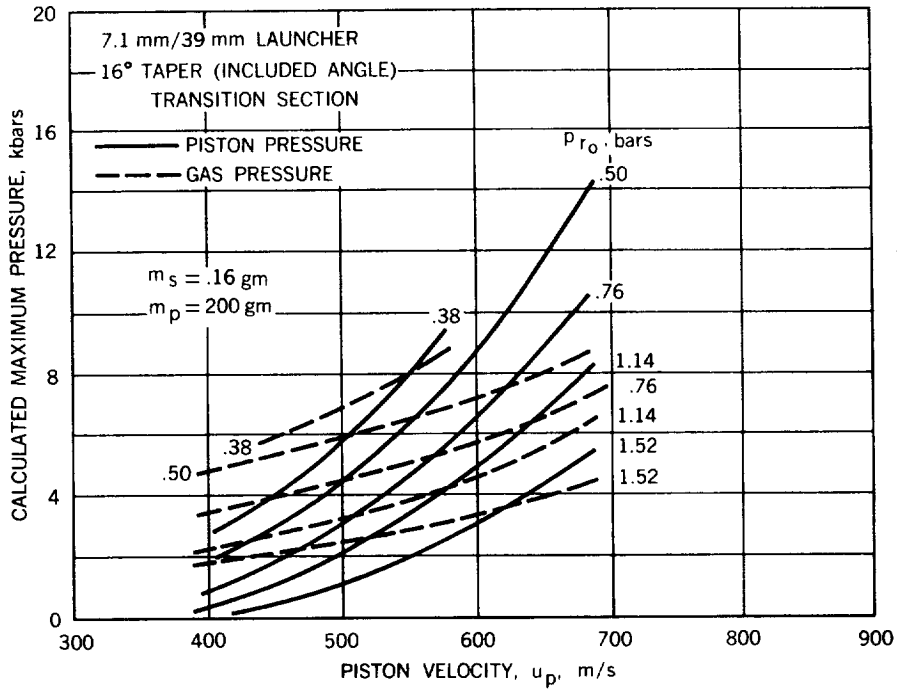

2.51 Calculated maximum pressures exerted on 16°-taper transition section by piston and gas as a function of piston velocity, for constant values of initial hydrogen pressure

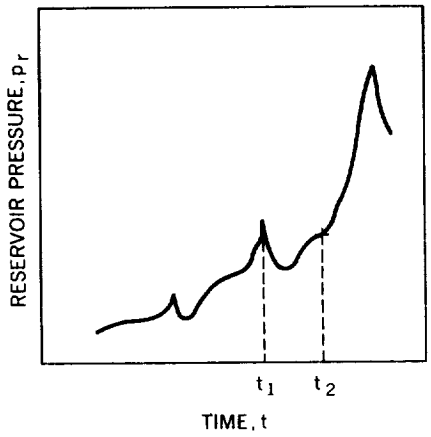

2.52 Example of variation of reservoir pressure during compression

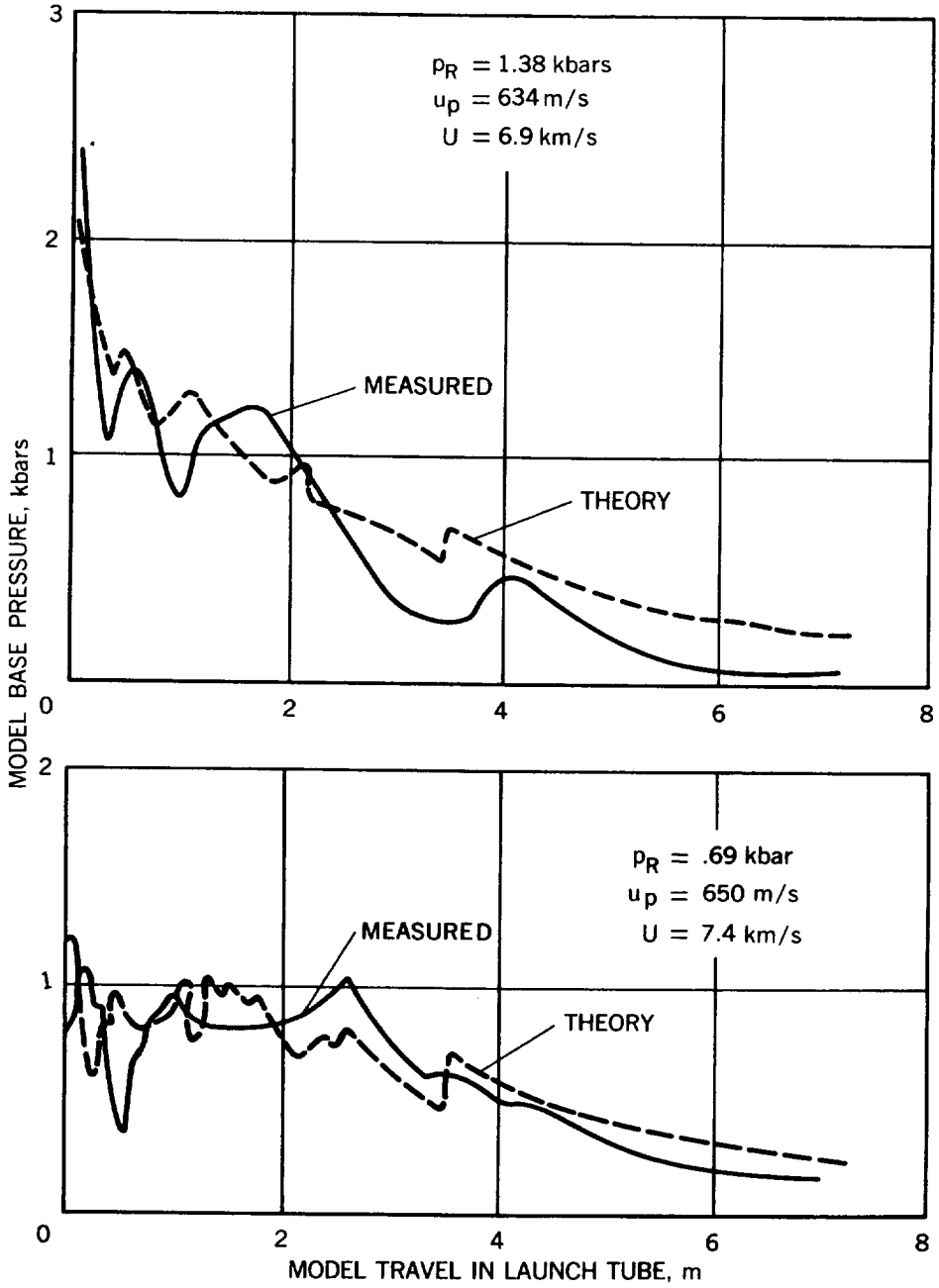

2.53 Effect of model-release pressure on the model-base pressure during launch; 25.4 mm/102 mm launcher

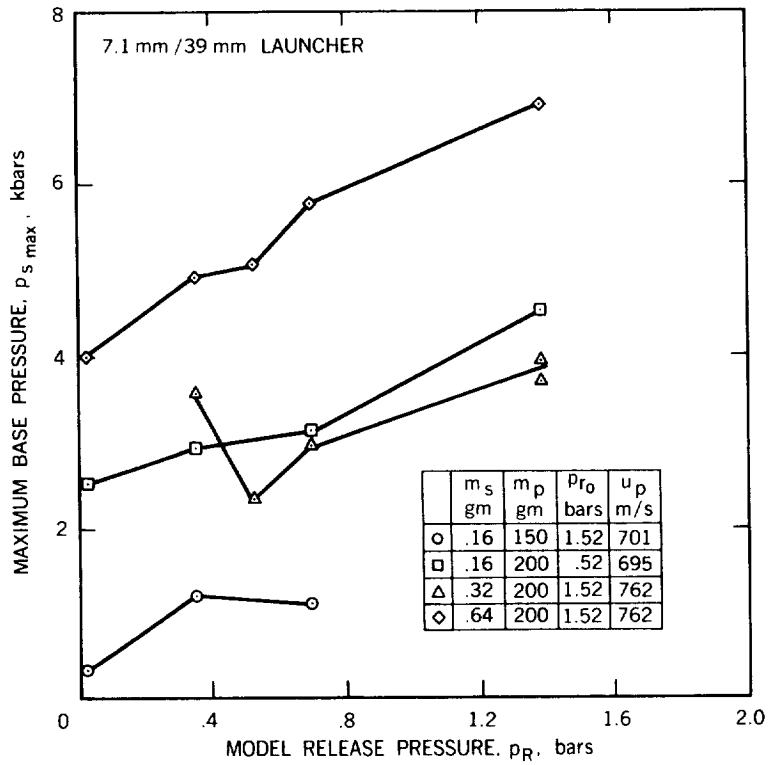

2.54 Effect of model-release pressure on maximum base pressure (experimental)

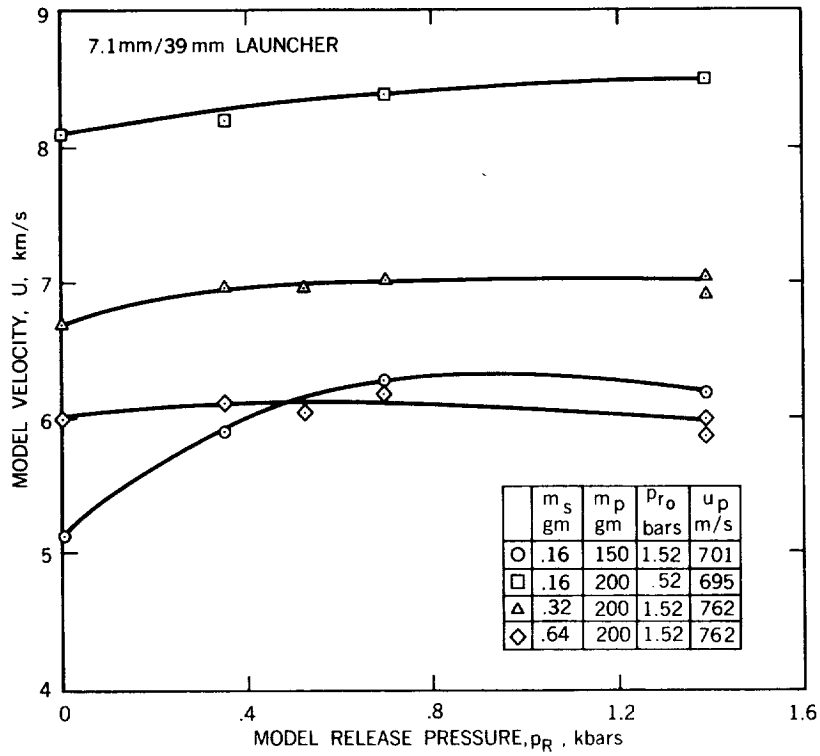

2.55 Effect of model-release pressure on model velocity for a variety of loading conditions (experimental)

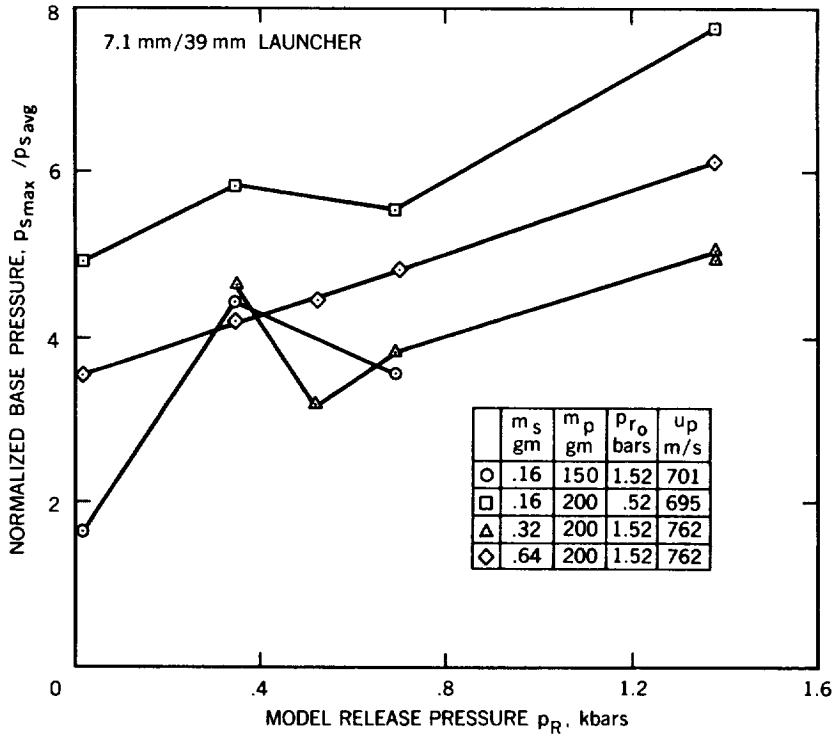

2.56 Effect of model-release pressure on normalized maximum base pressure (experimental)

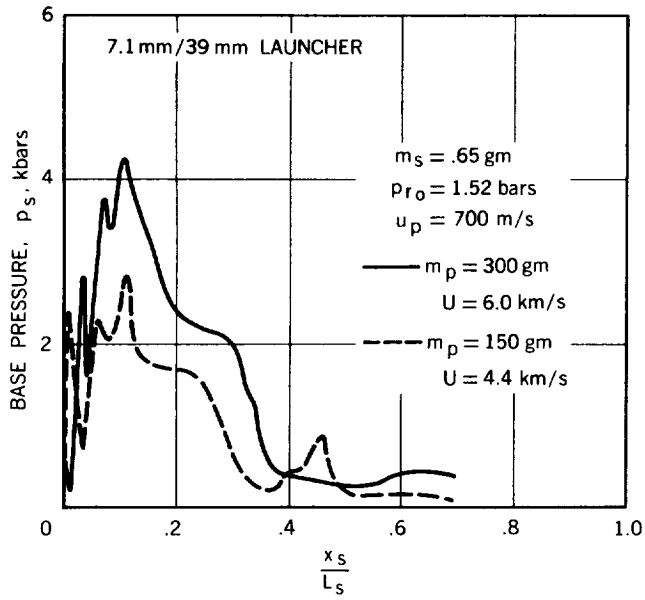

2.57 Effect of piston mass on model base pressure during launch (experimental)

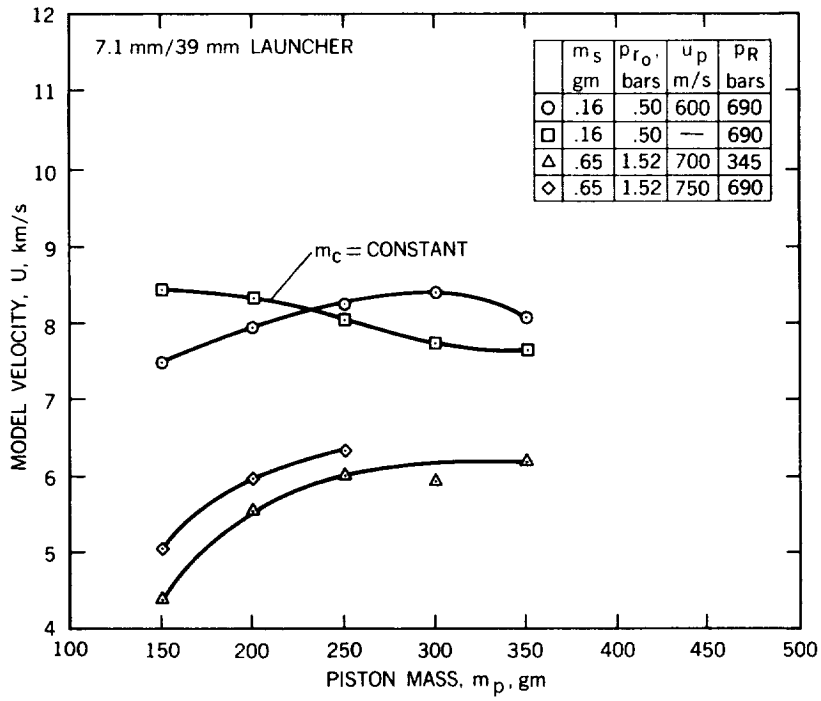

2.58 Effect of piston mass on model velocity for a variety of loading conditions (experimental)

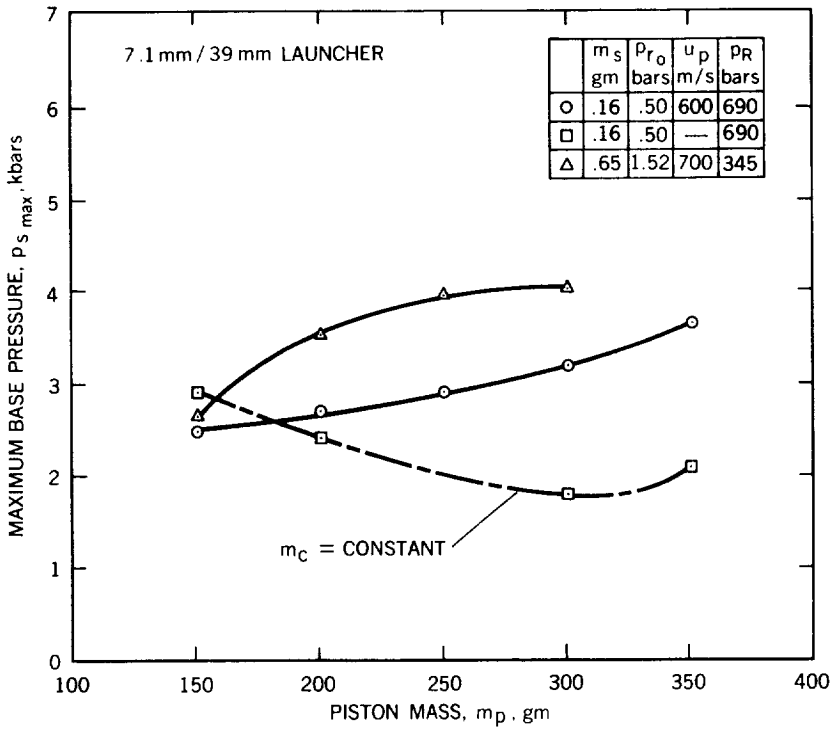

2.59 Effect of piston mass on maximum base pressure (experimental)

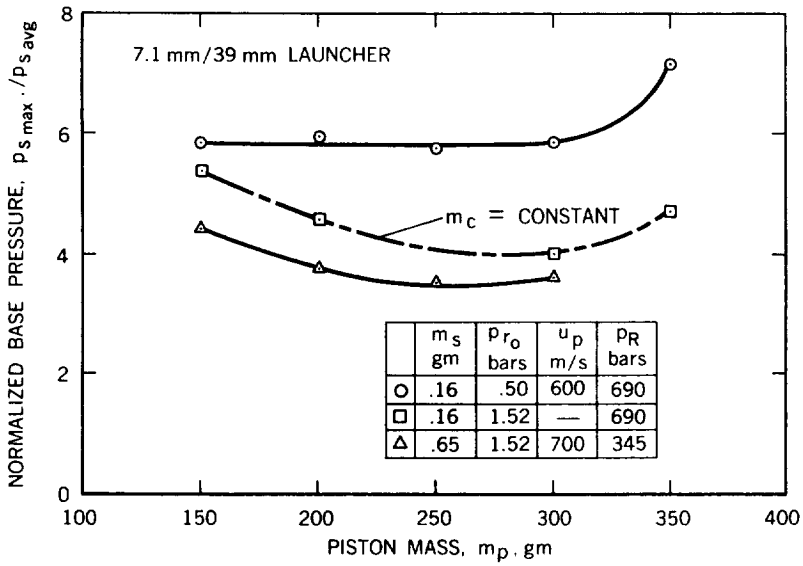

2.60 Effect of piston mass on normalized maximum base pressure (experimental)

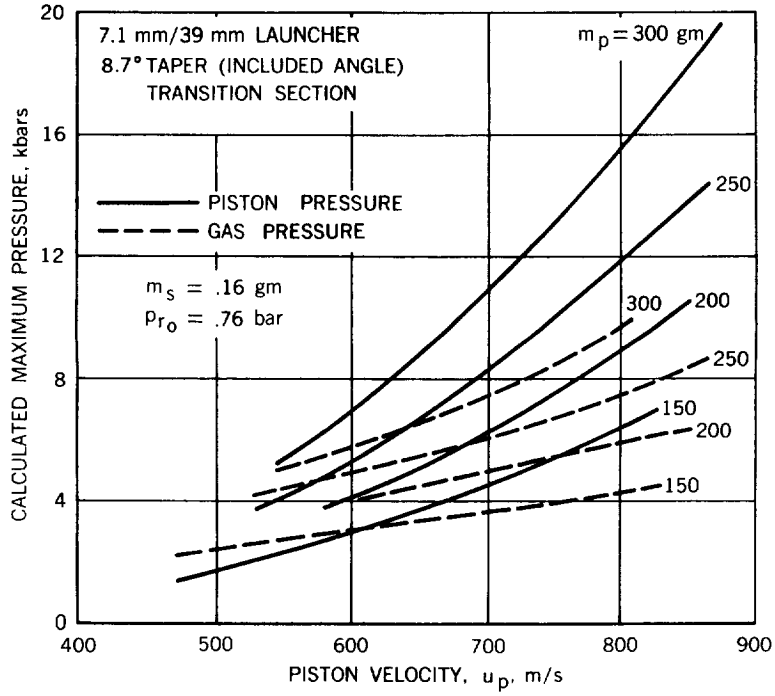

2.61 Calculated maximum pressures exerted on 8.7°-taper transition section by piston and gas as a function of piston velocity, for constant values of piston mass

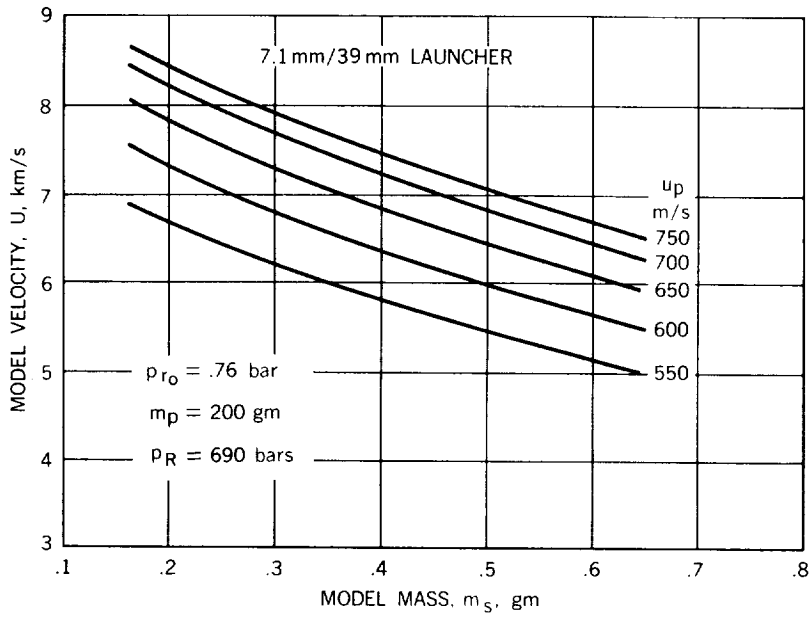

2.62 Effect of model mass on model velocity at constant values of piston velocity (experimental)

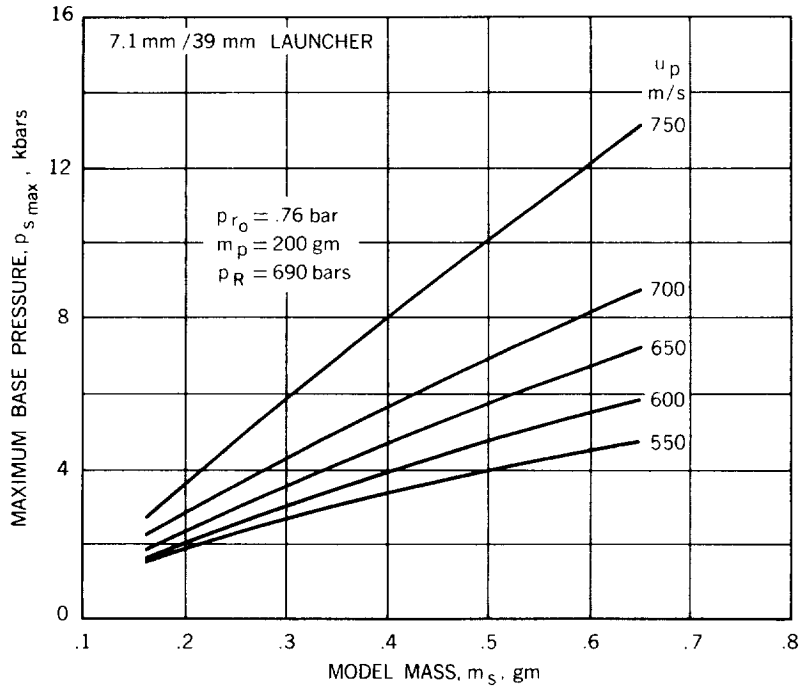

2.63 Effect of model mass on maximum base pressure at constant values of piston velocity (experimental)

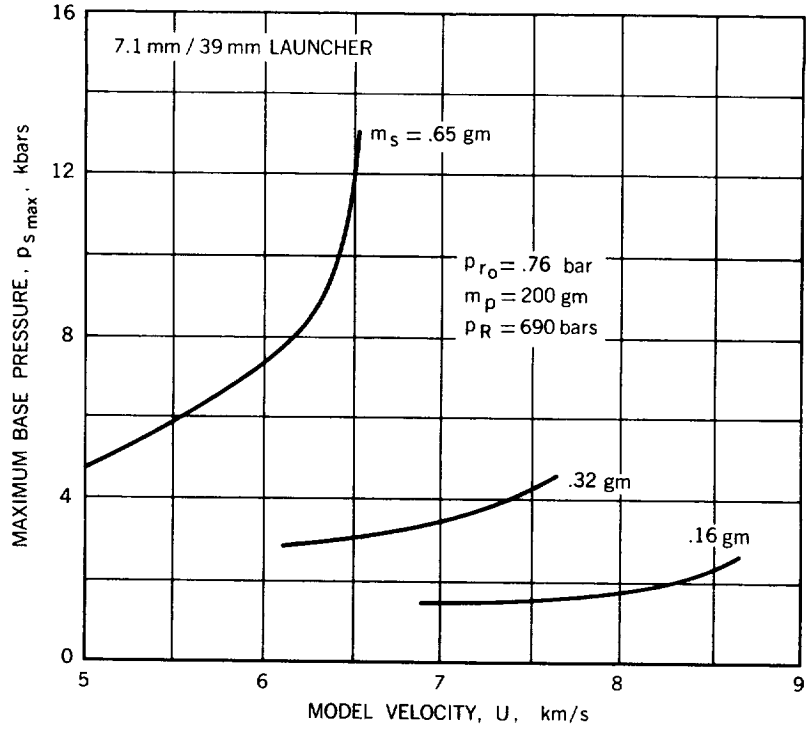

2.64 Variation of maximum base pressure with model velocity at constant values of model weight (experimental)

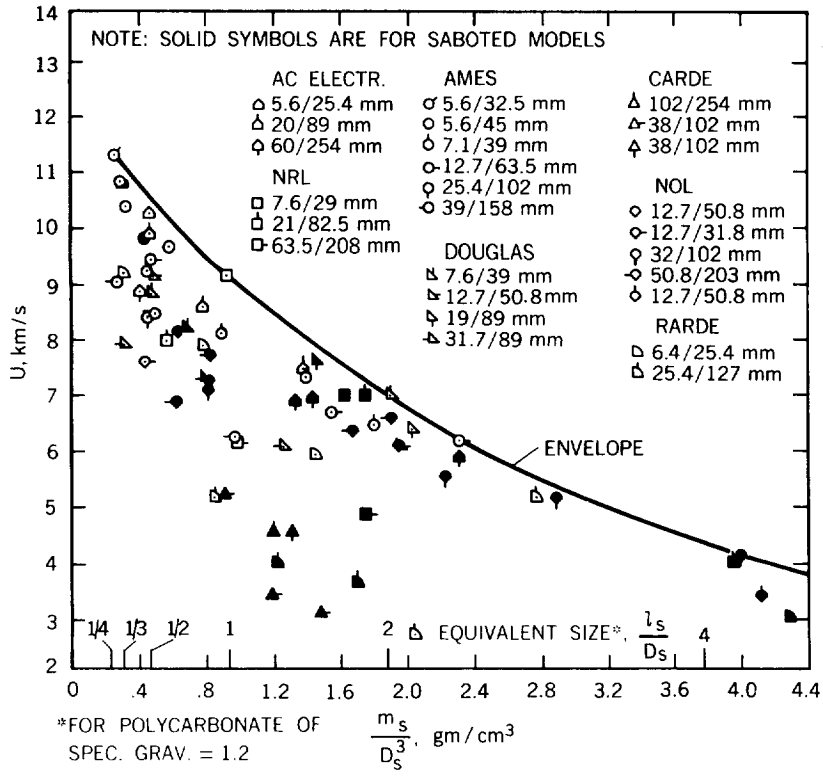

2.65 Launch velocities obtained for a wide variety of models with representative light-gas guns at a number of research laboratories

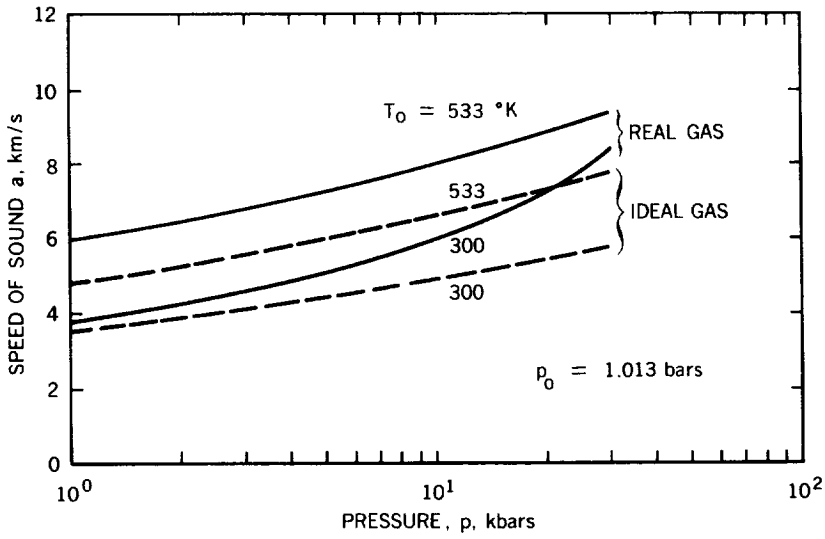

2.66 Comparison of speed of sound in ideal and real hydrogen, compressed isentropically to pressure, p, from initial pressure of 1.013 bars

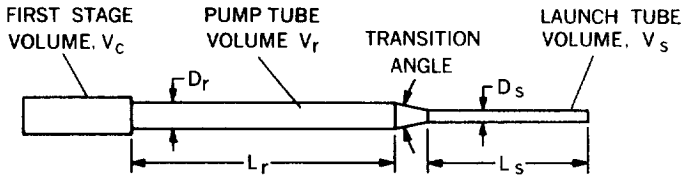

2.67 Notation for gun dimensions given in Table 2.2

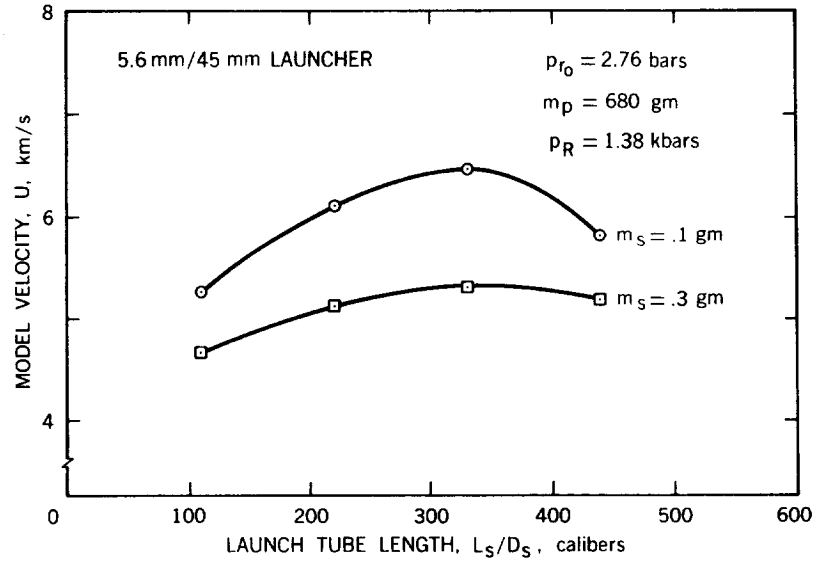

2.68 Effect of changes in launch-tube length on model velocity (experimental)

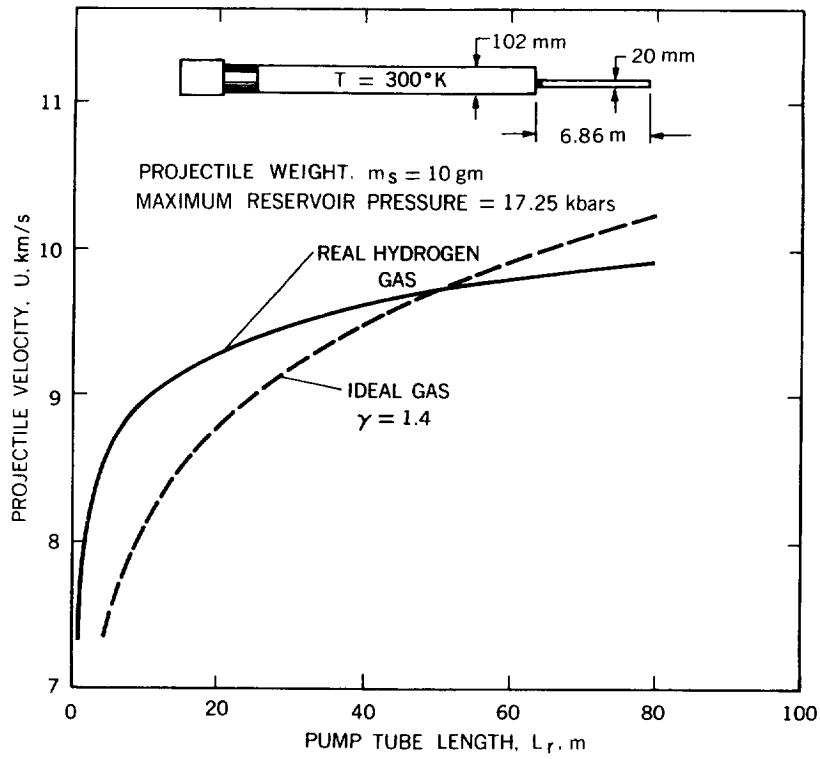

2.69 Effect of pump-tube length on calculated performance of gun operating with constant-base-pressure process. (From Seigel, Piacesi, and Bixler, US Naval Ordnance Laboratory, Ref. 2.78)

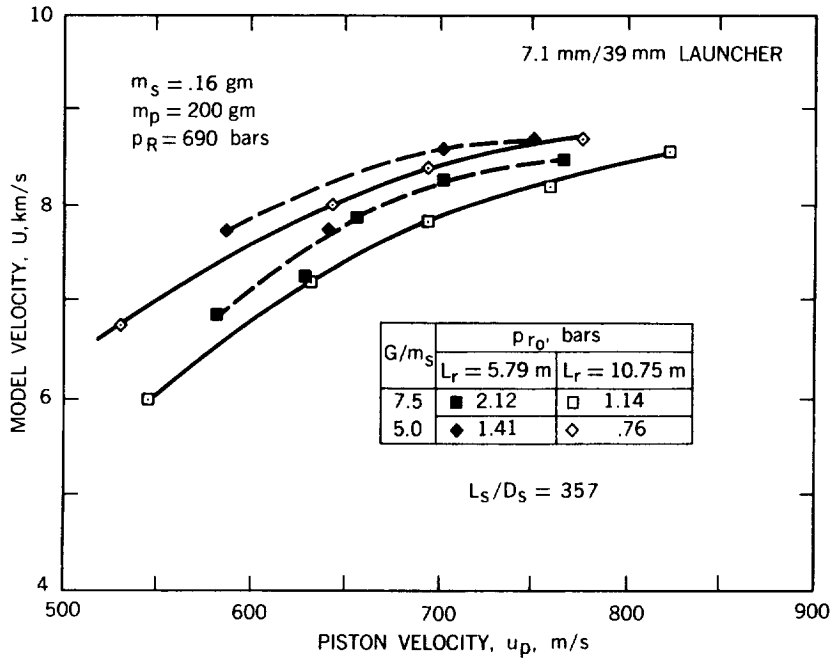

2.70 Effect of change in pump-tube length on variation of model velocity with piston velocity (experimental)

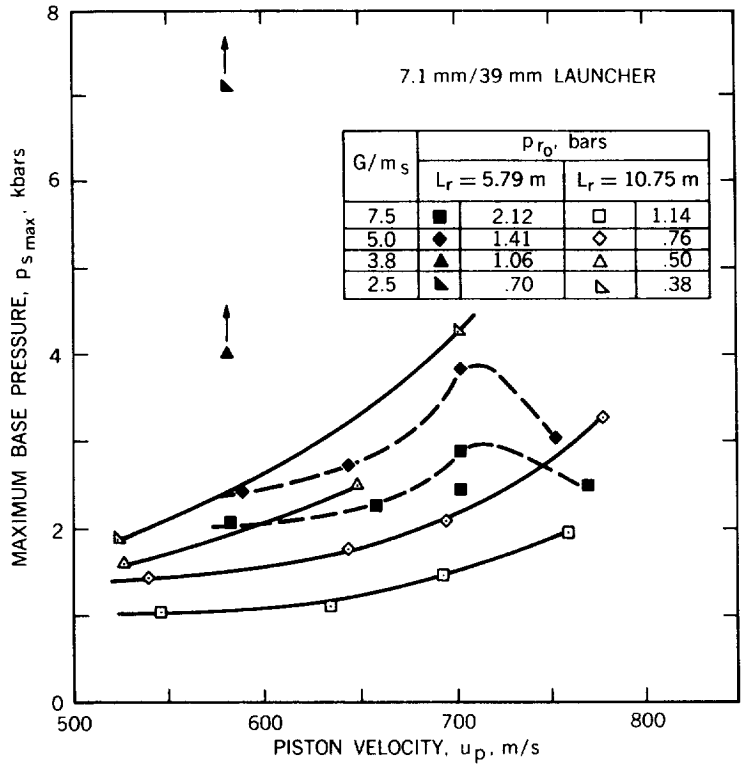

2.71 Effect of change in pump-tube length on variation of maximum base pressure with piston velocity (experimental)

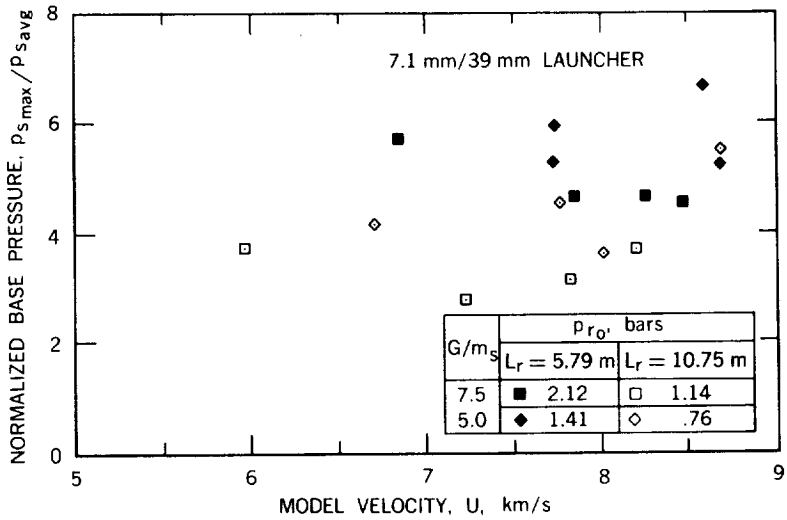

2.72 Effect of change in pump-tube length on variation of normalized maximum base pressure with model velocity (experimental)

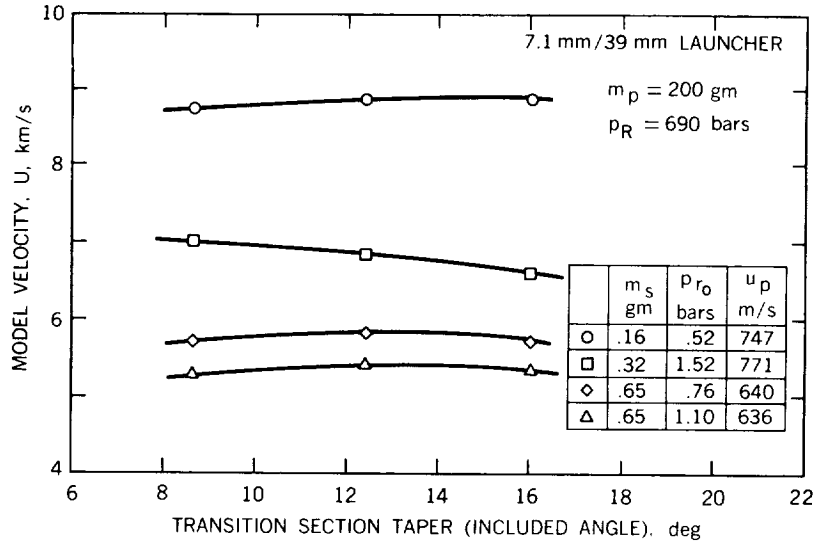

2.73 Effect of pump-tube to launch-tube transition-section taper angle on model velocity (experimental)

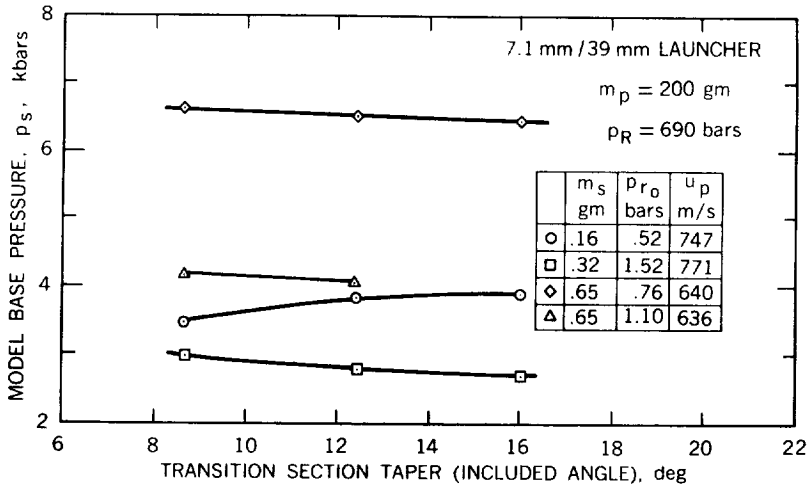

2.74 Effect of pump-tube to launch-tube transition-section taper angle on maximum base pressure (experimental)

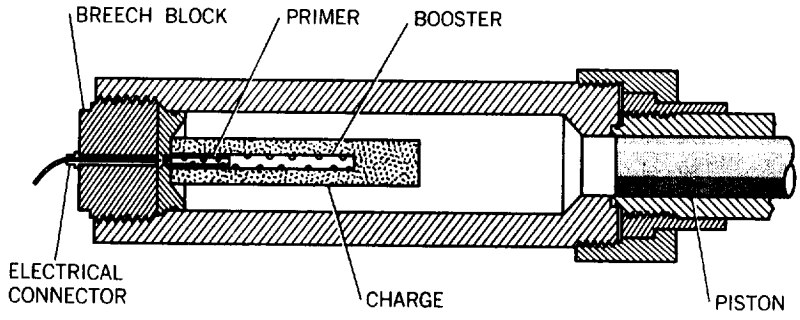

2.75 Light-gas gun powder chamber

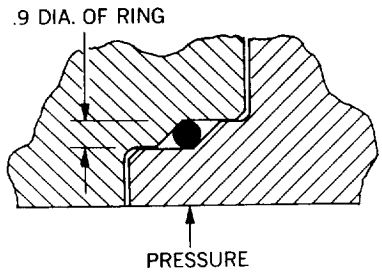

2.76 O-ring seal at gun joint

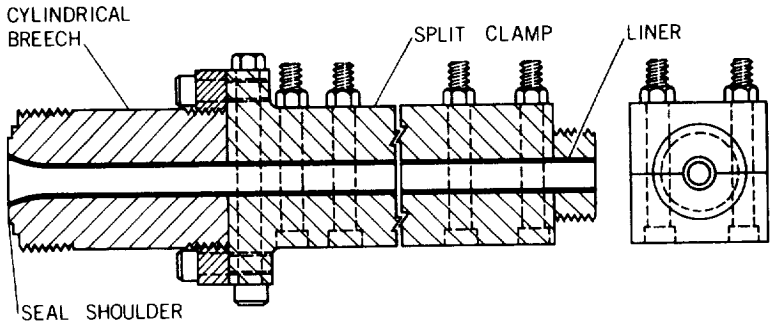

2.77 Split-clamp launch-tube design

2.78 Ames Research Center 25.4 mm/102 mm light-gas gun split-clamp launch tube

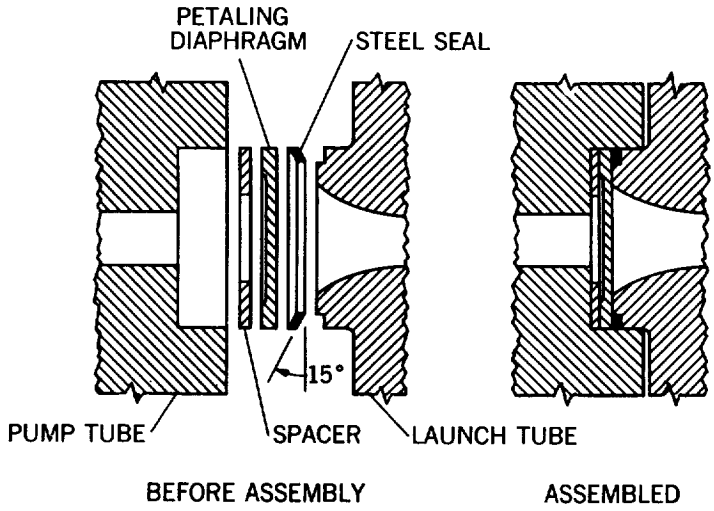

2.79 High-pressure gas seals

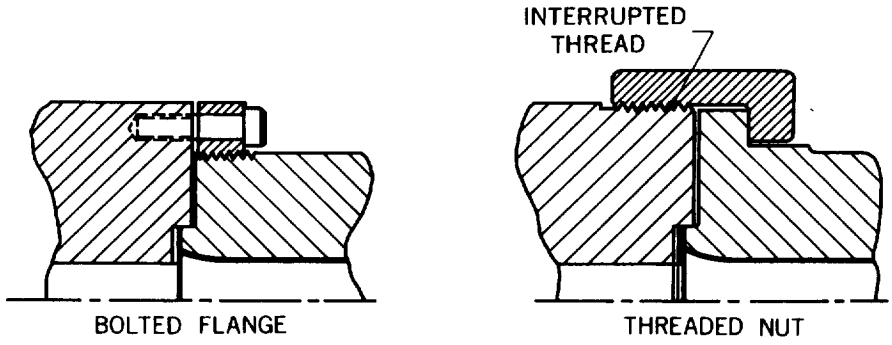

2.80 Launch- and pump-tube couplings for small guns

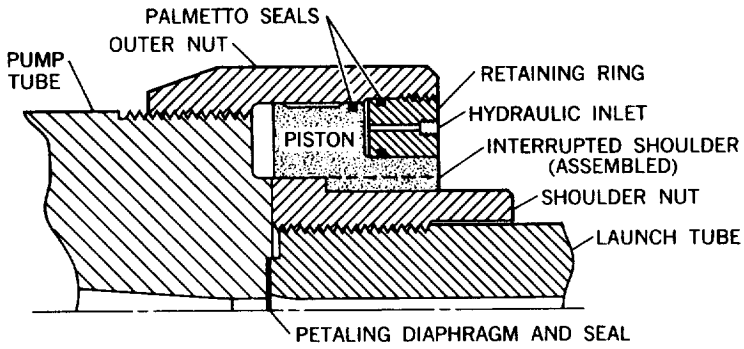

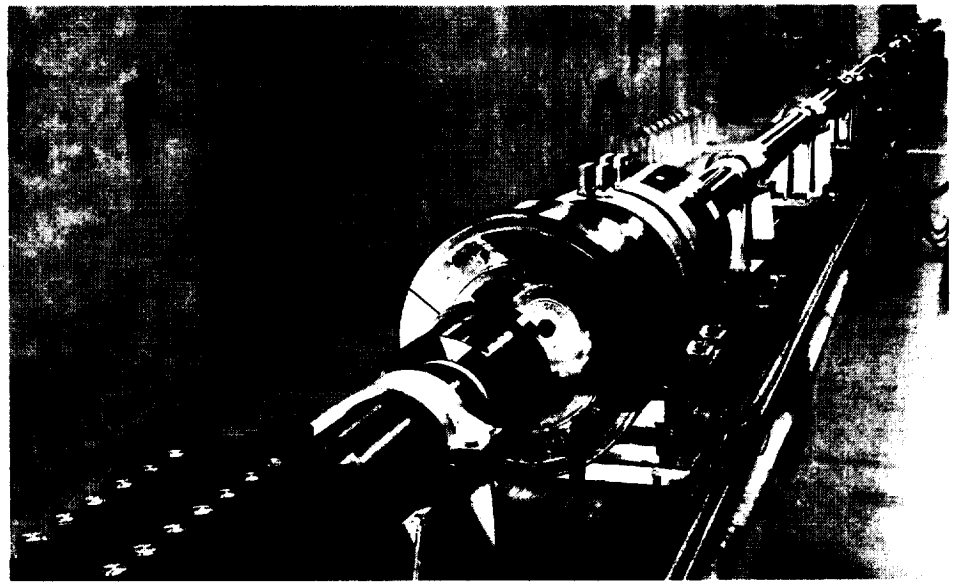

2.81 Ames Research Center 25.4 mm/102 mm light-gas gun launch-tube to pump-tube coupling

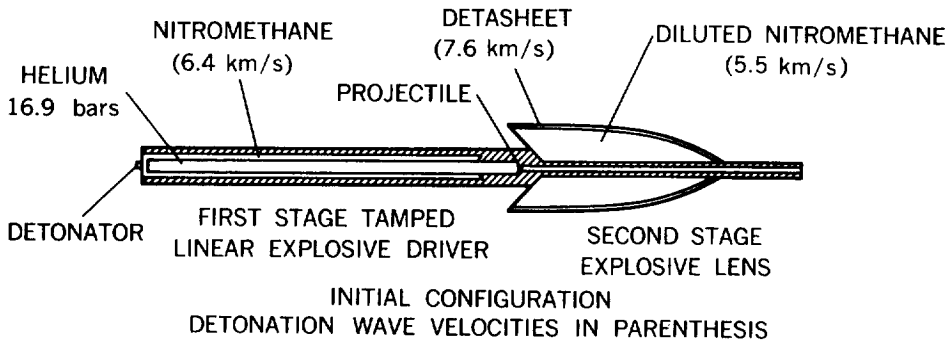

INITIAL CONFIGURATION
DETONATION WAVE VELOCITIES IN PARENTHESIS

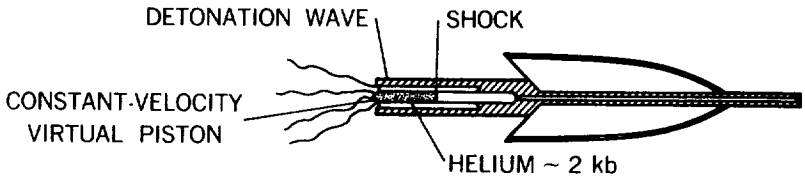

FIRST-STAGE LINEAR DRIVER OPERATION

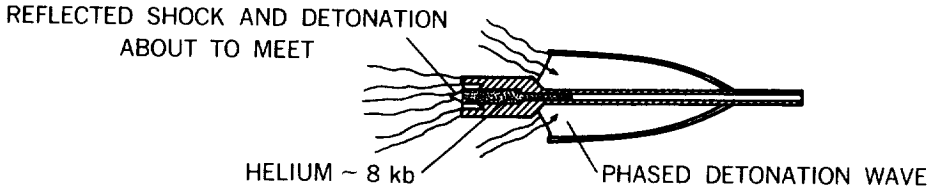

SECOND STAGE INITIATED
PROJECTILE AND DRIVER GAS BEING INJECTED INTO EXPLOSIVE LENS

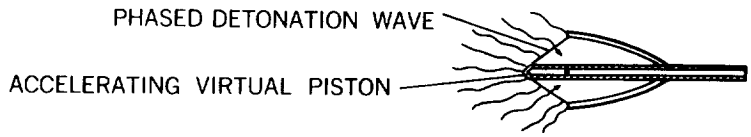

EXPLOSIVE LENS ACCELERATES PROJECTILE TO FINAL VELOCITY

2.82 Operation of a two-stage explosively-driven launcher. (From Moore, Physics International Co., Ref. 2.26)